1973

Neutron emission from fission fragments

Robin Lindsay Walsh
Wollongong University College

NEUTRON EMISSION FROM FISSION FRAGMENTS

Thesis Submitted to the

Department of Physics, Wollongong University College,

University of New South Wales, for the Degree of

Master of Science

by

Robin Lindsay Walsh, B.Sc. (Hons.)

October 1973

8080044

This work is dedicated to my father and mother,

James and Josephine, with love.

SUMMARY

This thesis presents the results of a multiparameter experiment involving the spontaneous fission of californium, ^{252}Cf. The aim was to measure the neutron emission $\nu(A)$, $\nu(Z)$ from ^{252}Cf fission fragments as a function of the mass A and charge Z of the fragments and also as a function of the fragment total kinetic energy.

The 'sawtooth' behaviour of both the $\nu(A)$ and $\nu(Z)$ curves was observed. The $\nu(Z)$ data imply that there is no odd-even Z effect in fragment neutron emission. The slope of the $\nu(Z)$ curve for the heavy fragment was found to be substantially lower than that previously reported. No 'plateau' effect was seen in the heavy group $\nu(Z)$ data. Fine structure in the ^{252}Cf $\nu(A)$ curves was observed which correlated in position with the fine structure peaks of the ^{252}Cf mass yield curves.

ACKNOWLEDGEMENTS

This work was undertaken with the permission of the Australian Atomic Energy Commission. The Commission paid my university fees and granted study leave where necessary, and for this I am most grateful.

I am greatly indebted to my good friend and colleague, Dr. John Boldeman, for much helpful advice and constructive criticism throughout the course of the experimental work, and for a knowledgeable examination of the preliminary manuscript. My University supervisor, Dr. Jagdish Mathur, was a constant source of encouragement. Both he and my second supervisor, Dr. John Symonds, ably reviewed the manuscript and suggested worthwhile amendments. Professor Austin Keane and Dr. Roger Bird also critically read the thesis and made helpful comments.

The experiment could not have got off the ground without the efforts of a number of people. Mr. Harry Broe provided expert guidance in the re-design, installation and subsequent high vacuum operation of the fission chamber and cryostat assembly. Mr. Alfred 'Greg' Beech fabricated and installed the silicon X-ray detector, while Mr. Pat Weir made the surface barrier fission detectors. Mr. John Eberhardt constructed the X-ray detector preamplifier, placidly putting up with my persistent calls for more haste. Mr. Ken Brown advised on the draining and refilling of the liquid scintillator tank.

During the period of data taking, Mr. Paul Parton was always prompt to attend to malfunctions of the magnetic tape deck and associated tape control unit. Similarly, Mr. Bob Phillips suffered my occasional requests for rush repair jobs on the electronic instrumentation with resignation and skill. Mr. Peter Ellis spent some time developing an

interface for a 1K ADC on the X-ray pulse height line.

Numerous people gave valuable assistance in the computer analysis of results. Mr. Les Sullivan and Mrs. Marcelle Inkster wrote the programs XDIST and NBDIFF, used in the analysis of the $\nu(Z)$ data. Les was particularly patient in the face of a number of requests for changes to the program format. Messrs. Hugo Ferguson, Graham Trimble and Bob Cawley gave expert advice on the many software problems that arose in the $\nu(A)$ analysis program MASSIVE. Mr. Tony Musgrove wrote the bulk of the program PCALC, which calculated the neutron geometry emission probabilities. Mr. Alan Emery assisted in the calculation of the $\nu(M,E_T)$ reference matrix (section 5.1).

The thesis was typed with a great deal of skill and accuracy by Mrs. Lillian Woodland. Mr. Allan Aston prepared the majority of the diagrams.

My former flatmate, Mr. Graham King, was always very considerate in not disturbing me during those times when I was working on this thesis at home.

To all those mentioned above is due my deepest gratitude and thanks.

CONTENTS

CHAPTER 1

INTRODUCTION

The possibility of neutron emission as a de-excitation mode for the primary fission fragments was realised in the very earliest fission studies[1]. The systematics of the nuclear charge density indicated that the primary fragments would be neutron rich and unstable towards β decay. Since it was also known that the excitation energy involved was very large, approximately 200 MeV[2,3], neutron emission seemed probable and was soon observed by a number of groups[4,5]. With the realisation that the fission neutrons could be used to sustain nuclear 'chain reactions' a great deal of effort was devoted to examining their properties in detail. The successful outcome of this work is summarised well in the 1955 and 1958 Geneva Conferences on the 'Peaceful Uses of Atomic Energy'[6,7].

Studies of the neutrons emitted in the fission process also yield a wealth of information about the fission act itself, information which often cannot be obtained by any other means. Measurements of the angular distribution of fission neutrons showed that the neutrons are emitted from the two moving fragments, and further, that they are emitted after the fragments have attained their peak velocities. Measurements of the neutron energy spectrum showed that the neutron emission could be thought of as a 'boil-off' or 'evaporation' process from excited fragments which were themselves characterised by one or more nuclear temperatures. Experiments investigating the numbers of fission neutrons emitted ('multiplicity') have cast much light on the energy balance in fission. The variation of $\bar{\nu}$ (the average number of prompt neutrons emitted per fission) with the excitation energy of the compound nucleus (E^{*}) tells us that the excitation energy is dissipated almost wholly as neutron emission while ever neutron

emission is energetically possible. The interpretation of the $\bar{\nu}$-E^{*} relationship in terms of the discrete saddle point energy levels permits an estimate of the strength of the coupling between the saddle point degrees of freedom and those at scission. That is to say, an estimate of whether the distribution of the available energy at the saddle point is preserved or lost in the passage to scission. Further, the $\bar{\nu}$-E^{*} relationship can also yield valuable data on the relative heights of the two Strutinsky potential barriers in fission.

Studies of the neutron emission as a function of the mass of the emitting fragments show in a remarkably direct way the role of shell effects in the fragments. The deformation parameters of the individual fragments may be calculated directly from data of this type. Data on the variation of total neutron emission with total fragment kinetic energy is related to the competition between neutron emission and fragment kinetic energy for the saddle point excitation energy. Data of this type is complementary to the $\bar{\nu}$-E^{*} data mentioned above.

In the last five years, measurements of the neutron emission from a fragment of given nuclear charge Z have become possible. This has been due to the advent of high resolution silicon X-ray detectors. These detectors are used to measure the energy of the K X-ray characteristic of a particular fragment charge. These X-rays are emitted by the fragments within a few nanoseconds (mostly) of fission. The high resolution obtainable, better than 500 eV FWHM for a 30 keV X-ray, enables identification of individual elements.

The interest in ν versus Z measurements is two fold. Firstly, we would like to observe that the $\nu(Z)$ curve exhibits the same 'sawtooth'

behaviour as the ν versus mass curve, as we expect it should. Resolutions of one charge unit are equivalent to mass resolutions of about 2.5 amu, comparable to the best time-of-flight measurements. The second and more interesting aspect arises from the link between neutron emission and fragment excitation energy. It is expected that fission into two even charge fragments will produce about 2 MeV more fragment excitation than fission into two odd charge fragments[8,9]. Assuming all the excitation energy passes into neutron emission, this represents about 0.2 to 0.3 neutrons more from the even Z pair than from the odd Z pair. Thus, an odd-even Z effect should appear in the total neutron emission. The only measurements of this effect which have been reported at present are by the French groups at CEN, Saclay, and at CEA, Bruyères le Châtel, on the spontaneous fission of ^{252}Cf[9,10,11]. These groups found no odd-even Z variation in the ^{252}Cf neutron emission and also no such variation in the fragment kinetic energy E_K. The problem then arises that if the semi-empirical mass formulae calculations[8,9] are correct, just where has the excess fragment excitation energy gone? The present work is an attempt to measure the ^{252}Cf $\nu(Z)$ and $E_K(Z)$ dependences with a higher charge resolution than was used for the French measurements. In addition, the ^{252}Cf ν versus mass dependence is also obtained.

As well as the experimental work reported herein, a survey of developments in the field of fission neutron studies is also given in Chapters 2 and 3. The candidate has previously made some contribution to this field

(12,13,14,15,16) (see attachment). Similar surveys are scarce in the literature.

CHAPTER 2

SOME GENERAL PROPERTIES OF THE FISSION NEUTRONS

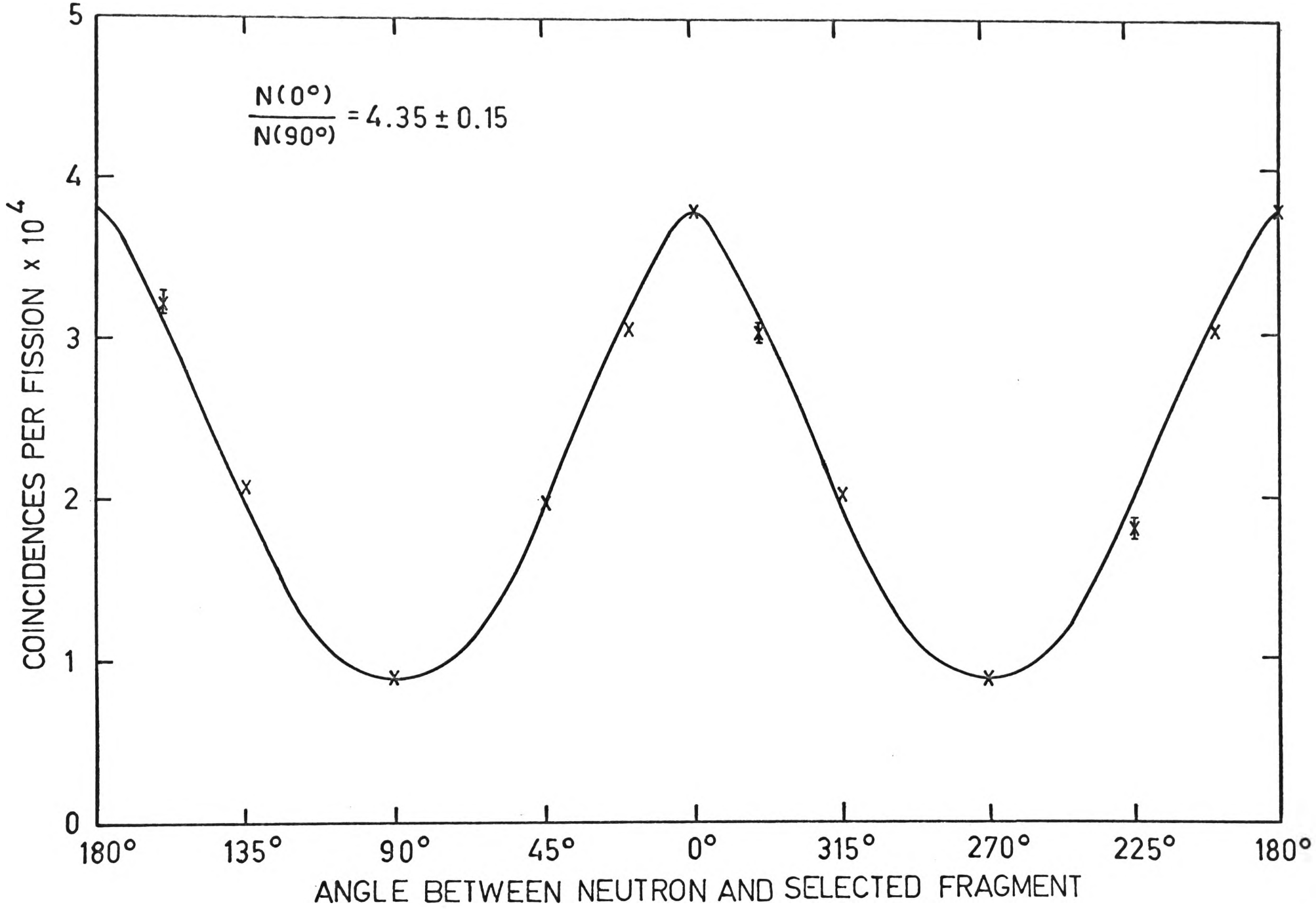

Fig 2.1 Angular distribution of prompt neutrons from Pu^{239} induced to fission with thermal neutrons. From reference [17].

As mentioned earlier, measurements of the angular and energy distributions of fission neutrons gave important evidence as to the origin of the neutrons. The first two sections of this chapter review some of these measurements, and relate their findings to the conclusion of neutron emission from two moving fragments. The third section treats the neutron multiplicity and its direct relationship to the question of the dissipation of the energy of the compound nucleus after scission.

2.1 Neutron Angular Distribution

In angular distribution studies, the angle of emission of the neutron is usually measured with respect to the direction of fragment motion. The most significant feature of the distribution - in the laboratory - is the strong peaking in this fragment motion direction.

In one of the earliest such studies Fraser[17] examined the thermal neutron fission of ^{233}U, ^{235}U and ^{239}Pu. The collimated fission fragments were detected in a gridded ionisation chamber, and coincident prompt neutrons in a given direction were counted by proton recoils in an electron-collecting chamber filled with methane. Fraser's results for ^{239}Pu are shown in Figure 2.1. There is a strong peaking of the distribution in the fragment direction of motion. $\frac{N(0^o)}{N(90^o)}$, the ratio of the number of neutrons at 0^o to that at 90^o, was found to be 4.35 ± 0.15.

The ^{233}U and ^{235}U distributions also displayed this strong peaking. Fraser accommodated his results to the assumption of isotropic emission of neutrons from the fragments, i.e. isotropic in the fragment frame of reference, the neutrons being emitted after the fragment has attained its

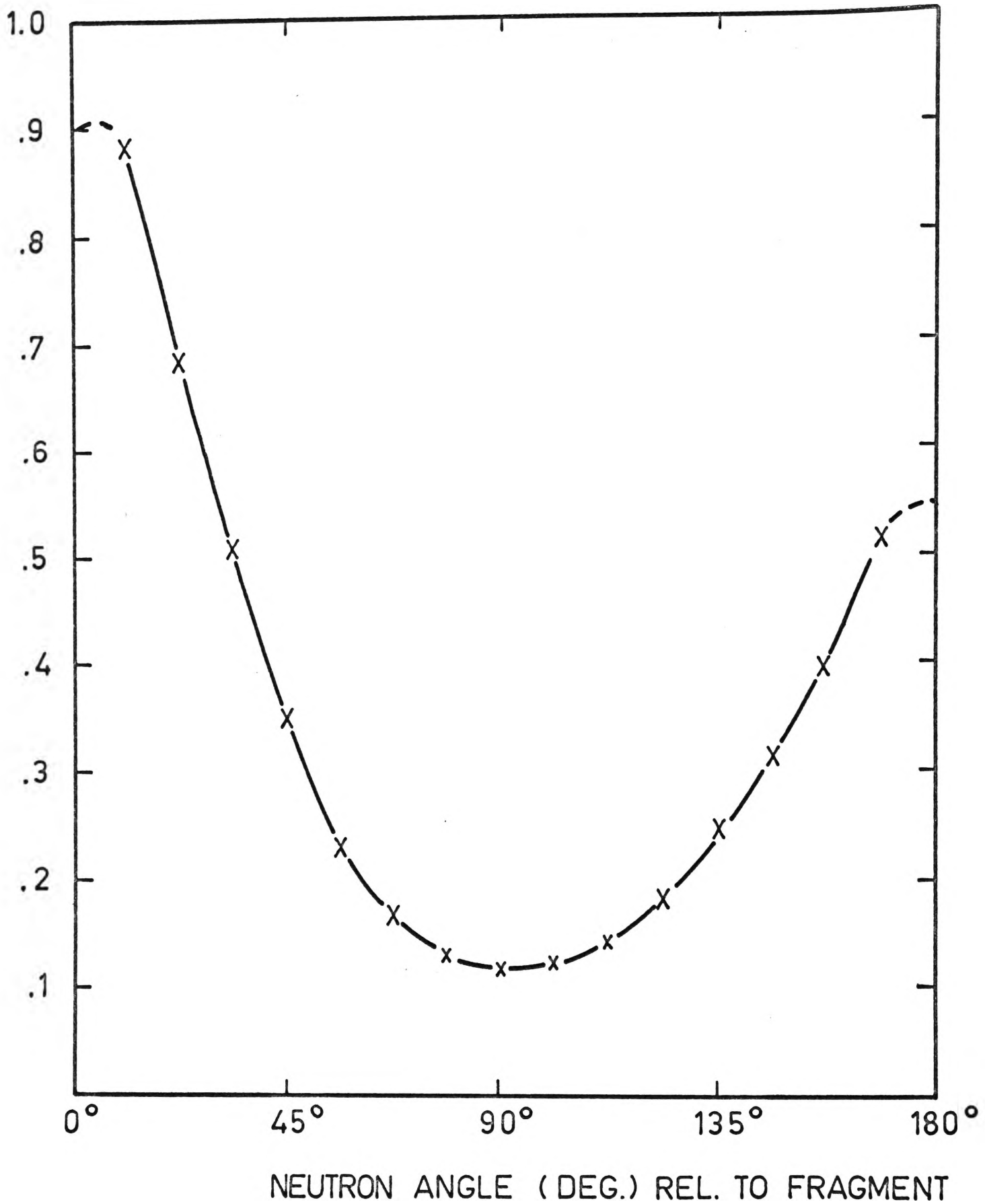

Fig 2.2 The measured angular distribution (lab) of neutrons from Cf^{252}. From [18].

peak velocity ($\sim 10^9$ cm/sec). The neutrons therefore have a velocity component in the fragment direction, producing the peaking of the laboratory spectrum.

A much more exhaustive work was performed by Bowman et al. in 1961[18]. These authors studied the spontaneous fission of ^{252}Cf. As well as measuring the angle of neutron emission with respect to a fragment, they also measured the velocities of the two fragments and the velocities of the emitted neutrons, in each case by the time-of-flight method. The laboratory angular distribution they obtained is shown in Figure 2.2. $\frac{N(0^o)}{N(90^o)}$ can be seen to be about 9.1. Figure 2.3 is another representation of their data, showing the neutron distribution as a function of both angle and neutron velocity. The distribution shown is that of the density $\rho(V,\theta)$, where the probability per fission that a neutron making an angle θ with the fragment has a velocity V in the interval dV within the solid angle dw is $\rho(V,\theta)V^2$ dV dw. A visual examination of this figure suggests that the neutron distribution is consistent with approximately isotropic emission from two moving fragments. That is, the fact that the lines of constant ρ have the form of elongated ovals suggests that the neutrons have been emitted from two sources moving in opposite directions with velocities about the same as those of the fragments.

Bowman et al. then proceeded to examine their data more quantitatively in order to test the hypothesis of isotropic emission from the moving fragments. Their method was to represent the overall features of the data by simple analytic expressions corresponding to the assumption of emission of neutrons from the moving fragments, and to see how well the data could be fitted to such expressions. In the main, the results of this procedure

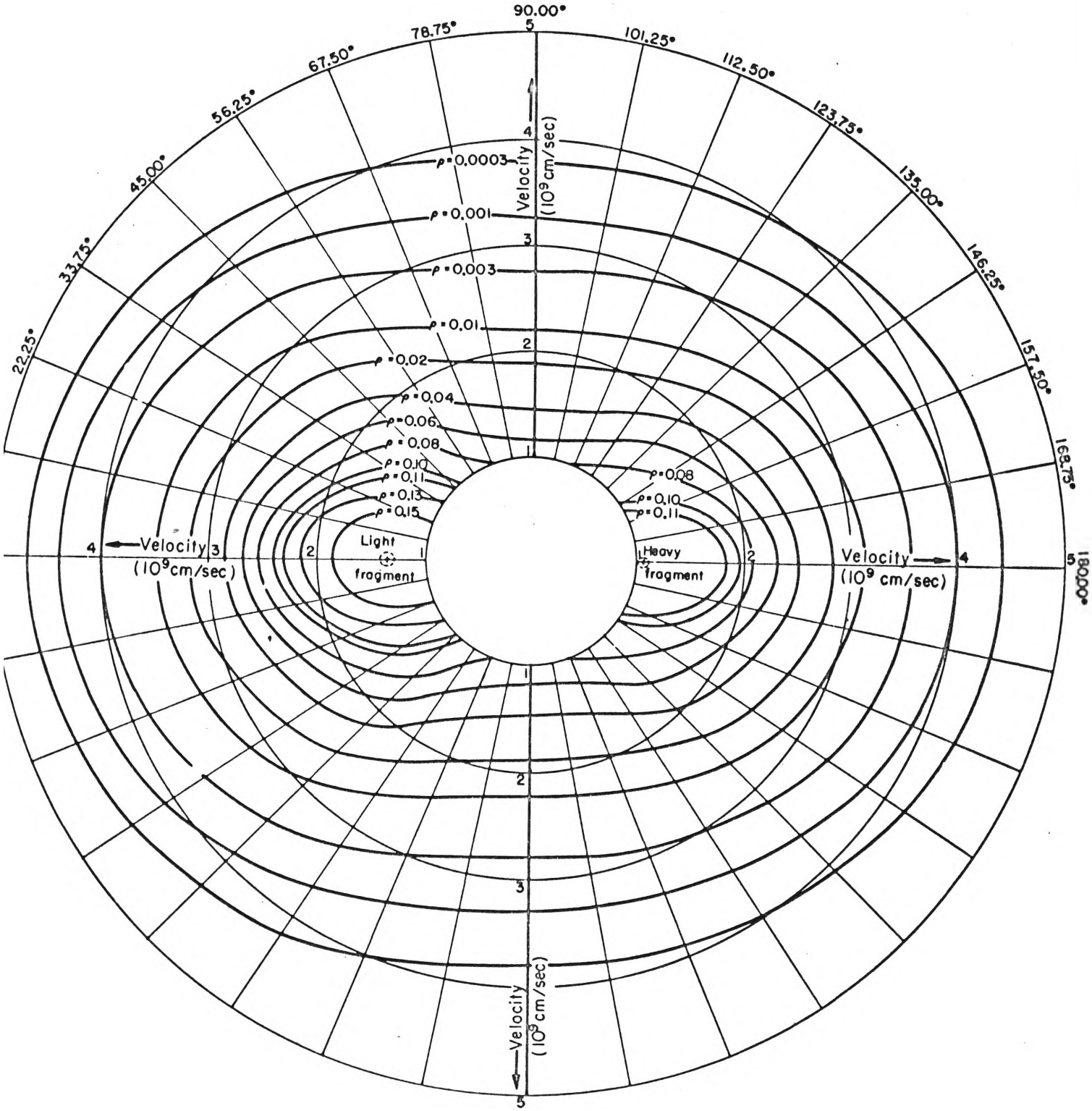

Fig 2.3 Contour diagram in polar coordinates of observed neutron density distribution $\rho(V, \theta)$ as a function of neutron velocity and angle. From BOWMAN, THOMPSON, MILTON, AND SWIATECKI. [18] The contour lines are lines of constant neutron density. The average velocities of the light and heavy fragments are also shown.

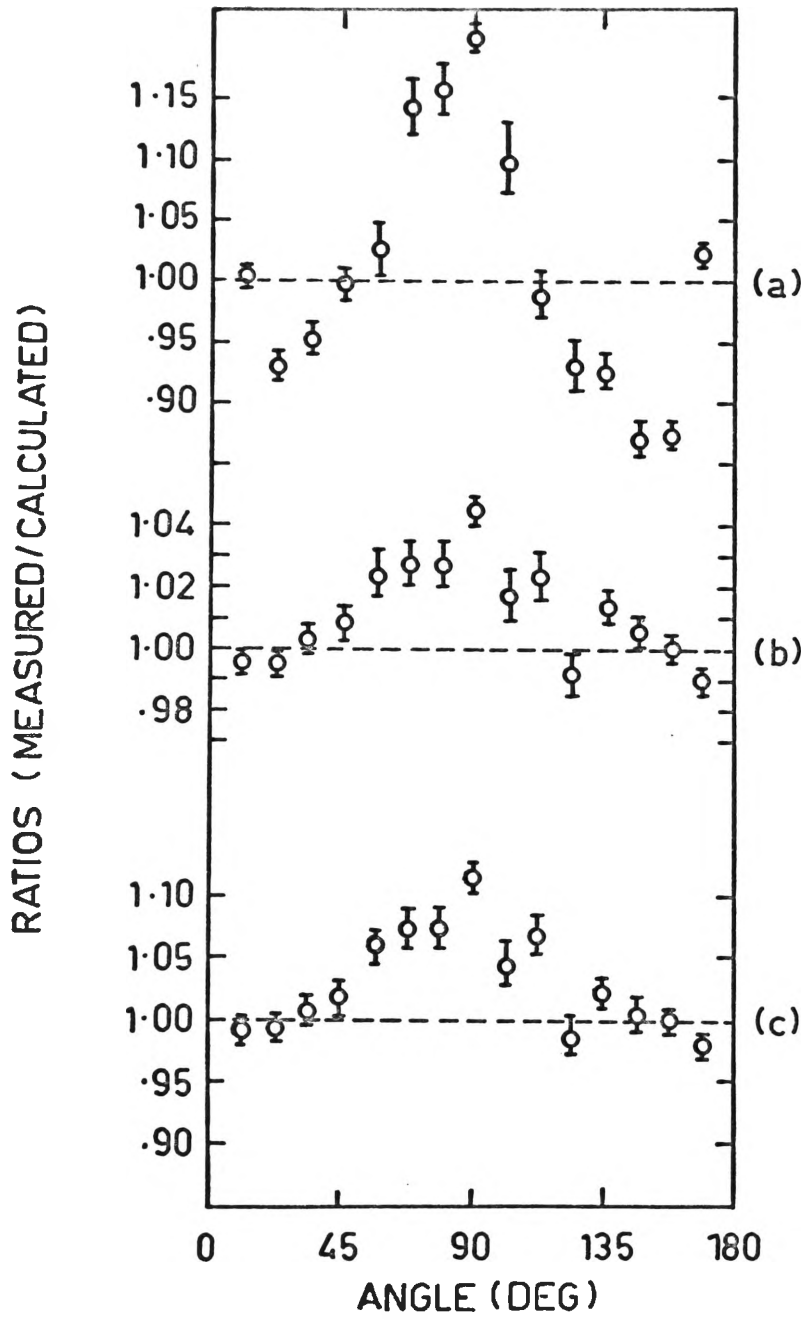

Fig 2.4 Ratio (measured / calculated) of neutron numbers versus angle. Initial calculation. From [18].

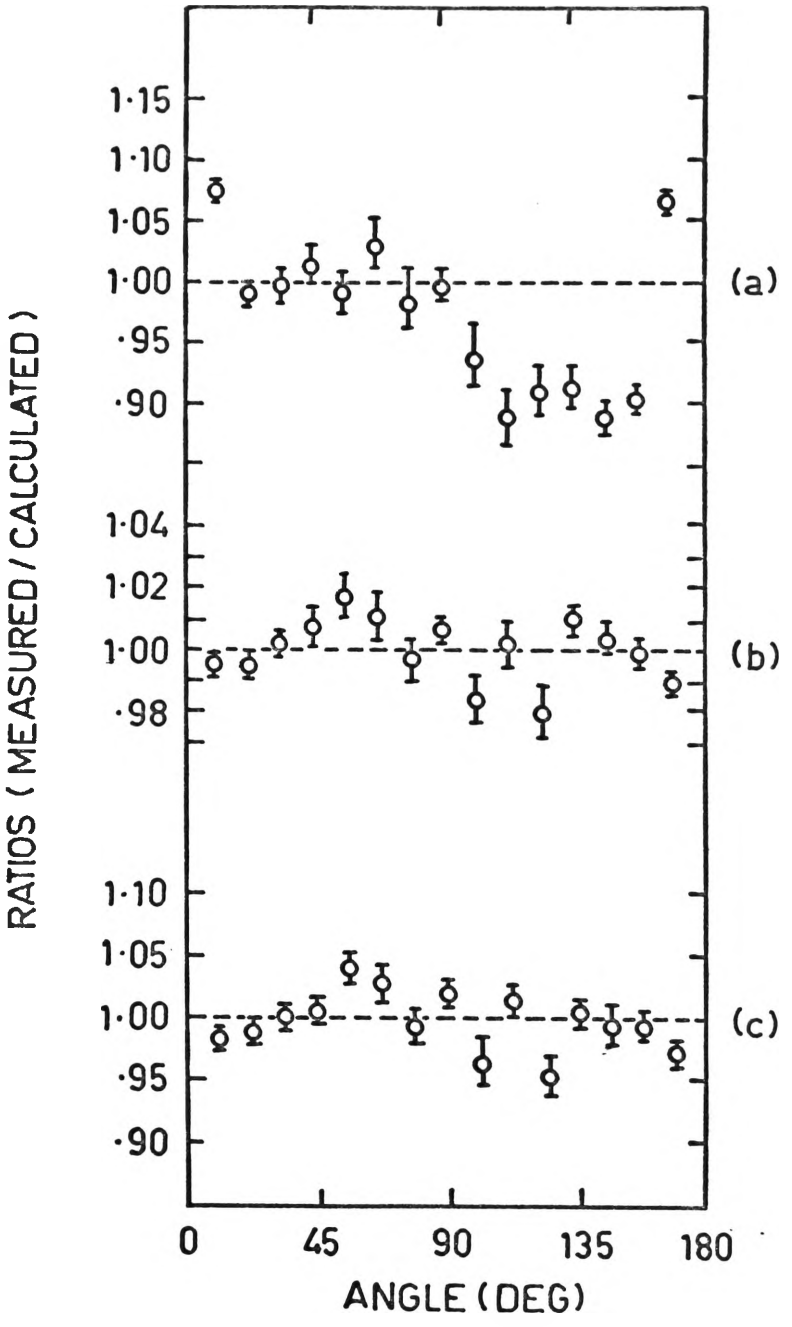

Fig 2.5 Same ratio, but with a 10% isotropic component in calculations.

confirmed the conclusions of the more qualitative approach above.

There did, however, exist a significant discrepancy between the calculated distribution and the measured one at an emission angle of 90^{o}. Figure 2.4 shows the ratio of measured to calculated values for numbers of neutrons, average velocities and average energies, as a function of emission angle. There is obviously a systematic rise in the observed number of neutrons as one approaches 90^{o}. This implies that a fraction of the neutrons, rather than being emitted from the moving fragments, is emitted isotropically in the laboratory system. Bowman et al. repeated their calculation of the neutron distribution, this time assuming 10 per cent of the neutrons to be distributed isotropically in the laboratory system with average energy 2.6 MeV (laboratory system). Their results are compared with the measured values in Figure 2.5. It is clear that the rise towards 90^{o} has been removed, confirming the existence of this second group of neutrons - the 'scission' neutrons. These neutrons are thought to be produced in the scission process itself, at about the time of rupture of the elongated 'neck' joining the two nascent fragments. They are distributed isotropically in the laboratory system. Thus only about 85 to 90 per cent of the neutrons produced in the fission process arise from the two fragments, the other 10 to 15 per cent being the scission neutrons.

2.2 Neutron Energy Spectrum

The energy distribution of fission neutrons is very close to a Maxwellian distribution. Figure 2.6 shows the data of Barton et al. and Frye and Rosen at Los Alamos for thermal fission of ^{235}U[19]. The

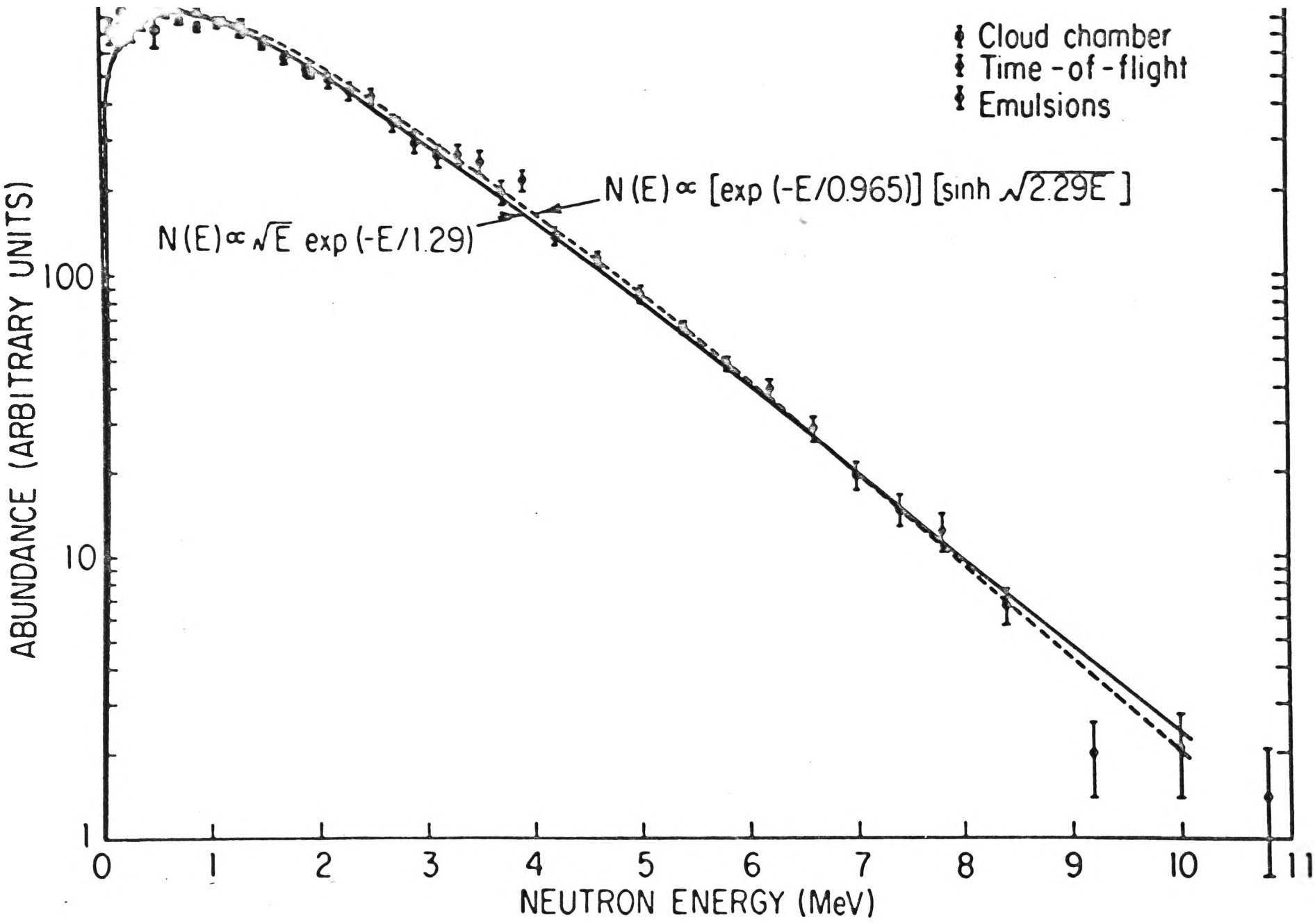

Fig 2.6 Comparison of semi-empirical expressions of the energy spectrum of fission neutrons with experimental measurements at Los Alamos on neutrons from thermal fission of U^{235}. From [19].

two fitted curves shown are

$$N(E) \propto E^{\frac{1}{2}} \exp \frac{-E}{1.29} \quad , \qquad \ldots(2.1)$$

a Maxwellian distribution, and

$$N(E) \propto \exp \frac{-E}{0.965} \cdot \sinh (2.29E)^{\frac{1}{2}} \quad , \qquad \ldots(2.2)$$

the so-called 'Watt' spectrum.

N(E) is the number of fission neutrons with energy E, in the laboratory system.

Equations (2.1) and (2.2) represent the two different approaches made in fitting the measured spectrum. The assumption of a Maxwellian distribution does not have a rigorous theoretical basis: its justification lies purely in the fact that it provides a good fit to the data. The constant 1.29 in equation (2.1) is chosen to provide the best fit to the data, and is merely a parameter of the spectrum. It does not represent a nuclear temperature. The Watt spectrum is derived by assuming that the neutron emission spectrum in the centre-of-mass system (CMS) is a Maxwellian (see below). The more general form of the Watt spectrum is

$$N(E) = \exp\left(\frac{-E_f}{T}\right) \cdot (\pi E_f T)^{-\frac{1}{2}} \cdot \exp \frac{-E}{T} \cdot \sinh \left[2(E E_f)^{\frac{1}{2}}/T\right] \qquad \ldots(2.3)$$

where E_f is the energy of a neutron having the velocity of the fragment and T is a spectrum parameter.* For the Maxwellian distribution, the average energy $\bar{E}$, and the most probable energy E_p are given by

---

*The Watt distribution includes the Maxwellian as a special case, viz the case $E_f = 0$

$$\bar{E} = \frac{3T}{2} \qquad \ldots(2.4)$$

and $$E_p = \frac{T}{2} = \frac{\bar{E}}{3} \qquad \ldots(2.5)$$

(T is the Maxwellian spectrum parameter)

For the Watt spectrum[20]

$$\bar{E} = E_f + \frac{3T}{2} \qquad \ldots(2.6)$$

and $$\tanh(2E_p^{\frac{1}{2}} E_f^{\frac{1}{2}}/T) = 2(E_p E_f)^{\frac{1}{2}}/(E_p + E_f) \qquad \ldots(2.7)$$

For most nuclides, E_p lies in the range 0.6 to 0.7 MeV, with $1.8 < \bar{E} \lesssim 2.1$ MeV. The neutron intensity varies as $E^{\frac{1}{2}}$ at low energies and exponentially at high energies.

Derivation of Energy Spectrum Formulae

The major difficulty in deriving an expression for the neutron energy spectrum in the laboratory system is that the energy spectrum in the CMS is not known with certainty. If it is assumed that the neutrons are all emitted from the fragments after they (the fragments) have reached their peak velocities, and also that the neutron emission is isotropic in the CMS, then

$$\bar{E} = \bar{E}_f + \bar{E}_{CM} \quad . \qquad \ldots(2.8)$$

$\bar{E}$ and E_f are as defined above (2.3) and (2.4) and $\bar{E}_{CM}$ is the average centre-of-mass neutron energy. Following Feather[21], isotropic emission results in a uniform distribution of energies in the labroatory system,

$$N(E) = (E_f E_{CM})^{-\frac{1}{2}} \qquad \text{for } (E_{CM}^{\frac{1}{2}} - E_f^{\frac{1}{2}})^2 < E < (E_{CM}^{\frac{1}{2}} + E_f^{\frac{1}{2}})^2 \qquad \ldots(2.9)$$

and $N(E) = 0$ elsewhere ...(2.10)

If the CMS energy distribution is $\phi(E_{CM})$, then for a given E_f,

$$N(E) = \int_{(E - E_f)^2}^{(E^{\frac{1}{2}}+E_f^{\frac{1}{2}})^2} \frac{\phi(E_{CM})\, dE_{CM}}{4(E_f\, E_{CM})^{\frac{1}{2}}} \qquad ...(2.11)$$

The form of the $\phi(E_{CM})$ in equation (2.11) now determines the final expression for N(E). Feather assumed an emission spectrum of the form

$$\phi(E_{CM}) = (E_{CM}/T^2)\, \exp(-E_{CM}/T) \qquad ...(2.12)$$

where T is the nuclear temperature of a fragment.*

This is simply the neutron 'evaporation' spectrum predicted by Weisskopf's statistical model of the nucleus[22]. It was thought that the highly excited fission fragments should be appropriate systems for the application of this model.

Combining equations (2.11) and (2.12) gives

$$N(E) = (\pi^{\frac{1}{2}}/8\, E_f^{\frac{1}{2}}\, T^{\frac{1}{2}}) \left\{F\left[(2\,E/T)^{\frac{1}{2}} + (2\,E_f/T)^{\frac{1}{2}}\right] - F\left[\left|(2\,E/T)^{\frac{1}{2}} - 2\,E_f/T)^{\frac{1}{2}}\right|\right]\right\} \qquad ...(2.13)$$

where

$$F(x) = -2x(2\pi)^{-\frac{1}{2}} \exp(-x^2/2) + (2\pi)^{-\frac{1}{2}} \int_{-x}^{x} \exp(-t^2/2)dt \qquad ...(2.14)$$

and is composed of tabulated probability functions[23].

---

*It should be emphasised that whereas the 'T' in the Maxwellian and Watt spectra is only a parameter, the 'T' in equation (2.12) does describe a nuclear temperature. It is related to the excitation energy E^* of the compound nucleus by $E^* = aT^2$, where a is a constant which increases slowly with mass.

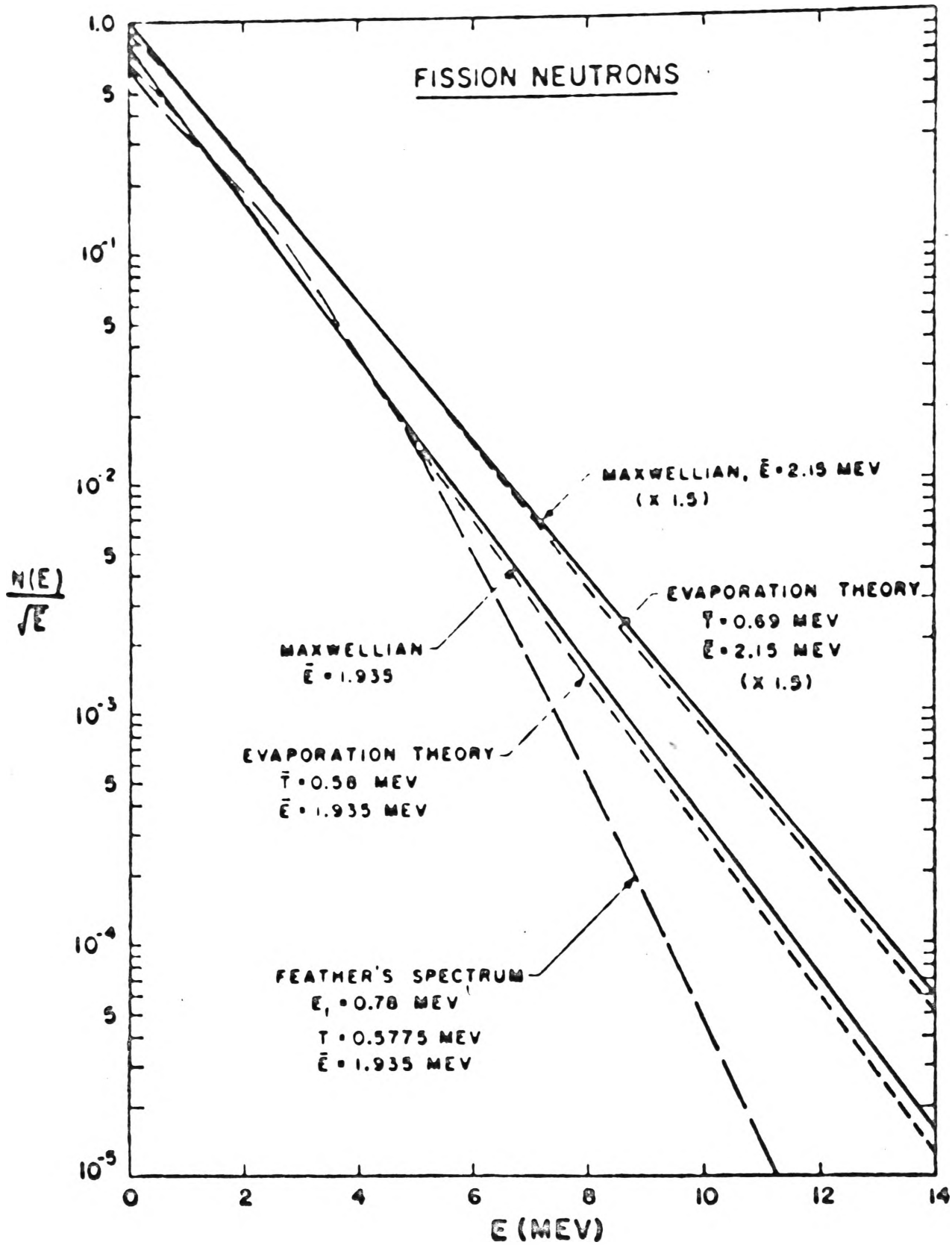

Fig 2.7 Normalized fission neutron spectra based on evaporation theory, compared with Maxwellian distributions for the same average energy. Two examples are shown, chosen to represent $U^{235}+n(\bar{E}=1.935$ Mev) and $Cf^{252}(\bar{E}=2.15$ Mev). These spectra were produced by combining a number of Feather spectra to give the expected distribution of temperature and fragment velocity. Feather's spectrum for a single temperature and fragment velocity is shown for comparison. From [20].

The average laboratory energy $\bar{E}$ and most probable energy E_p for this Feather distribution are given by

$$\bar{E} = E_f + 2T \qquad \ldots(2.15)$$

and $$\tanh(2E_p^{\frac{1}{2}} E_f^{\frac{1}{2}}/T) = (E_f/E_p)^{\frac{1}{2}} \qquad \ldots(2.16)$$

The Watt distribution (equation (3.3)) may be obtained in similar fashion to the above by assuming a Maxwellian form for $\phi(E_{CM})$ and substituting in equation (2.11).

Even though the Feather spectrum has the more sound theoretical derivation, it does not fit the experimental data nearly so well as do the Maxwellian and Watt spectra. Figure 2.7 compares a Feather spectrum with temperature T = 0.5775 MeV (corresponding to an average laboratory energy $\bar{E}$ of 1.935 MeV, i.e. the case of ^{235}U plus thermal neutrons) with a Maxwellian distribution of the same average energy (centre curve, continuous line). The agreement is poor, particularly for $E \gtrsim 5$ MeV.

In the above (equations (2.12) through (2.16)) T is assumed single-valued. A significant improvement to the theory can be made by taking into account the fact that the second and subsequent neutrons will be emitted from a less-excited nucleus, corresponding to a lower nuclear temperature. It has been shown[17,24] that even a simple combination of two evaporation components with different values of T can produce good agreement with the neutron spectra in the laboratory system. Terrel[20] performed a more complete analysis in which he weighted together fourteen Feather spectra using a separate fragment velocity for the light and heavy fragments and seven different nuclear temperatures. These

temperatures were weighted in accordance with a nuclear temperature distribution which itself was derived from the distribution of initial fragment excitation energies. This 'multi-component' Feather (or 'evaporation') spectrum is also shown in Figure 2.7, for the two cases ^{235}U plus thermal neutrons ($\bar{E}$ = 1.935 MeV, and average temperature $\bar{T}$ = 0.58 MeV) and spontaneous fission of ^{252}Cf ($\bar{E}$ = 2.15 MeV, $\bar{T}$ = 0.69 MeV). Note the close agreement in each case with the simple Maxwellian expression of the same average energy. This agreement is very convenient, in view of the simple properties of the one-parameter Maxwellian distribution[*]. The Maxwellian form is therefore commonly used in calculations involving the neutron energy spectrum.

Recent measurements, however,[25,26] of fission-spectrum-averaged values of energy-dependent cross sections have raised doubts regarding both the shape and mean energy of fission neutron spectra. They suggest, for example, that $\bar{E}$ for ^{235}U is about 2.2 MeV, rather than the 'accepted' value of about 1.95 MeV. The situation is rather unsatisfactory at present.

2.3 Multiplicity

The term neutron 'multiplicity' refers to the numbers of neutrons emitted in the fission process. In any given fission event any number of neutrons ranging from zero up to about six or seven neutrons may be emitted (higher numbers are relatively rare). The average number

---

[*] For a Maxwellian: $E_p = \bar{E}/3$, $\sigma^2(E) \equiv \langle E^2 \rangle - \bar{E}^2 = 2\bar{E}^2/3$, $\langle E^{\frac{1}{2}} \rangle = (8\bar{E}/3\pi)^{\frac{1}{2}}$, and $\langle \bar{E}^{\frac{1}{2}} \rangle = (6/\pi\bar{E})^{\frac{1}{2}}$

(average over all fission modes) emitted per fission event, $\bar{\nu}$, is an important parameter in reactor calculations. Note: $\bar{\nu}$ throughout this thesis is meant to describe the prompt neutrons emitted in fission, within about 10^{-14} secs after scission. It does not include the delayed neutrons associated with fission, which are emitted some seconds after scission. These delayed neutrons arise from fission products which, when formed in the fission chain decay scheme, have an excitation greater than their corresponding neutron binding energy. The number $\bar{\nu}$ needs to be known with a high degree of accuracy for various fissile nuclides (better than one per cent for thermal reactors). One reason for this is that estimates of the critical mass of fuel needed for a given reactor configuration are directly related to $\bar{\nu}$. Uncertainties of 2 per cent in $\bar{\nu}$ give rise to uncertainties of from 6 to 20 per cent in critical mass estimates[27].

Another reason for an accurate knowledge of $\bar{\nu}$ is the information this gives on the energy balance in fission. The energy of the fissioning compound nucleus is dissipated mainly either as kinetic energy of the two fragments or as fragment excitation energy. The excitation energy then passes primarily into prompt neutron emission, with some going into prompt gamma ray emission. $\bar{\nu}$ data is thus a valuable probe into the mechanism of the competition between the different modes of energy release.

2.3a $\bar{\nu}$ versus Energy

In this section the way in which the average number of neutrons emitted varies with the energy of the fission-inducing neutron will be treated. Discussion will be initially restricted to ^{235}U.

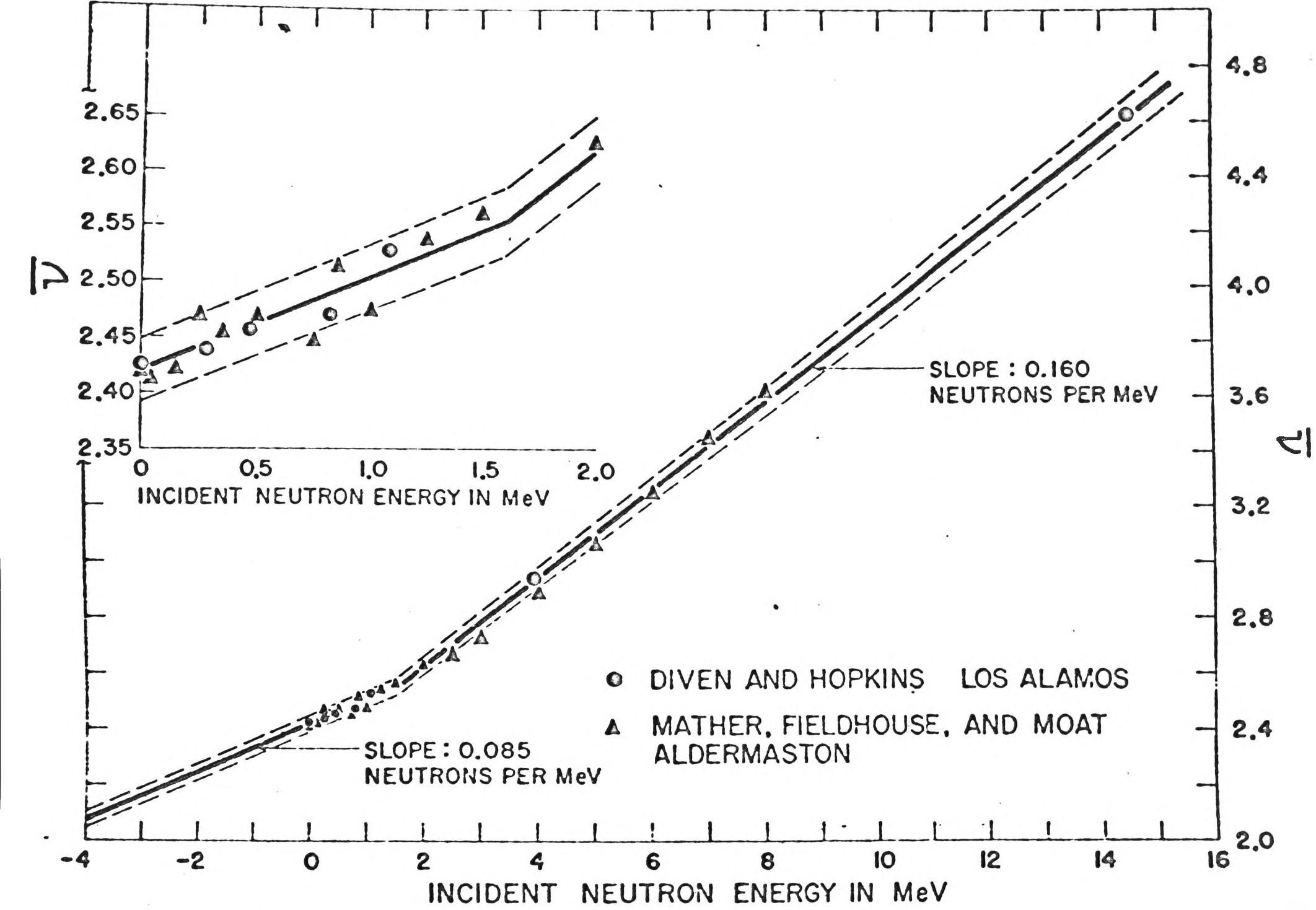

Fig 2.8 $\bar{\nu}$ versus incident neutron energy

Figure 2.8 shows results of some of the early ^{235}U work in this field: by Hopkins and Diven at Los Alamos[28] and by Mather et al. at Aldermaston[29]. Each of these groups used the large liquid scintillator tank method to count fission neutrons. It can be seen that over most of the range of incident neutron energy E_n, the $\bar{\nu}$ behaviour can be well represented by a straight line, with slope 0.16 neutrons per MeV. For $E_n \lesssim 2$ MeV the line changes slope, to 0.085 neutrons per MeV.

The value 0.16 for the slope was about that expected at first guess: the average binding energy of a neutron to a ^{235}U fission fragment is about 5 MeV, while the average kinetic energy carried away by the neutron is about 2 MeV (laboratory system). Thus for approximately every 7 MeV of added energy one would expect a neutron to be emitted from the fragment. More exactly:

$$\bar{\nu} = \frac{\bar{E}_n^{\star}}{\bar{B}_n + \bar{\epsilon}} \qquad \ldots(2.17)$$

where $\bar{B}_n$ is the average binding energy of a neutron to a fragment,

$\bar{\epsilon}$ is the average kinetic energy of an evaporated neutron in the fragment system,

and $\bar{E}_n^{\star}$ is the average fragment excitation carried off by the neutrons. $\bar{E}_n^{\star}$ is given by

$$\bar{E}_n^{\star} = \bar{E}_M + B_o + E_n - \bar{E}_K - \bar{E}_\gamma \qquad \ldots(2.18)$$

where $\bar{E}_n$ is the average energy obtained from a hypothetical spontaneous fission of the compound nucleus with zero excitation energy,

B_o is the binding energy of a neutron to the fissioning nucleus,

$\bar{E}_K$ is the average kinetic energy of the fission fragments, and

$\bar{E}_\gamma$ is the average total energy of the prompt fission gamma rays.

These averages are all made over the mass-yield distribution.

By differentiating equation (2.17) with respect to $\bar{E}_n^*$, assuming that $\bar{E}_K$ and $\bar{E}_\gamma$ are independent of E_n, and by substitution for the relevant quantities, one finds

$$\frac{d\bar{\nu}}{dE_n} = 0.14 \text{ MeV}^{-1} \qquad \ldots(2.19)$$

which is close to the 0.16 MeV^{-1} value mentioned above.

The lower slope for $\bar{\nu}$ versus E_n below 2 MeV was difficult to explain. The most likely reason was that the above assumption of constant $\bar{E}_K$ and $\bar{E}_\gamma$ was incorrect. That is, either or both of these quantities displays a dependence on E_n, between 0 and 2 MeV. For example, if $\bar{E}_K$ increased with E_n in this region, less of the energy of the compound nucleus would be available to pass into excitation energy of the fragments, that is into neutron emission. Similarly for $\bar{E}_\gamma$. However, measurements by Okolovich et al.[30] indicated that $\bar{E}_K$ was the same for both thermal and 5 MeV fission of ^{235}U to within ± 0.1 per cent. Further, Protopopov and Shiriaev[31] found no difference in the total γ emission from thermal, 2.8 and 14.7 MeV neutron induced fission of ^{235}U. It seemed some other

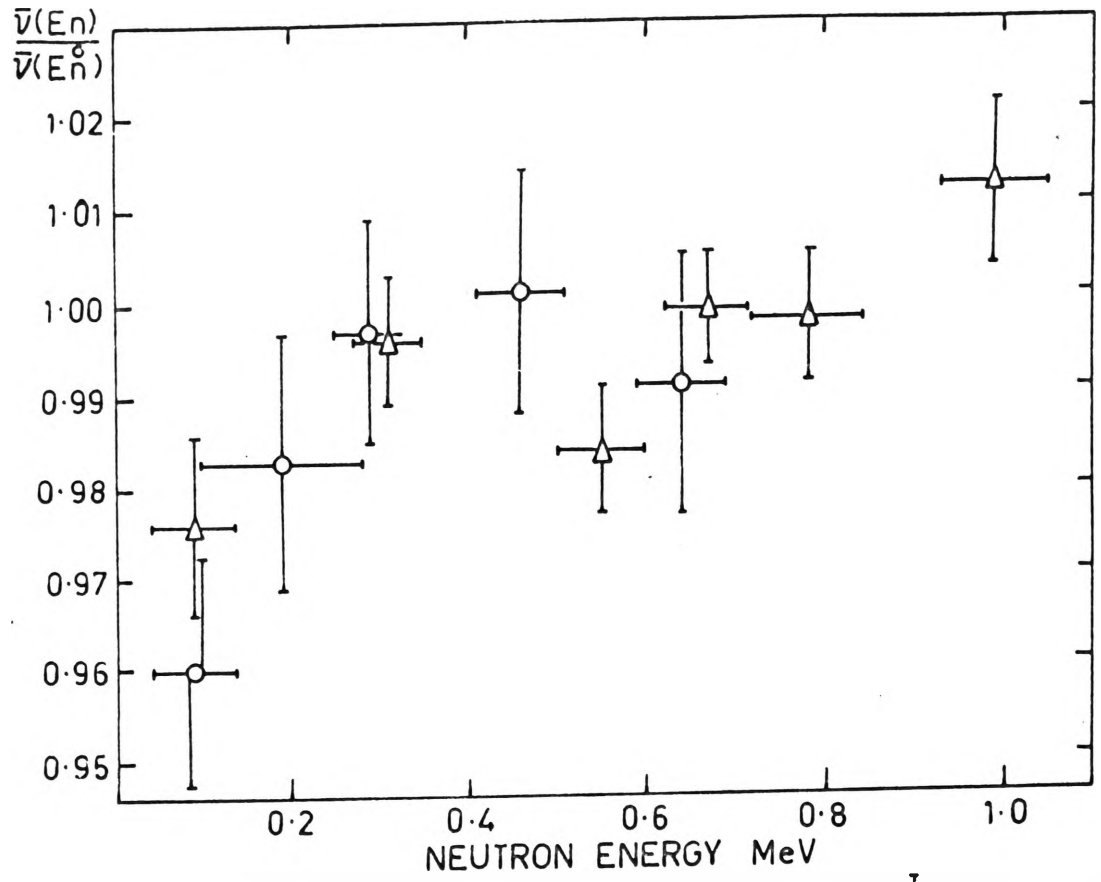

Fig 2.9 Results of the relative measurements of $\bar{\nu}(En)$. Δ designates the scintillation detector of neutrons, φ the thorium fission chamber. Obninsk results [32].

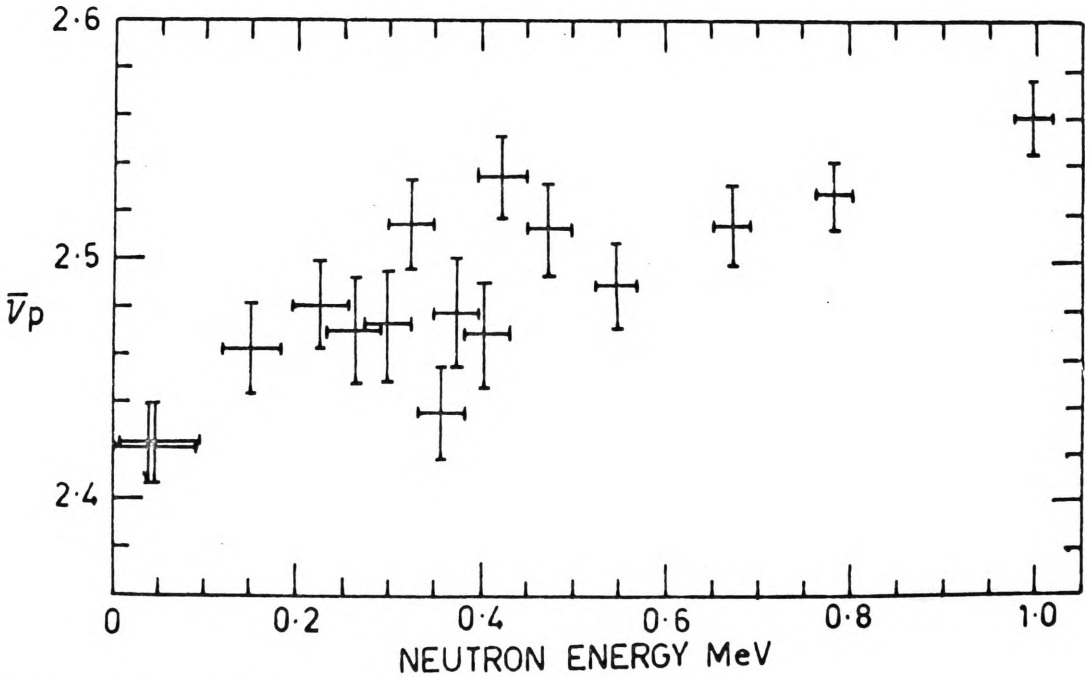

Fig 2.10 A.N.L $\bar{\nu}(En)$ results [33]

explanation was needed to explain the slope change.

The picture became even more complicated when two groups, Blyumkina et al. at Obninsk[32] and Meadows and Whalen at Argonne National Laboratory[33] reported finding fine structure in the $\bar{\nu}$ energy dependence below 1 MeV. Figures 2.9 and 2.10 show their results. Both groups observed a peak in the $\bar{\nu}(E_n)$ curve at about 400 keV incident neutron energy. The ANL group even found evidence for an associated minimum at 350 keV. Above 600 keV the curve returned to a straight line relationship, with $\frac{d\bar{\nu}}{dE_n} \sim 0.15$ neutrons MeV^{-1}. The amplitude of the fine structure was about 3 per cent in each case. As the quoted errors on the experimental points were ~1 per cent, the effect seemed a real one - not one attributable to statistical scatter.

The fine structure could be tentatively explained in terms of the Bohr model of a fissioning nucleus[34]. It is assumed that the energy of the low-lying rotational bands of the saddle point spectrum passes into a part of the fragment kinetic energy. As E_n increases, parity considerations force the fission to take place through particular bands. Knowing the band separation[35-37], the variation of $\bar{E}_K$ with E_n, and hence of $\bar{\nu}$ with E_n, could be calculated. Such calculations[32] were in good agreement with the experimental data.

In 1968-69 the candidate, in collaboration with Dr. J. W. Boldeman, examined closely the $\bar{\nu}$ behaviour below 2 MeV for ^{235}U (12, copy attached). A large liquid scintillator tank was used as the neutron detector. For full details of the experimental method see references (38) and (12). No evidence whatsoever was found of the fine structure reported by Blyumkina et al. and Meadows and Whalen. Our data are shown in Figure 2.11.

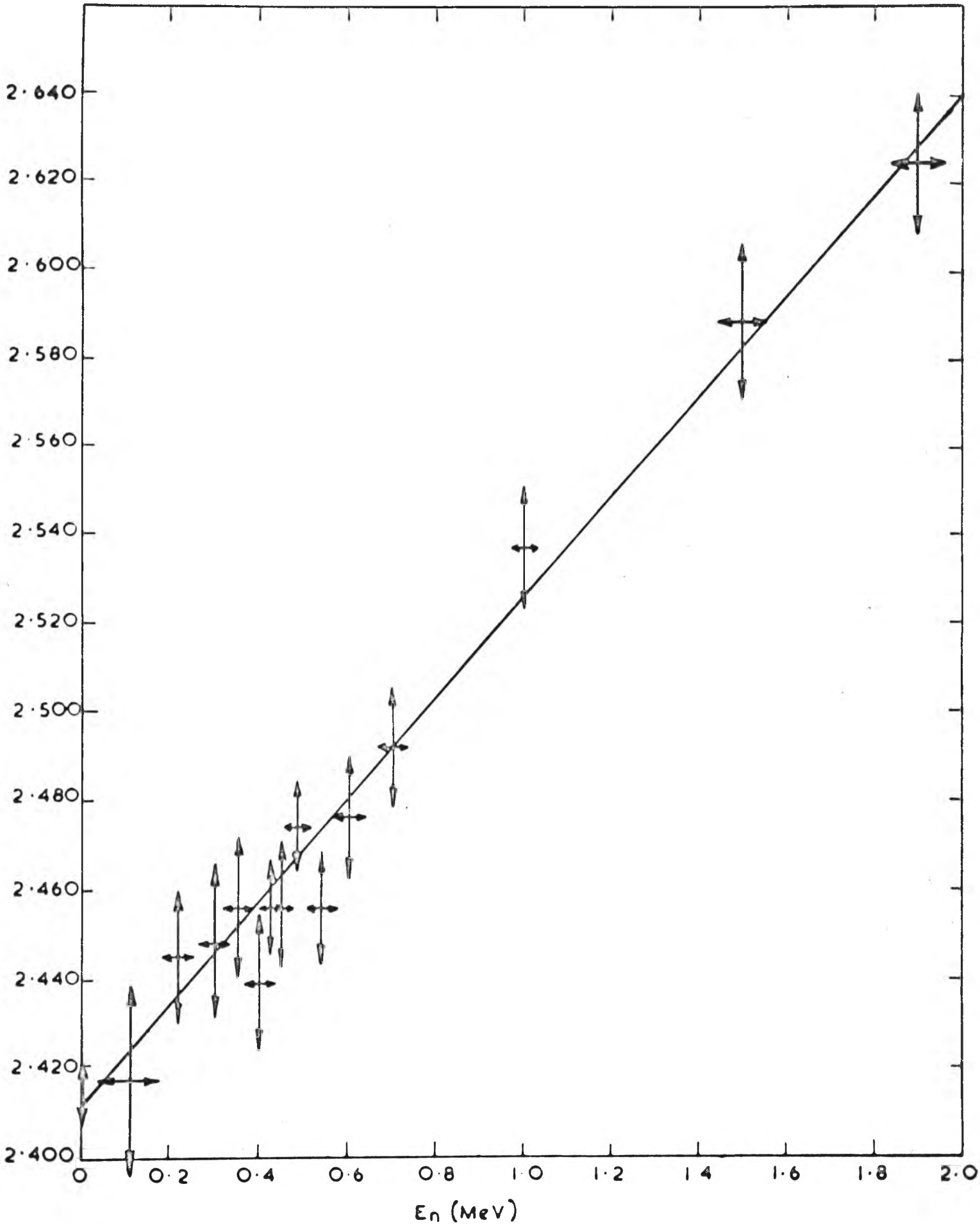

Fig 2.11 $\bar{\nu}_p$ VERSUS INCIDENT NEUTRON ENERGY (En)— BOLDEMAN & WALSH (1970). REF [12].

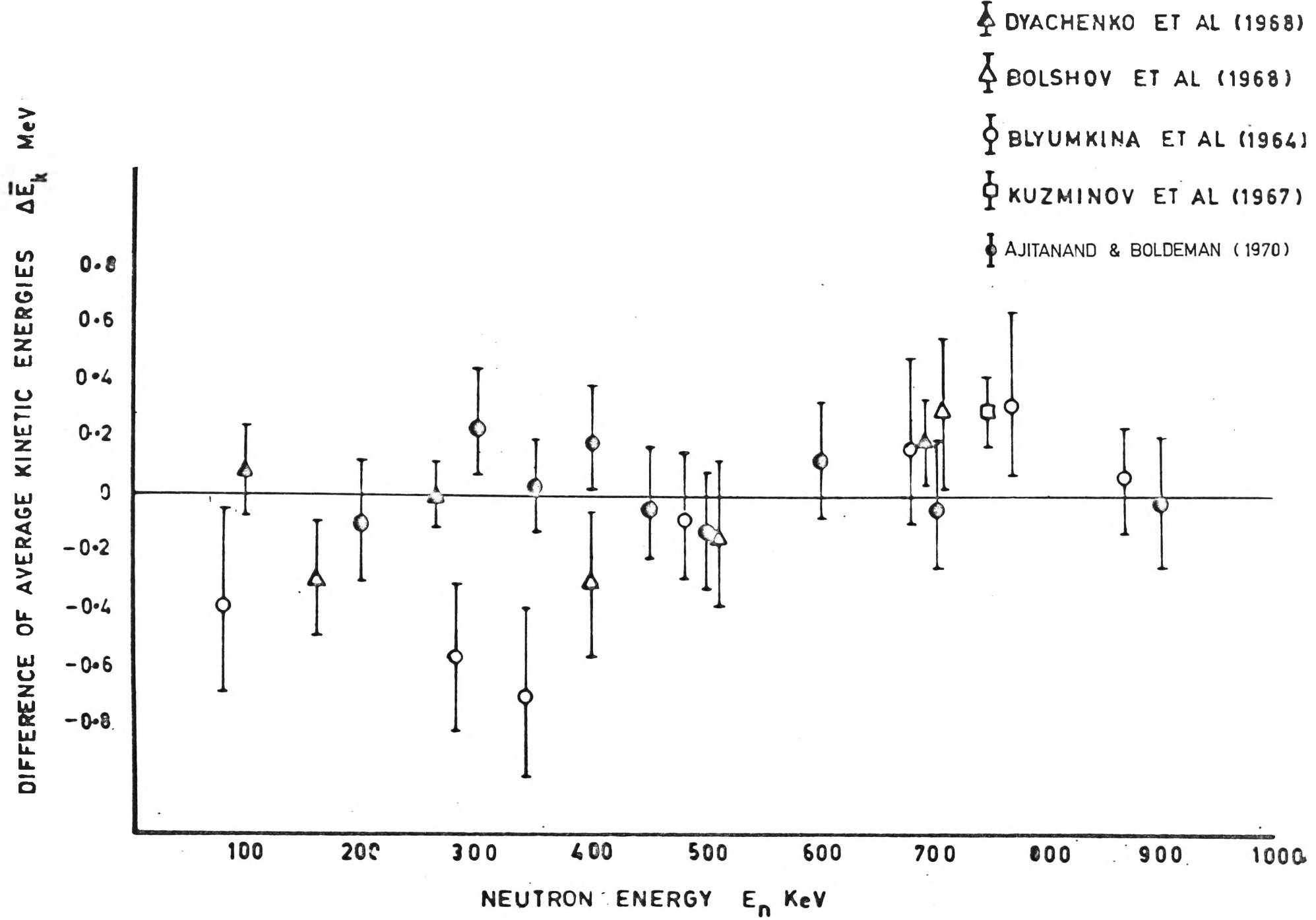

Fig 2.12 $\Delta \bar{E}_k$ versus incident neutron energy E_n : Comparison of data by different authors for U235.

The results are considerably more accurate than the other two sets, especially in the region of primary interest (300-600 keV).

As a check on our $\bar{\nu}(E_n)$ findings, the variation with E_n of the ^{235}U fragment average total kinetic energy $\bar{E}_K$ was studied at Lucas Heights by Ajitanand and Boldeman[39]. It was found that over the measured energy range ($0 < E_n < 1$ MeV) $\bar{E}_K$ is independent of E_n. Figure 2.12 shows the kinetic energy results of Ajitanand and Boldeman[39], together with the data of some other authors[32,40,41,42]. A flat $\bar{E}_K(E_n)$ dependence is in good agreement with the assertion of a linear $\bar{\nu}_p(E_n)$ relationship.

The $\bar{\nu}$ studies mentioned above allow certain conclusions to be drawn as to the interaction or coupling strength between the collective saddle point degrees of freedom and the nucleonic degrees of freedom at scission. If one assumes that the potential energy barrier in fission is single-humped, as was generally accepted to be the case up to the mid-1960's then the Boldeman and Walsh[12] conclusion of no fine structure implies that the saddle to scission coupling must be strong. That is, the distribution of the available energy at the saddle point is not preserved in the passage to scission, but passes wholly into fragment excitation energy. However, the more recent description of the fission potential barrier by Strutinsky[43,44] results in rather different coupling strength conclusions. The Strutinsky 'double-humped' potential barrier is shown in Figure 2.13. With each barrier there are associated collective levels of the A. Bohr type. The higher of the two barriers corresponds to the (d,pf) fission threshold of Northrop et al.[35] For the ^{236}U compound nucleus, it is not at present known with certainty

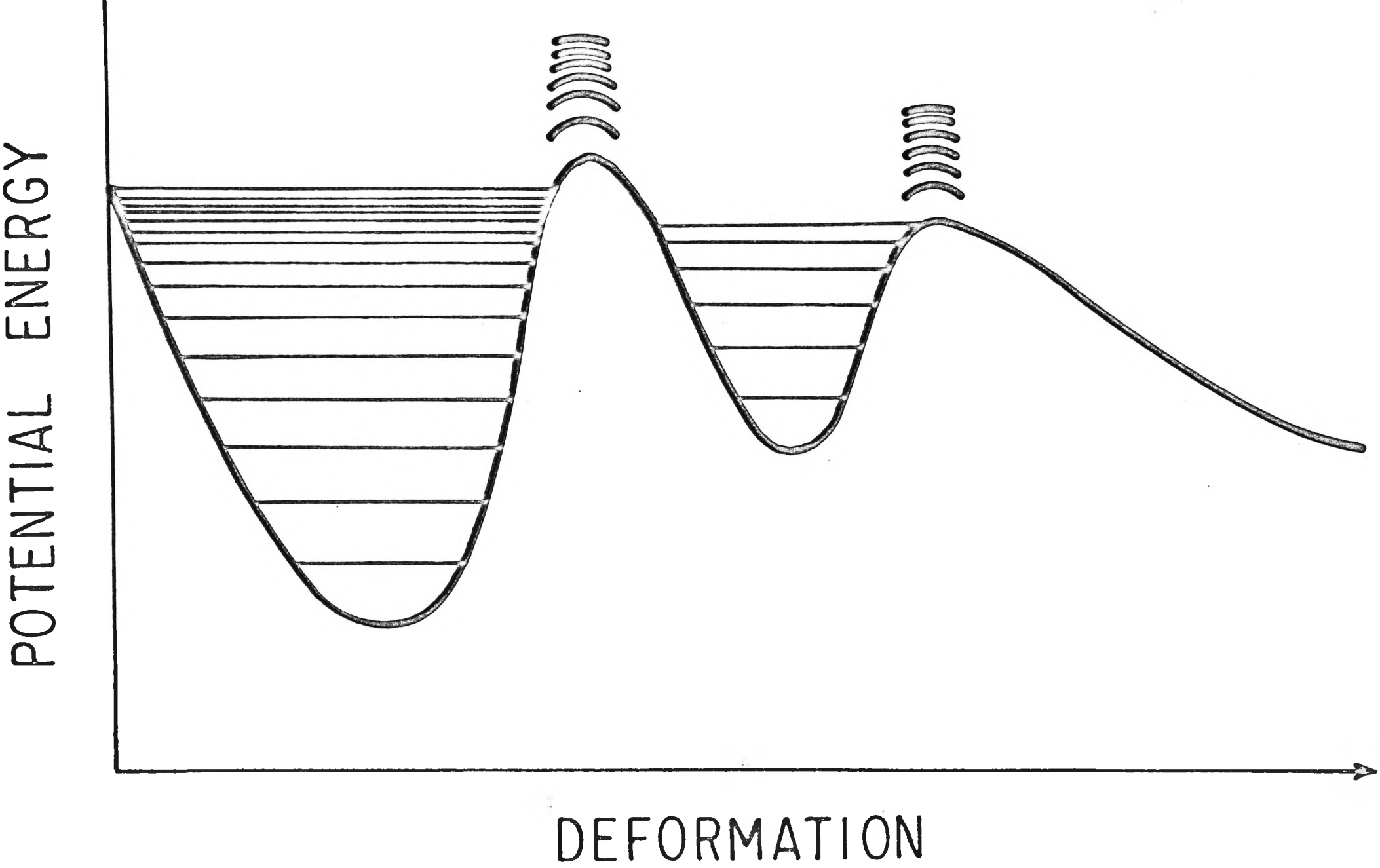

Fig 2.13 THE DOUBLE HUMPED BARRIER IN THE DEFORMATION ENERGY OF A HEAVY NUCLEUS (SCHEMATIC) FROM [43].

which barrier is the higher. If the second barrier is higher for ^{236}U then it may be concluded that the saddle to scission coupling is strong, as in the single-humped barrier case. However, if the second barrier is lower than the first, then for a particular entry channel at the first, a large number of channels may be available at the second. This could result in an averaging out of any effects arising from the discrete nature of the collective channels available at the first barrier. No clear-cut indication of the coupling strength would exist. Fine structure could be absent, and yet the coupling could still be weak.

Further $\bar{\nu}$ versus energy studies have been made by Boldeman and Walsh on ^{233}U and on ^{239}Pu[13,15] (copies attached). No fine structure was observed for either ^{233}U or ^{239}Pu. The authors came to the conclusion that for all three nuclides, the saddle to scission coupling is weak. They suggested that in the cases of ^{235}U and ^{239}Pu, the weak coupling does not produce any fine structure effects simply because barrier B (second barrier) for these two is lower than barrier A. For ^{233}U, which probably has barrier B higher than A and therefore should show up some fine structure, it was pointed out that the first ^{233}U fission threshold lies 1.5 MeV below the binding energy of the incoming neutron. Thus, in the region of excitation energy corresponding to neutron induced fission, a number of different K bands, each with its own set of I (total spin) levels, would be expected (e.g. K = 1 bending mode band, K = 2 γ vibration band[45]). This would serve to smear out the fine structure effects which one would expect if only two K bands were present at the first barrier.

Basic to the above argument is the idea that in passing from neutron fission of ^{233}U to neutron fission of ^{235}U and ^{239}Pu, barrier B drops from the higher to the lower of the two barriers. Evidence for this fact lies in the fission fragment angular anisotropy studies of a number of authors (see 46). These studies showed a marked change in anisotropy between compound nuclei A = 234 and A = 240. This change can be attributed to a shift in barrier heights, B becoming lower than A.

At the present time, the existence of fine structure in the $\bar{\nu}$-E_n curve is still a matter of some disagreement.

However, the phenomenon of a change in slope in the curve, as shown in Figure 2.8, has been fairly well established for ^{235}U and ^{233}U(12,13). Below the pairing gap energy[A], de-excitation by gamma emission competes with neutron emission for the available energy of the saddle point nucleus; that is the average total gamma energy increases slightly with E_n. The gamma competition is weaker, the more unpaired nucleons present in the compound nucleus(48). Therefore at the pairing gap the gamma competition decreases, perhaps vanishing altogether(49). This results in a sudden increase in the neutron emission at the pairing gap, and shows up as a change in the $\bar{\nu}$-E_n slope.

2.3b Distribution of Neutron Emission Numbers

As well as the mean number of fission neutrons emitted by a particular nuclide, the distribution of neutron numbers around this mean is of importance. From equation (2.18) above, for a given mass

---

[A] The energy above threshold needed to induce single-particle transitions in the saddle point nucleus(47).

ratio the distribution of fragment excitation energy (σ_{E_x}) around the mean value $\bar{E}_x$ is equal to the distribution of fragment kinetic energy (σ_{E_K}) around the mean $\bar{E}_K$. As the excitation energy passes mainly into neutron emission, measurements of the width of the neutron number distribution should give results in close agreement with those of the kinetic energy studies. Another important reason for measuring neutron number widths is the information that may be gained on the correlation between the excitation energies of the light and heavy fragment of a given split. As discussed in Chapter 1, if

$$\sigma^2_{E_x} = \sigma^2_{E_{xL}} + \sigma^2_{E_{xH}} \qquad \ldots(2.20)$$

that is if

$$\sigma^2_{\nu_{TOTAL}} = \sigma^2_{\nu L} + \sigma^2_{\nu H} \quad , \qquad \ldots(2.21)$$

then the two fragment excitations are independent. The procedure here entails determining the neutron emission width for each fragment group, i.e. light and heavy.

A number of $\bar{\nu}$ studies have included a measurement of the P_ν distribution[50,51,38]. P_ν is the probability of emission of an integral number, ν, of neutrons per fission. In the case of the liquid scintillator experiment of Boldeman and Dalton[38], the P_ν determinations were made by including in the neutron counting system a 'multiple event counter'. For each particular fission event, this unit stored the number of neutrons detected in both the counting gate and in the background gate. The P_ν values are given by

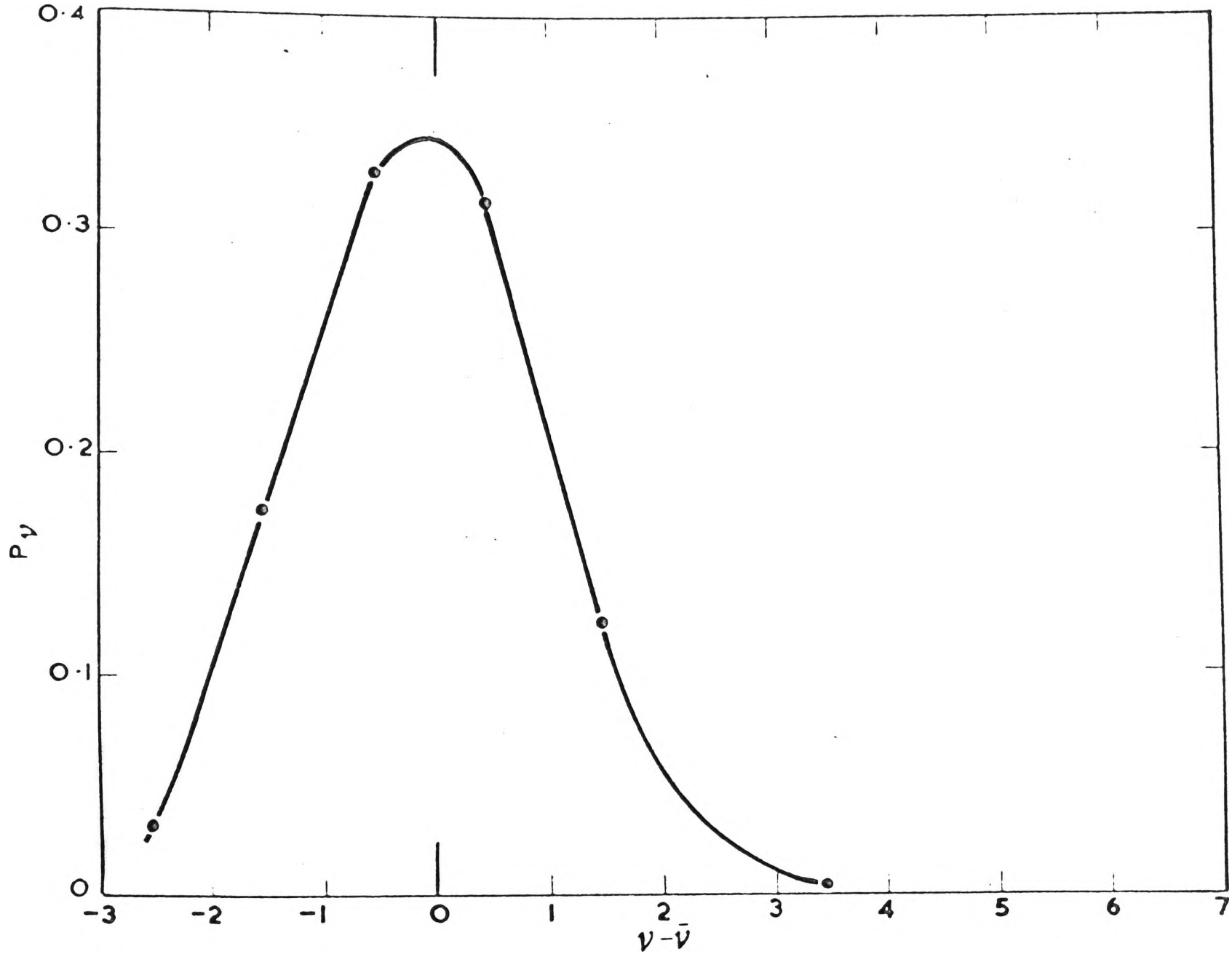

Fig 2.14 NEUTRON EMISSION PROBABILITY DISTRIBUTION FOR U235

From [38]

$$P_\nu = \sum_{x=\nu}^{x=10} \frac{x!}{\nu!(x-\nu)!} \left(1 - \frac{1}{\varepsilon}\right)^{x-\nu} \left(\frac{1}{\varepsilon}\right)^{\nu} D_x \qquad \ldots(2.22)$$

where D_x = experimentally determined probabilities of observing x neutrons per fission

ε = neutron detection efficiency of the scintillator.

Equation (2.22) is due to Diven et al.[50] Figure 2.14 shows the P_ν distributions measured in this experiment for ^{235}U.

The continuous curve shown in Figure 2.14 is drawn 'by eye'. It is close to a Gaussian, which is to be expected since the fragment total kinetic energy distribution is Gaussian in shape[52]. The standard deviation, σ, of the ^{235}U neutron number distribution is about 1.1. From Terrel[53], if the average fragment excitation energy change caused by the emission of one neutron is E_o, then the RMS width of the excitation energy distribution must be σE_o. For $E_o \sim 10$ MeV (see section 3.2) this gives an RMS width of ~11 MeV, corresponding to a FWHM of ~26 MeV. This value agrees well with recent results for the ^{235}U total kinetic energy FWHM of 27 MeV[54] and ~26 MeV[55].

Terrel[53], Leachman[56] and Gordon and Aras[57] have attempted to calculate theoretically the P_ν shape. The Gordon and Aras treatment is the more recent and important and will be discussed here. Their procedure was to calculate the total energy release E_T for a particular mass and charge split by the equation

$$E_T = \Delta M(^{236}U^{*}) - (\Delta M_L + \Delta M_H) \qquad ...(2.23)$$

The mass excesses ΔM for the excited ^{236}U compound nucleus and for the light and heavy fragments are calculated from Seeger's semi-empirical mass formula[58]. If $\bar{E}_K$ is assumed independent of the charge split $\left(\frac{Z_L}{Z_H}\right)$ for a particular mass split $\left(\frac{A_L}{A_H}\right)$, then the excitation energy E_x is given by

$$E_x = E_T - E_K\left(\frac{A_L}{A_H}\right) \qquad ...(2.24)$$

The kinetic energy values are taken from experiment. Equation (2.24) requires the excitation energy distribution to be the same as the kinetic energy distribution, i.e.

$$\sigma_{E_x} = \sigma_{E_K} \qquad ...(2.25)$$

It was further assumed that the light and heavy fragment excitation energies are uncorrelated

$$\sigma^2_{E_{xL}} + \sigma^2_{E_{xH}} = \sigma^2_{E_x} \qquad ...(2.26)$$

and that

$$\frac{\sigma^2_{E_{xL}}}{\sigma^2_{E_{xH}}} = \frac{\bar{E}_{xL}}{\bar{E}_{xH}} \qquad ...(2.27)$$

$\frac{\bar{E}_{xL}}{\bar{E}_{xH}}$ was left a free parameter in the calculations, being allowed to vary until the correct ratio was obtained for $\frac{\nu_L}{\nu_H}$.

After selecting, in line with the above, an excitation energy for a given primary fragment, de-excitation of the fragment by the emission of neutrons and γ-rays was determined by a Monte Carlo method. Finally, the results were averaged over the excitation energy distribution and over the fragment mass yield. Whereas nearly all aspects of the calculation agreed well with experiment (e.g. total γ-ray energy release) the calculated σ_ν value of 1.39 was considerably larger than the ^{235}U value of 1.112 ± 0.004. To resolve this important discrepancy, the authors considered the effect of assuming either positive or negative correlation between the light and heavy fragment excitation energies. No improvement was obtained. Gordon and Aras concluded that the next most obvious method of reducing the calculated σ_ν value was by relaxing the assumption implied by equation (2.24), that is by allowing $\bar{E}_K$ to vary with $\left(\frac{Z_L}{Z_H}\right)$ for a given $\left(\frac{A_L}{A_H}\right)$. However, recent experimental data of Glendenin et al.[59] found $\bar{E}_K$ to be independent of the charge division. At present this anomaly in the calculated and measured neutron emission widths remains unresolved.

CHAPTER 3

NEUTRON EMISSION FROM INDIVIDUAL FRAGMENTS

The previous chapter was concerned with properties of the fission neutrons which were average properties - averaged over the entire range of fragment mass, charge and kinetic energy. The important conclusions drawn from the average data were:

(a) the majority of the neutrons are emitted from the fragments after they have separated and after they have reached their terminal velocities;

(b) the neutrons are emitted by an evaporation process, best described by a number of nuclear temperatures.

The discussion now turns to the situation where the neutrons can be identified with the particular fragment which emitted them.

3.1 ν Versus Mass

3.1a Experimental Studies

The first experiment in which the prompt fission neutrons were identified with a fragment of given mass was that of Fraser and Milton at Chalk River in 1954[60]. They studied the thermal neutron fission of ^{233}U. An earlier study by Fraser[17] on the angular distribution of fission neutrons found that on average the light fragment group emitted 30 per cent more neutrons than the heavy fragment group. The Fraser and Milton (1954) study was designed to examine this interesting result more closely. Their fission chamber was a double back-to-back grid ionisation chamber, containing the ^{233}U. The amplitude of a pulse from one side of the chamber is proportional to the ionisation energy of the fragment initiating it. The fission neutrons were detected in methane filled, knock-on-proton cylindrical ionisation chambers.

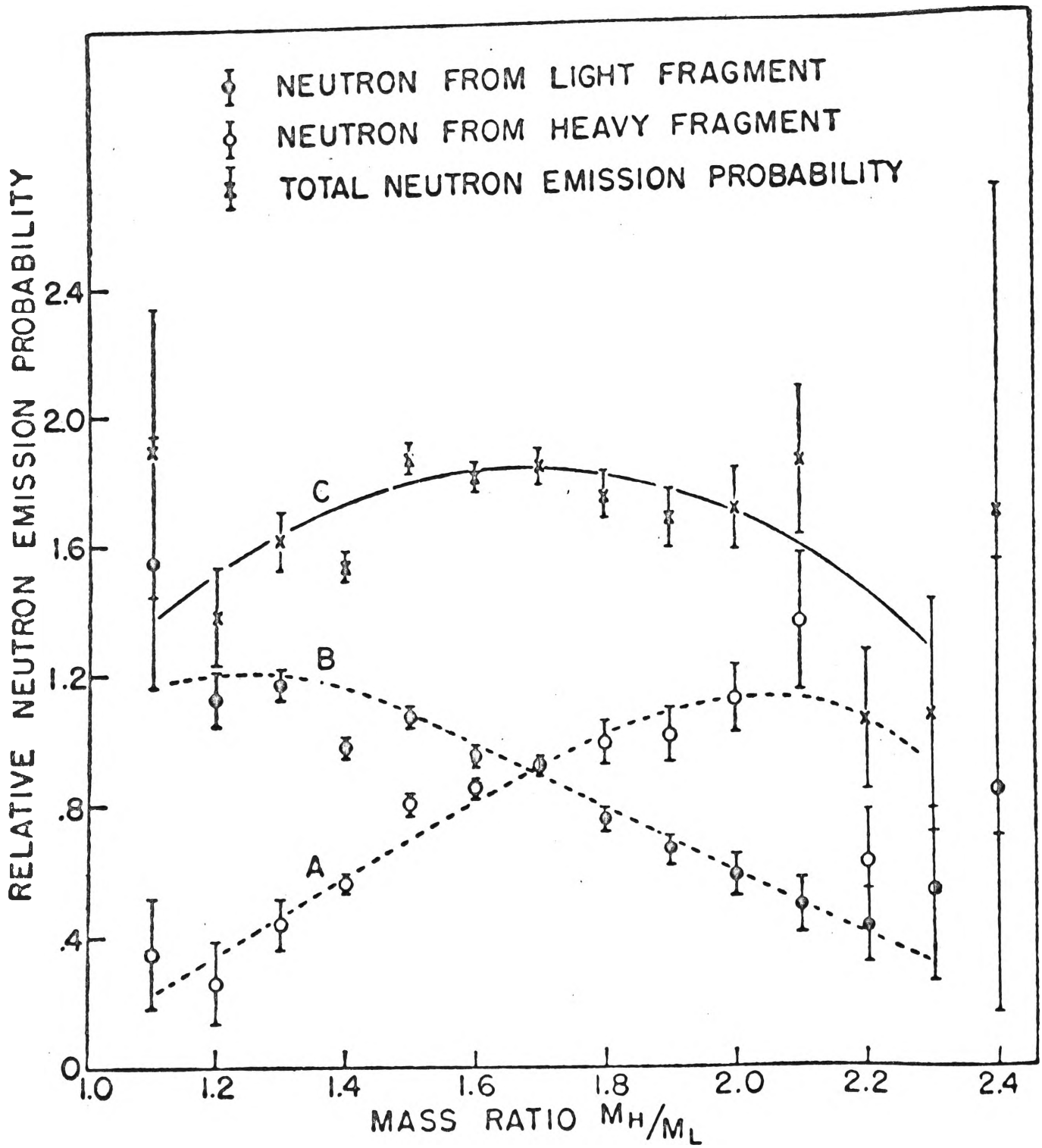

Fig 3.1a Relative neutron emission probability as a function of mass ratio for the light and heavy fragments. From [60]

The strong peaking of the neutrons in the direction of motion of the fragment (discussed in section 2.1) enabled identification of the emitting fragments. The ratio of the two fragment ionisation energies in the fission chamber is approximately proportional to the mass ratio of the fragments. Data were only recorded when a triple coincidence between two fragments and a prompt neutron was established.

The outstanding result of this experiment was that the neutrons were found to be emitted predominantly by the heaviest light fragments and by the heaviest heavy fragments. Figure 3.1a shows the neutron emission versus mass ratio curves presented by the experimenters[60] while Figure 3.1b shows an alternative presentation[61] of the same data superimposed on the ^{233}U mass yield distribution. There is an apparent discontinuity near symmetry between the ν_L and ν_H curves of Figure 3.1b. (ν_L describes neutron emission from the light fragment group, ν_H from the heavy fragment group.) Also the individual ν_L and ν_H curves have a considerable slope through each mass peak, while the total neutron yield $\nu(= \nu_L + \nu_H)$ is approximately constant. These surprising results met with some scepticism at first. A major reason for this was uncertainty in the neutron detection efficiency correction. The ionisation chamber neutron detectors were strongly energy dependent in efficiency. Furthermore, the neutron counting efficiency depended strongly on the angular correlation of the neutrons with fragment direction, an effect which varies with fragment mass and which is very sensitive to the precise form of the centre-of-mass emission spectrum chosen. Also the counting efficiency of the neutron detectors was low, of the order of a few per cent.

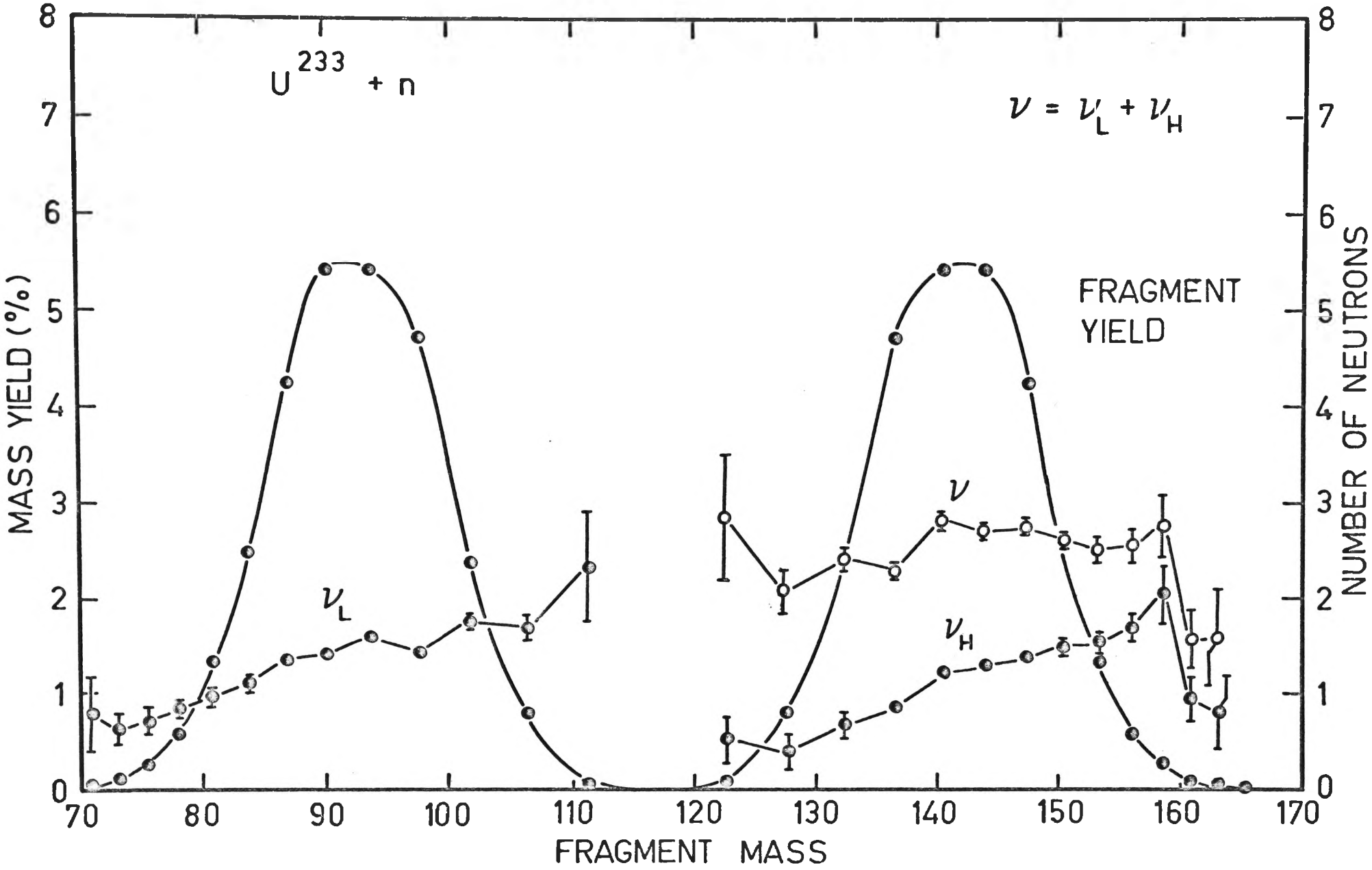

Fig 3.1b Neutron and mass yields for fission of U^{233} + n (data of Fraser and Milton, uncorrected). From [61].

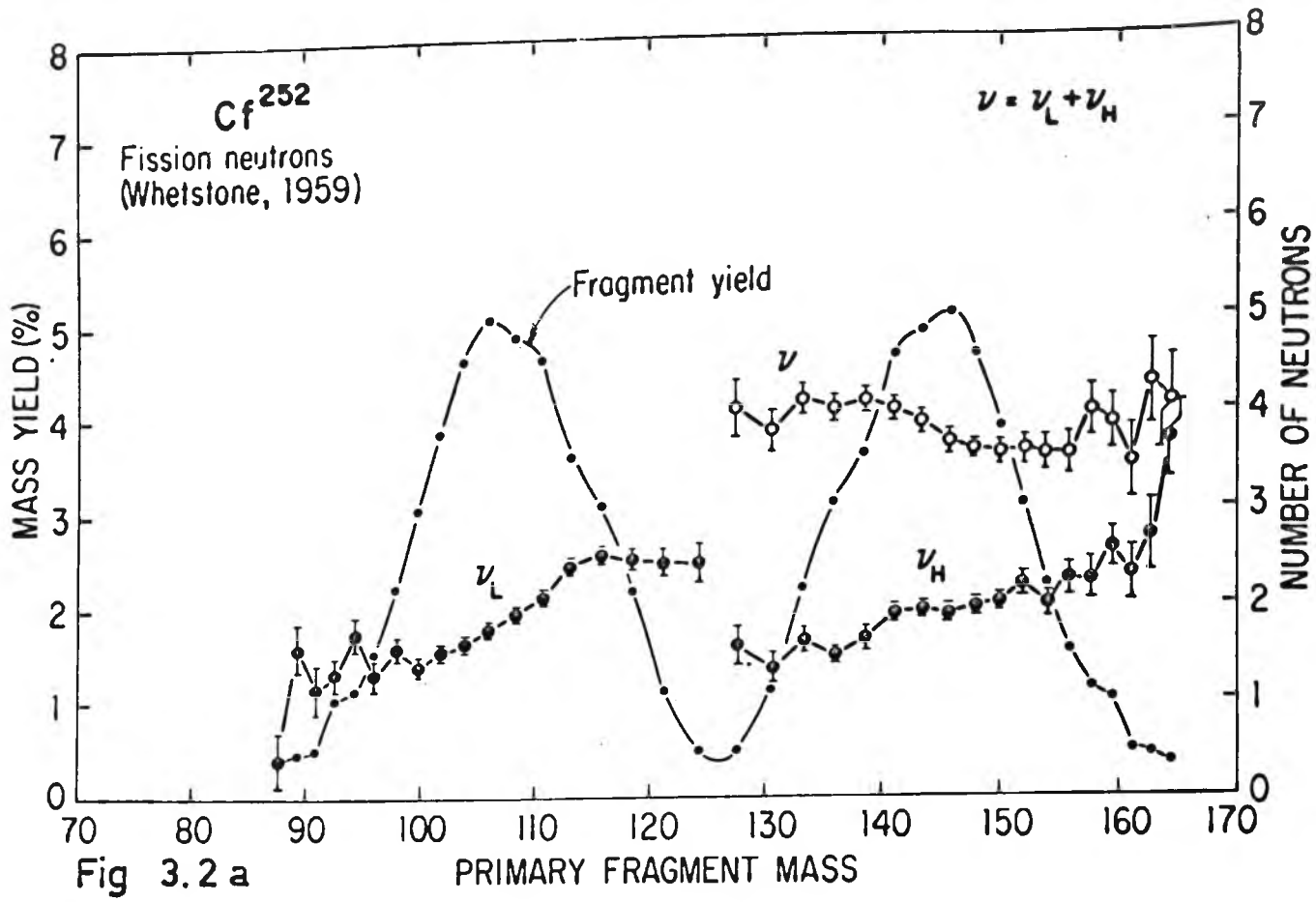

Fig 3.2 a

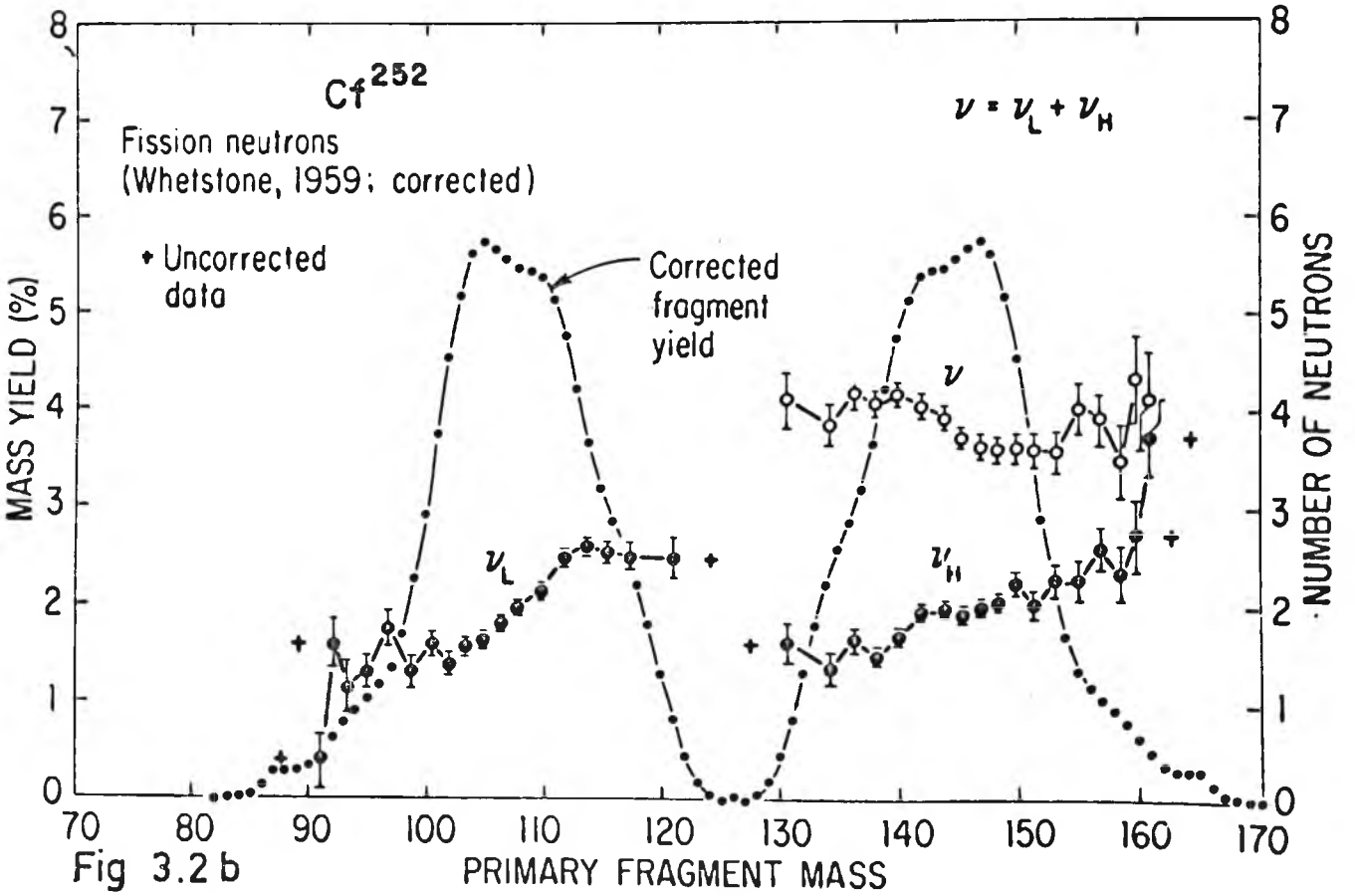

Fig 3.2 b

Fig 3.2 a,b WHETSTONE's data on the average number of neutrons per fragment in Cf^{252} as a function of the fragment mass. Standard deviations are shown for neutron yields. The prompt mass yields are also shown. The upper curve shows uncorrected data; the lower shows data after corrections of TERRELL for mass dispersion and dispersion shift of neutron data points. A few uncorrected points are shown as crosses. From [62].

However, in 1959, the above result was verified by Whetstone[62] who found a similar 'sawtooth' shape for the $\nu(A)$ curve, in this case for the spontaneous fission of ^{252}Cf. Whetstone's experimental technique was superior to that of Fraser and Milton[60]. He used a large liquid scintillator tank as neutron detector. The flat response of the liquid scintillator to neutrons of different energies resulted in neutron data of higher accuracy. The energies of the two fission fragments were determined by the time-of-flight technique, which enabled higher mass resolution (5 mass units (FWHM) compared with probably about 8 to 10 mass units for Fraser and Milton[60]). Whetstone's results are presented in Figure 3.2a.

Terrel[61] has pointed out that the $\nu(A)$ results of Fraser and Milton[60] and Whetstone[62] need a considerable 'dispersion shift' correction. This dispersion shift arises from inadequate mass resolution which has the effect of flattening and broadening each of the two segments (ν_L and ν_H). The dispersion shift correction amounts to as much as 3 or 4 mass units for $\nu(A)$ points on the extreme edges of the mass yield peaks. The effect of applying this correction is to make the $\nu(A)$ discontinuity less pronounced. In the case of Whetstone's data[62], the discontinuity reduces from one neutron unit at a mass number corresponding to symmetric fission, to one neutron unit spread over about 6 to 8 mass units. Figure 3.2b shows Whetstone's data after dispersion shift correction.

During the last decade, a considerable number of experiments have definitely established the existence of the sawtooth $\nu(A)$ curve for a number of nuclides[55,63-66]. Within the general $\nu(A)$ shape, however,

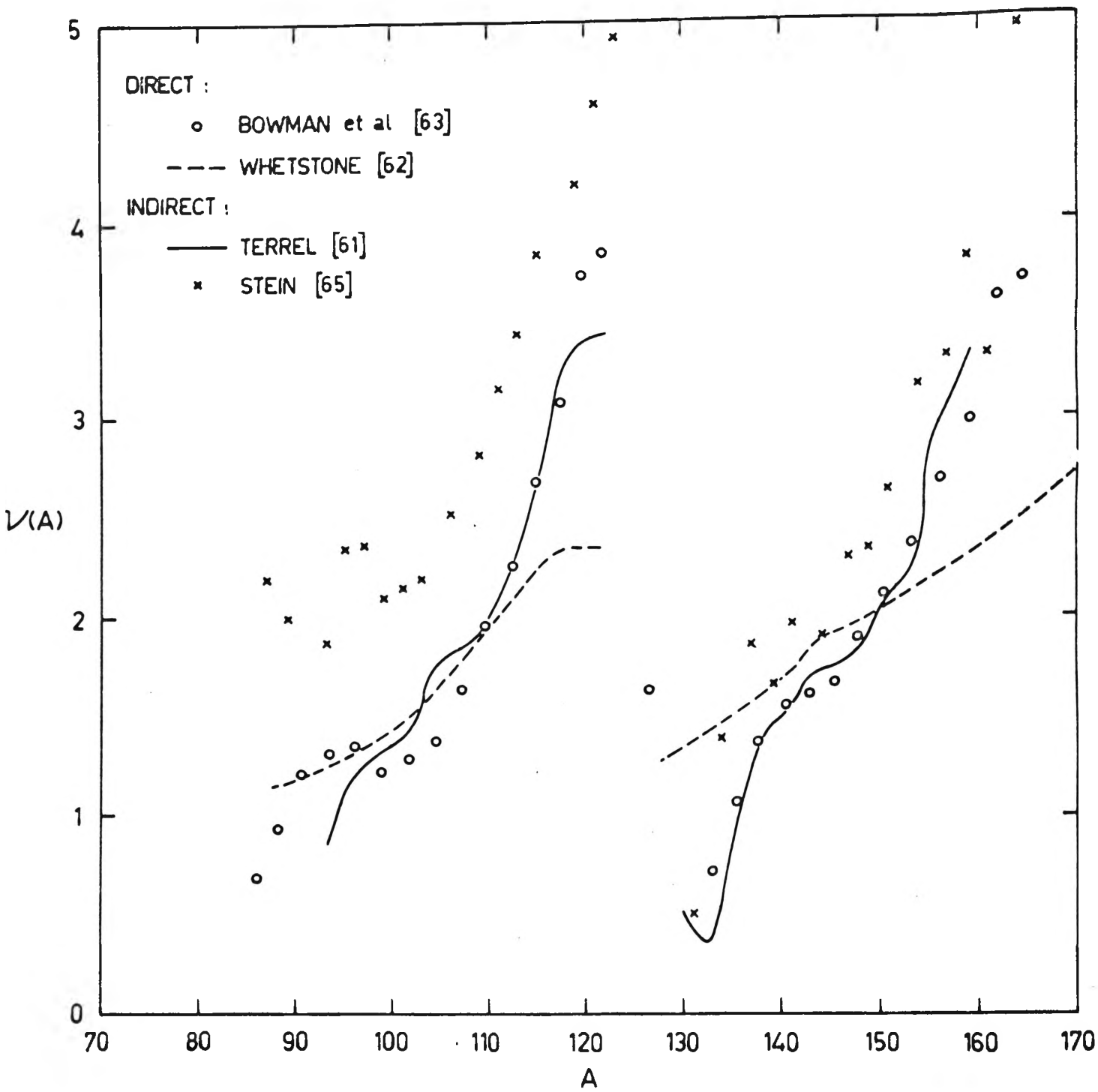

Fig 3.3 Neutron emission versus fragment mass - direct and indirect data.

there are discrepancies between different sets of data. For example, for the case of ^{252}Cf spontaneous fission, the results of Bowman et al. (1963)[63] and the indirect results of Stein (1965)[65] are in considerable disagreement in places, with the earlier result of Whetstone[62]. These three data sets are shown in Figure 3.3. It is clear that the later experiments show a much more rapid variation with mass than the earlier experiment. Also the data of (63) and (65) imply a levelling off of $\nu(A)$ in the region of the most probable mass yields, with Bowman et al. even claiming a statistically significant peak at about mass 95. Thirdly, (63) found a $\frac{\nu_L}{\nu_H}$ ratio of 1.17 ± 0.03, while Whetstone reported a value of 1.02 ± 0.02. Figure 3.3 also shows up a discrepancy between the Bowman et al. results and the Stein results. While they follow the same general shape as the former, the Stein data lie consistently higher, except for the heavy fragment region A = 135-145. Also given in Figure 3.3 is the ^{252}Cf $\nu(A)$ curve of Terrel (1962)[61], determined by an indirect method (see below). Clearly the Terrel data agrees well with the data of Bowman et al., not so well with the data of Stein, and poorly with the data of Whetstone.

Thermal neutron fission of ^{235}U is another example where the $\nu(A)$ data sets differ. Figure 3.4 shows some recent experimental results [55,64,66,14]. The heavy fragment $\nu(A)$ peak of Apalin et al.[64] is some 70 per cent higher than the trend of the other three measurements. Similarly, the light fragment $\nu(A)$ peaks of both Apalin et al.[64] and of Milton and Fraser[66] are about 50 per cent higher than the corresponding peaks of references (55) and (14). Milton and Fraser found significant fine structure peaks at masses 90, 96 and 101, which correlate with

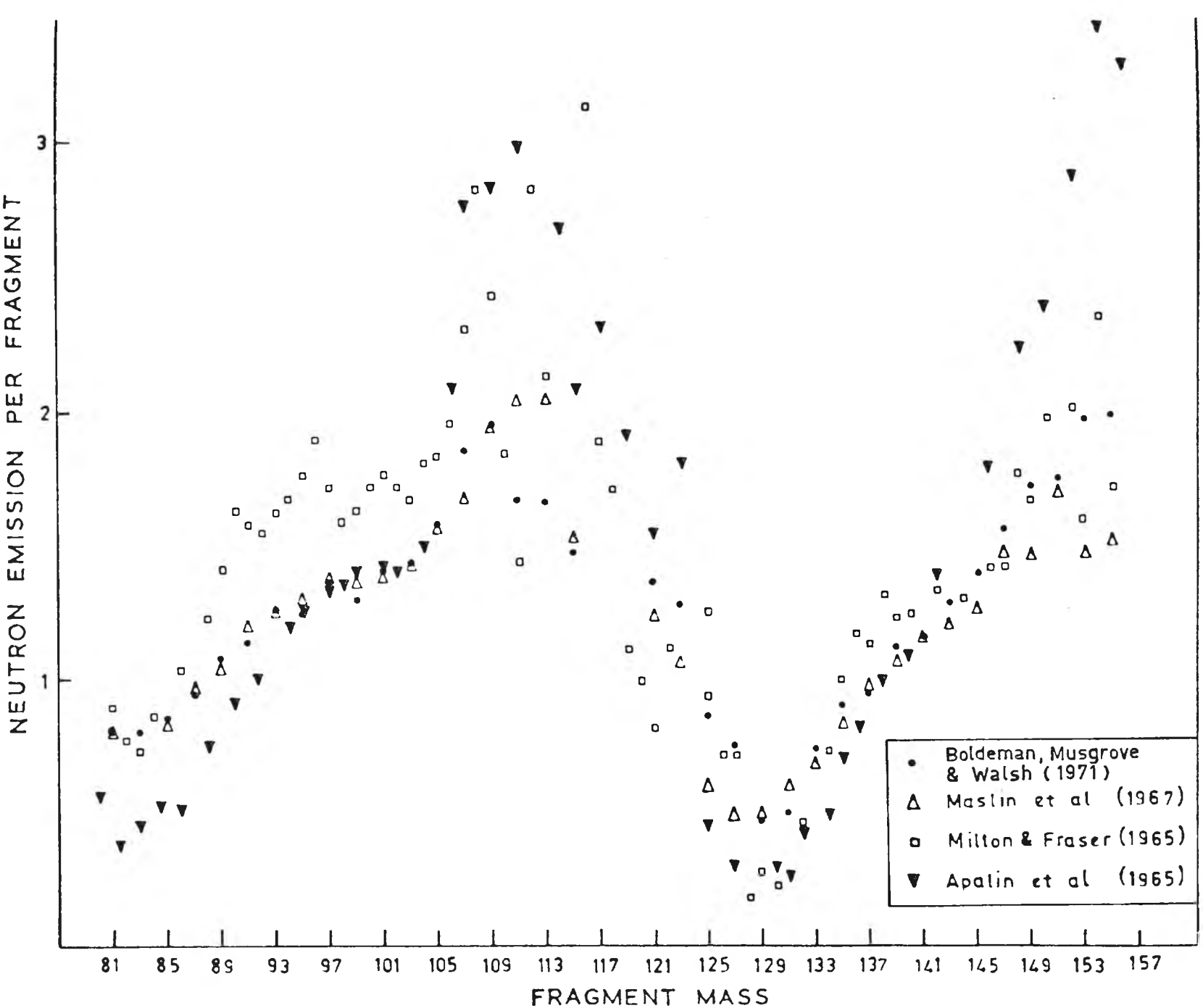

Fig 3.4 COMPARISON OF PRESENT NEUTRON EMISSION DATA WITH PREVIOUS DIRECT NEUTRON COUNTING DATA FOR U235

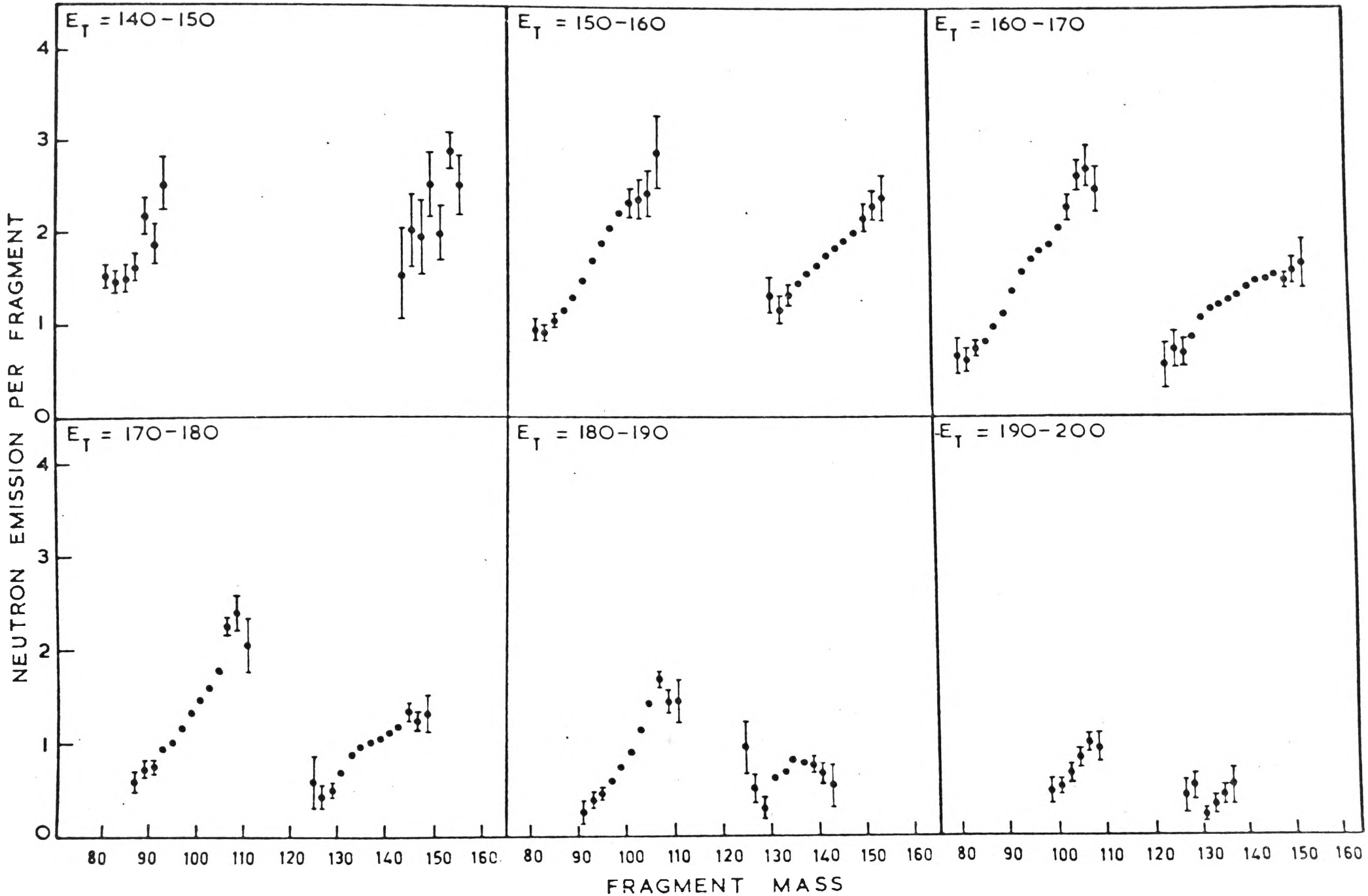

Fig 3.5 NEUTRON EMISSION PER FRAGMENT VERSUS FRAGMENT MASS FOR U^{235} FOR SIX RANGES OF TOTAL FRAGMENT KINETIC ENERGY

From [14]

reported fine structure in the mass yield curve[67]. However, none of the other three data sets shown found this fine structure. This could be because of the poorer mass resolution of double-energy measurements, compared with time-of-flight measurements. An important feature of Figure 3.4 is that it shows there to be no discontinuity in the ^{235}U $\nu(A)$ curve at symmetric fission. Thus it is probable that the light and heavy fragment data of ^{252}Cf (Figure 3.3) may also be validly joined by a straight line through symmetry.

It is notable that the sawtooth $\nu(A)$ behaviour still persists when the data are restricted to regions of (almost) constant total fragment kinetic energy. This is seen in Figure 3.5, taken from the ^{235}U work of Boldeman, Musgrove and Walsh[14]. An important feature here is the flattening of the $\nu(A)$ curve for the higher kinetic energy groups, for masses > 140. This flattening was also observed by Maslin et al. for ^{235}U[55] and by Bowman et al. for ^{252}Cf[63]. Mass 140 is the beginning of the region of nuclei with large quadrupole movements[68] indicating nuclei with stable ground state deformations. It is thought that the excitation energy of these fragments is released by de-excitation from the levels of the deformed nuclei through low energy γ-ray transitions, rather than by neutron emission.

Before going on to examine the various theories explaining the $\nu(A)$ behaviour, it is necessary to discuss the important work of Terrel[61] (mentioned above), who obtained neutron yield versus fragment mass curves for a number of nuclides using an indirect method.

Terrel's method is to derive the fragment neutron emission from a comparison of initial and final mass yield data. ('Initial' means pre-

neutron emission and 'final' means post-neutron emission). Assuming that all the neutrons are emitted by the fragments* gives

$$\bar{\nu}_L = \bar{M}_L - \bar{L} \qquad \ldots(3.1)$$

$$\bar{\nu}_H = \bar{M}_H - \bar{H} \qquad \ldots(3.2)$$

where M_L, M_H denote the initial mass numbers of the light and heavy fragments respectively, and L, H the corresponding final mass numbers. Also $M_L + M_H = A$, the mass number of the fissioning compound nucleus. At first glance it might seem an experimental impossibility to measure the initial mass yield distribution, since the neutrons are emitted within about 10^{-14} seconds after scission. However this difficulty is overcome when it is realised that neutron emission from a fragment changes the fragment velocity by only a small amount. The average velocity change is[62]

$$\langle \Delta v \rangle \sim \frac{1}{3} \left(\frac{m}{M}\right)^2 \frac{\langle v_{CM} \rangle^2}{v}$$

where m and M are neutron and final fragment masses respectively, and $\langle v_{CM} \rangle$ is the average velocity of an emitted neutron in the CMS. v is the initial fragment velocity (laboratory system). Since $\langle v_{CM} \rangle \sim v$, $\langle \Delta v \rangle$ is only about 0.01 per cent of v. Thus, fragment double-velocity studies, while actually detecting fragments <u>after</u> they have emitted neutrons, give a measure of the <u>pre</u>-neutron emission velocities. The initial masses are then found from the relation

---

*Not strictly correct, of course, in view of the 10 to 20 per cent 'scission' neutron contaminant. See section 2.1.

$$\frac{M_L}{M_H} = \frac{v_H}{v_L} \qquad \ldots(3.3)$$

$$M_L + M_H = A \qquad \ldots(3.4)$$

The final fragment masses are determined in double-energy measurements using

$$\frac{L}{H} = \frac{E_H}{E_L} \qquad \ldots(3.5)$$

Here E_H, E_L are the energies of the heavy and light fragments respectively. (The method of mass determination through double-energy measurements is described in Chapter 5).

The analysis uses two separate methods. In one, first and second moments and covariances of the initial and final mass yields are used to derive the relations

$$\left\langle \frac{d\nu_L}{dM_L} \right\rangle = \left[\sigma^2(M_L) + \sigma^2(\nu_L) - \sigma^2(L)\right]/2\sigma^2(M_L) \qquad \ldots(3.6)$$

$$\left\langle \frac{d\nu_H}{dM_H} \right\rangle = \left[\sigma^2(M_H) + \sigma^2(\nu_H) - \sigma^2(H)\right]/2\sigma^2(M_H) \qquad \ldots(3.7)$$

These expressions describe the average rate of change with mass of the neutron emission from the two fragment groups. The average rate of change of the total neutron emission is given by

$$\left\langle \frac{d\nu}{dM_H} \right\rangle = \left\langle \frac{d\nu_H}{dM_H} \right\rangle - \left\langle \frac{d\nu_L}{dM_L} \right\rangle \qquad \ldots(3.8)$$

$\sigma^2(L)$, $\sigma^2(H)$, $\sigma^2(M_L)$ and $\sigma^2(M_H)$ can be obtained from the experimental mass yield data. Terrel used the time-of-flight data of Milton and Fraser[69] and of Stein and Whetstone[70] for the initial masses, and the radiochemical results of Katcoff[71] and others[72,73] for the final masses. The problem of determining the quantities $\sigma^2(\nu_L)$ and $\sigma^2(\nu_H)$, for which no direct experimental evidence was available, was overcome by deriving new expressions relating $\sigma^2(\nu_L)$ to $\left\langle \frac{d\nu_L}{dM_L} \right\rangle$ and $\sigma^2(\nu_H)$ to $\left\langle \frac{d\nu_H}{dM_H} \right\rangle$, and solving simultaneous equations to eliminate $\sigma^2(\nu_L)$ and $\sigma^2(\nu_H)$ from the analysis.

The results of this procedure are summarised in Table 3.1 for four fissioning systems. The calculated slopes are in reasonable agreement with the measured slopes.

TABLE 3.1

Comparison of calculated and measured neutron emission parameters

	^{233}U+n	^{235}U+n	^{239}Pu+n	^{252}Cf(sp)
$\langle d\nu_L/dM_L \rangle$ (calculated)[a]	0.08±0.03	0.07±0.03	0.07±0.03	0.10±0.05
$\langle d\nu_H/dM_H \rangle$ "	0.11±0.03	0.07±0.03	0.11±0.03	0.09±0.05
$\langle d\nu/dM_H \rangle$ "	0.03±0.02	0.00±0.02	0.04±0.02	-0.01±0.03
$\langle d\nu_L/dM_L \rangle$ (experimental)[b]	0.04±0.03	0.05±0.03		0.06±0.03
$\langle d\nu_H/dM_H \rangle$ "	0.06±0.03	0.10±0.03		0.04±0.03
$\langle d\nu/dM_H \rangle$ "	0.02±0.03	0.02±0.02		-0.13±0.01

a Calculated by the method of Terrel[61]

b For references to the individual experiments see Terrel[61]

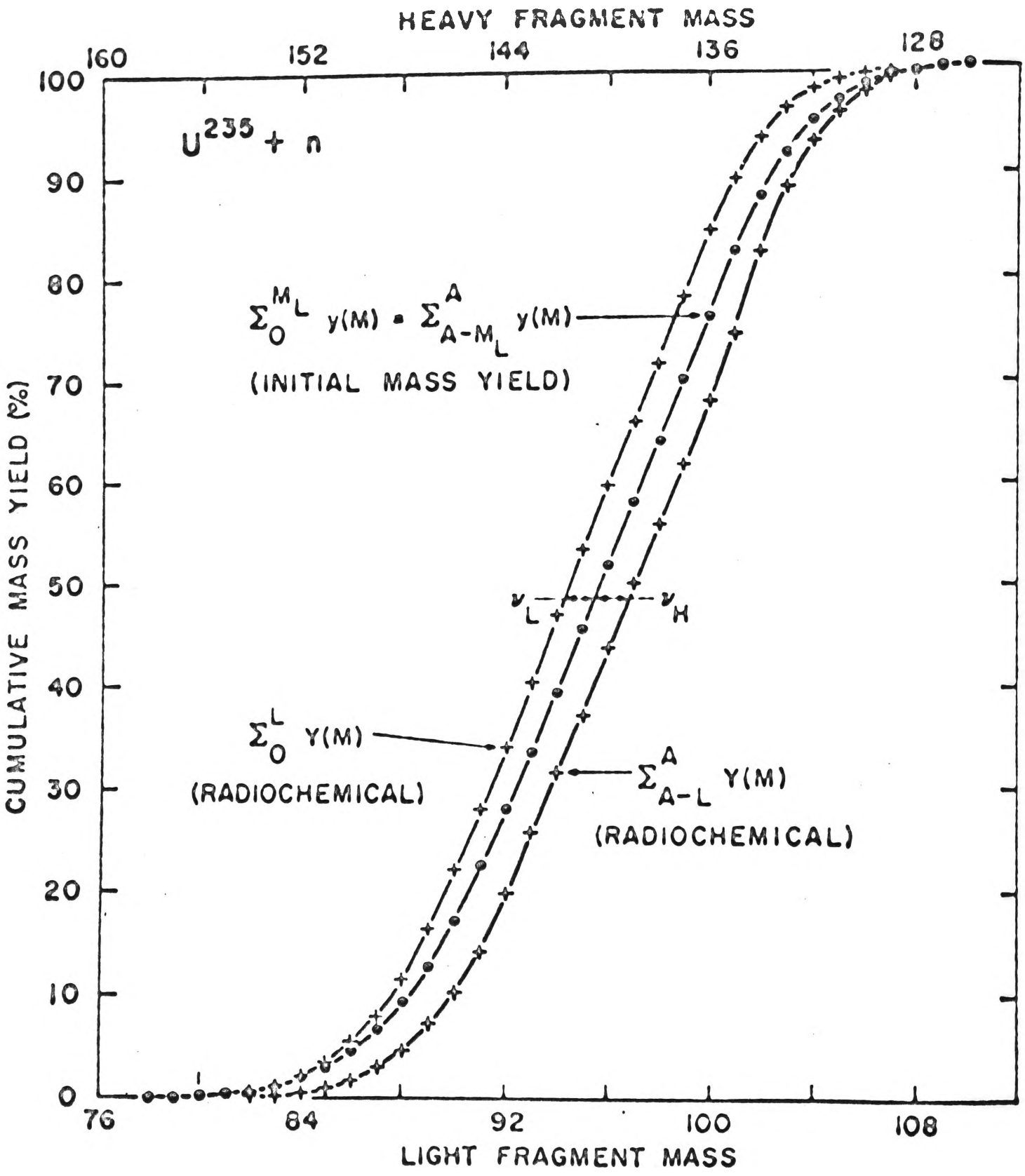

Fig 3.6 Cumulative mass yields used in determining neutron yields, for fission of $U^{235}+n$. The horizontal distances between cumulative yield curves, with slight corrections for curvature, determine neutron yields ν_L and ν_H as functions of initial fragment mass. From [61].

The above method calculates simple average slopes for the ν_L and ν_H mass dependences. Terrel's second method, however, extracts detailed information from the mass distribution. It calculates directly the neutron emission from each fragment mass. The method is one of matching initial and final cumulative fragment yields. The cumulative yield is the sum of the yields of all fragments of mass less than a given value. If y(M) is the initial (pre-neutron emission) yield of mass number M, and Y(M) the final (post-neutron emission) yield, then the initial and final cumulative yields for mass M_o are $\sum_{o}^{M_o} y(M)$ and $\sum_{o}^{M_o} Y(M)$ respectively. A full justification for the method involves rather exhaustive manipulations of arithmetic series, and will not be given here. Figure 3.6 shows how the final neutron emission calculation is performed. The horizontal distances between the radiochemical cumulative yield curves for the light and heavy fragment groups determine the yields ν_L and ν_H as functions of initial fragment mass (after slight correction for curvature of the yield curves). Terrel's results for neutron fission of ^{233}U, ^{235}U and ^{239}Pu, and for spontaneous fission of ^{252}Cf, are shown in Figure 3.7. The agreement between the Terrel calculation and experiment has been pointed out earlier, in Figure 3.3 for the case of ^{252}Cf.

3.1b Theoretical Explanations

The interesting sawtooth behaviour of the $\nu(A)$ curve stimulated numerous attempts to find an explanation. The fact that the total neutron emission in symmetric fission is considerably higher than the average total emission (e.g. $\nu_{TOT}^{SYM} \sim 3.5$ to 4 versus $\bar{\nu}_{TOT} \sim 2.5$ for ^{235}U, see Figure 3.4) led some authors to suggest that there existed

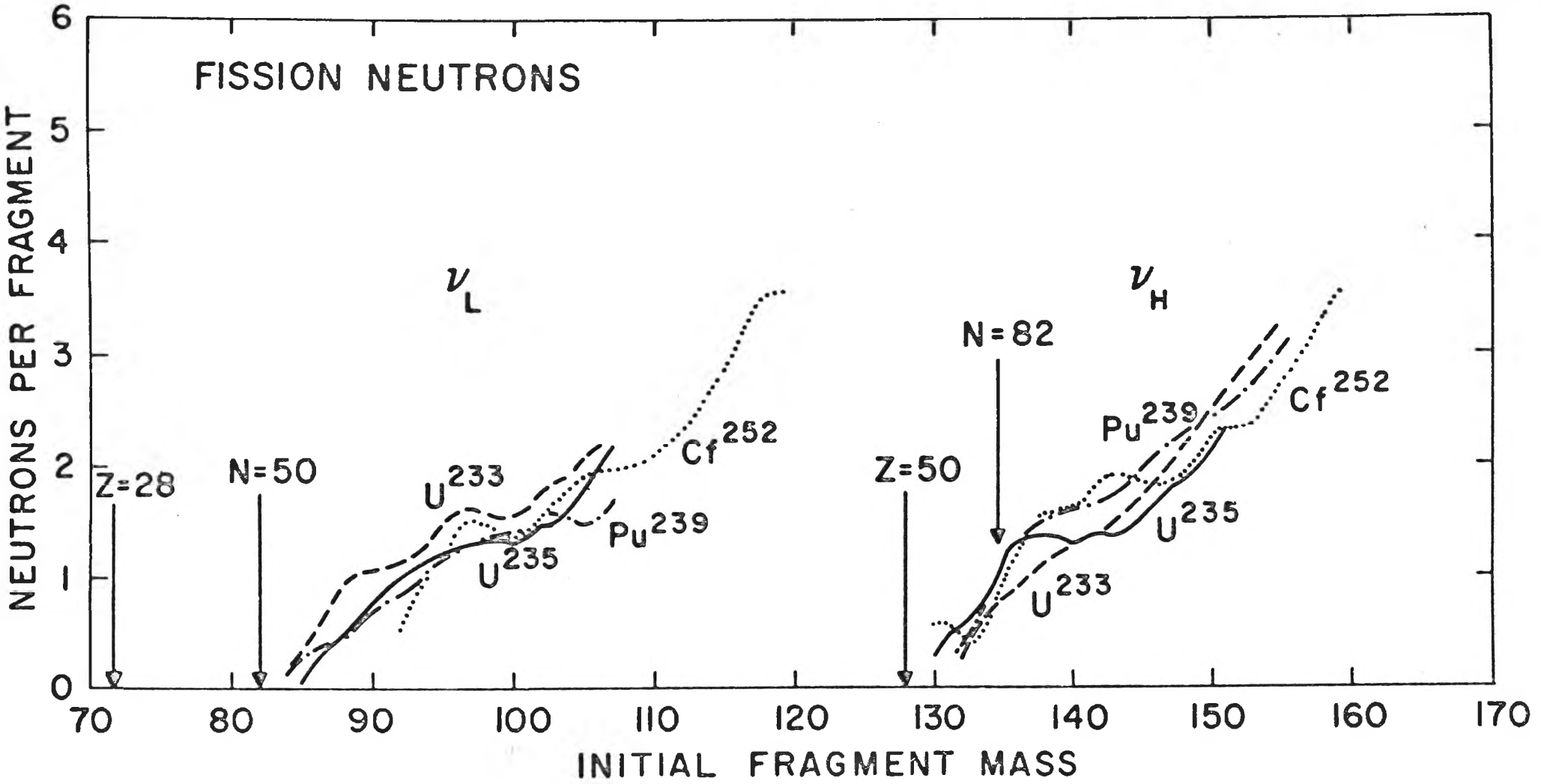

Fig 3.7

Neutron yields as functions of mass for four types of fission as determined from mass-yield data. Also indicated are the approximate fragment masses corresponding to magic numbers Z = 28 , 50 ; N = 50 , 82 (see § 3.1b) From [61].

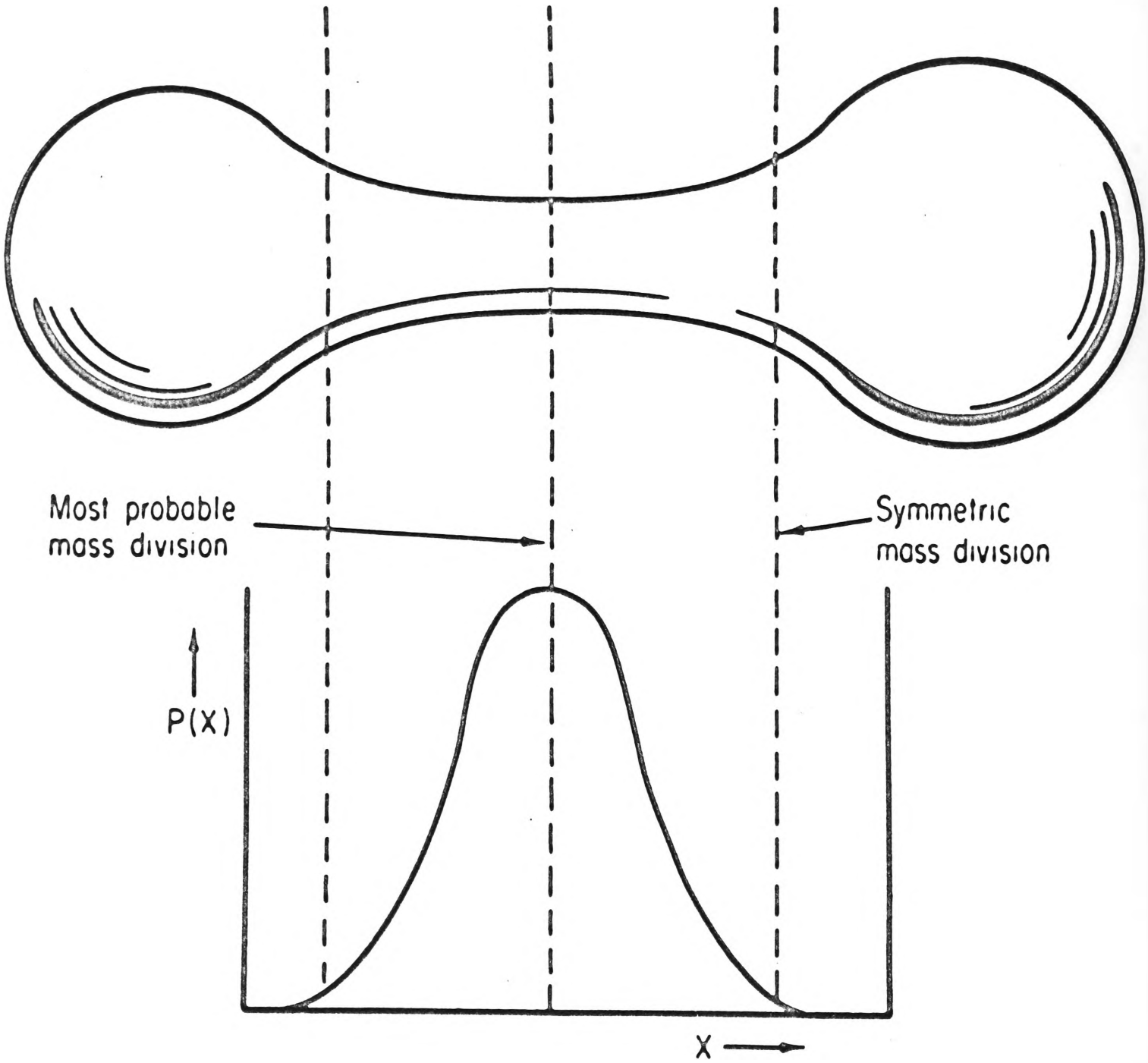

Fig 3.8 A picture of a fissioning nucleus shortly before it breaks in two. The two lobes are unequal in size. The mass ratio is determined by the point along the neck at which division occurs. The $P(x)$ curve is a probability curve for the points of division adjusted to give an overall distribution of fragment mass ratios in agreement with the observed distribution. According to this picture, a division of the nuclear mass into two equal parts will produce a nearly spherical heavy fragment and a markedly distorted (hence excited) light fragment. From WHETSTONE [62].

two different types of fission - symmetric fission with fragments of higher excitation, and asymmetric fission with fragments of lower excitation[74,75]. This idea is not generally favoured however. The apparent discontinuity in $\nu(A)$ at symmetry induced Whetstone to postulate his 'neck' model of fission[62]. This model notes that it is difficult to reconcile a neutron discontinuity with a symmetric saddle point shape, since such a shape should give rise to two fragments of almost equal internal excitation, i.e. equal neutron emission. The model assumes an asymmetric saddle point shape. Figure 3.8 shows the fissioning nucleus shortly before splitting. The two end lobes are unequal in size. The mass ratio is determined by the point along the neck at which the division occurs. P(X) is a point-of-splitting probability curve, calculated so as to reproduce the observed fragment mass distribution. The most probable split is into two fragments of unequal mass. Symmetric splitting corresponds to the relatively rare case of splitting near the larger end of the compound nucleus, in which case almost all the large amount of deformation of the neck is given to the light fragment. Splittings far from symmetry correspond to divisions close to the smaller end, with the neck deformation energy being given to the heavy fragment. Thus the observed $\nu(A)$ dependence could be reproduced quite well. However when it was shown experimentally that symmetric fragments emit approximately equal numbers of neutrons (i.e. no $\nu(A)$ discontinuity) the above model became rather untenable.

The most likely explanation of the $\nu(A)$ behaviour is that it is determined by the shell structure of the final fragments ('final' meaning in the latest stages of the fission process - at or near scission).

Referring to Figure 3.7, Terrel[61] has pointed out that for all four nuclei the regions of abnormally low neutron yield correspond closely to the magic numbers N = 50 (A ~83), Z = 50 (A ~130) and N = 82 (A ~133). It is well-known that nuclei at or near closed shells are more resistant to deformation, and prefer to retain a spherical shape. Thus, in the instant before scission, a closed shell (magic) fragment will tend to remain spherical, while its non-magic complementary fragment will be more susceptible to being deformed. After scission and separation, the closed shell fragment will have received little excitation energy from deformation energy and hence will emit few neutrons, whereas the complementary fragment, having been 'born' with larger deformation, will have a larger excitation energy and hence emit more neutrons. This qualitative argument describes the $\nu(A)$ behaviour well. Further, the low mass-yield of the magic number fragments (see for example Figure 3.2b) can also be explained, since the stiffness of the magic fragment will result in a higher Coulomb interaction energy, or fission barrier, and hence a lower fragment yield.

Vandenbosch[76] made a quantitative study of the fragment shell effect in fission. He assumed that the fissioning nucleus at the instant before scission can be represented by two uniformly charged tangent spheroids with co-linear major axes. He then computed the sum of the potential energy of Coulomb repulsion plus the deformation energy of the two spheroids. The expression used for the deformation energy included a 'shell effect' term, which itself contained a 'stiffness' parameter, k_A. For each mass ratio minimisation of the total potential energy (Coulombic plus deformation) gives the most probable scission

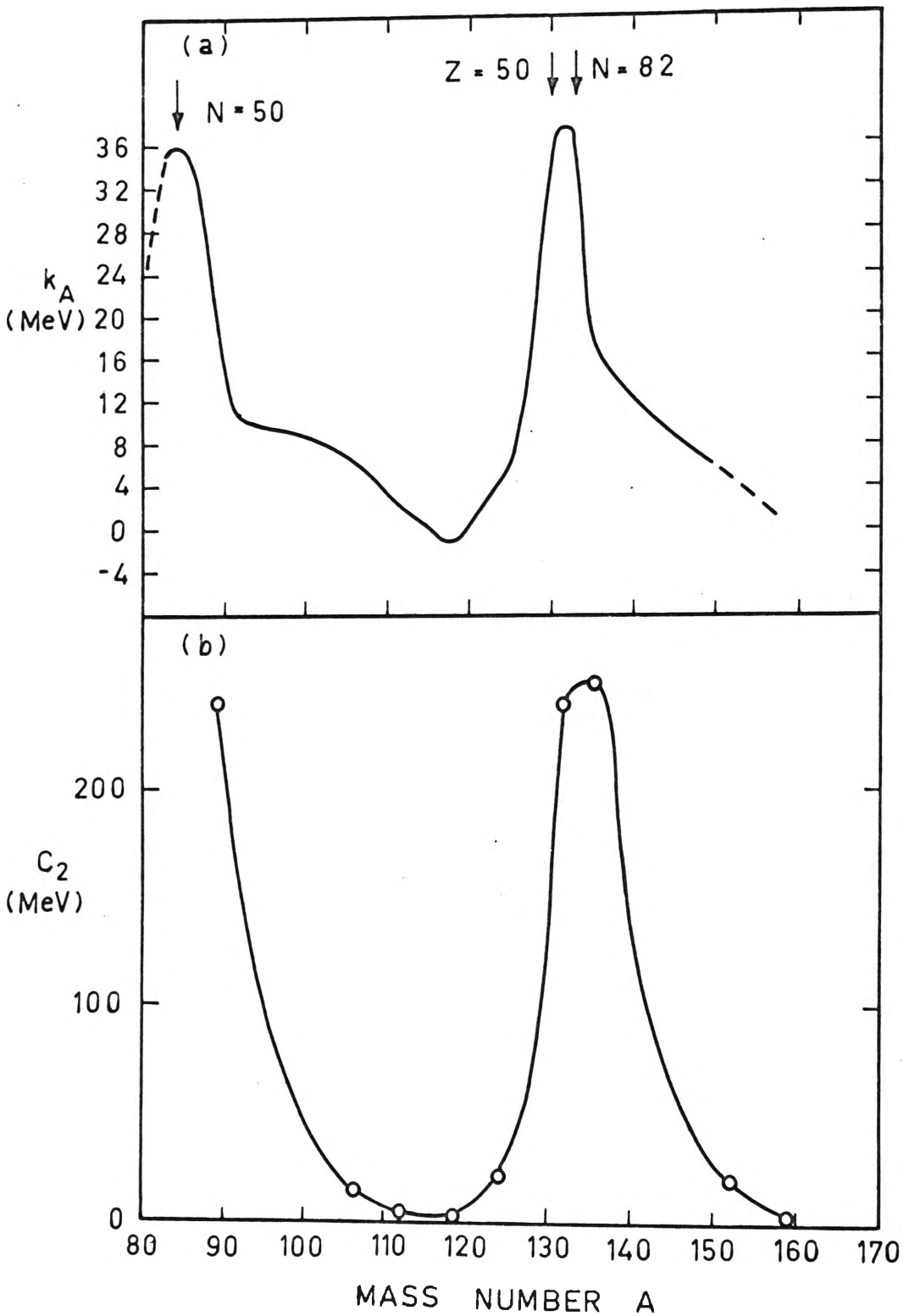

Fig 3.9 a,b Stiffness coefficient (k_A) and deformability parameter (C_2) versus mass number. From [76].

configuration. The Coulomb interaction energy at this most probable configuration gives the most probable kinetic energy of the fragments, while the corresponding deformation energies give rise to the neutron emission. By fitting the calculated kinetic energy and neutron emission expressions (involving k_A) to experimental data, a curve of k_A as a function of mass number can be derived. This curve is given in Figure 3.9a. It shows that the stiffness coefficient has large values in regions close to closed shells. Figure 3.9 b shows the nuclear deformability parameter C_2 obtained from Coulomb excitation studies of stable nuclei in the same mass range as the primary fission fragments[78]+. The C_2 curve provides good verification of Vandenbosch's calculations.

3.2 ν Versus Fragment Kinetic Energy

Information on neutron emission as a function of the total kinetic energy of the two fragments gives a direct look at the competition between fragment excitation energy and fragment kinetic energy for the available energy of the saddle point nucleus. Figure 3.10 shows the ν versus E_K result of Boldeman, Musgrove and Walsh, for ^{235}U[14]. This result is one averaged over the entire mass yield. The slope of the least squares fitted line is equivalent to -16.7 MeV per neutron for $\frac{dE_K}{d\nu}$. Using the Myers-Swiatecki mass formula[79] the variation of neutron emission with fragment kinetic energy can be converted into the variation of neutron emission with fragment excitation. The $\frac{dE^*}{d\nu}$ value

---

+The deformation energy of a nucleus with radius $R = R_o[1 + \beta_2 P_2(\cos\theta)]$ is $\frac{1}{2}C_2\beta_2^2$. P_2 is the second Legendre polynomial, β_2 specifies the deformation and C_2 is a constant[77].

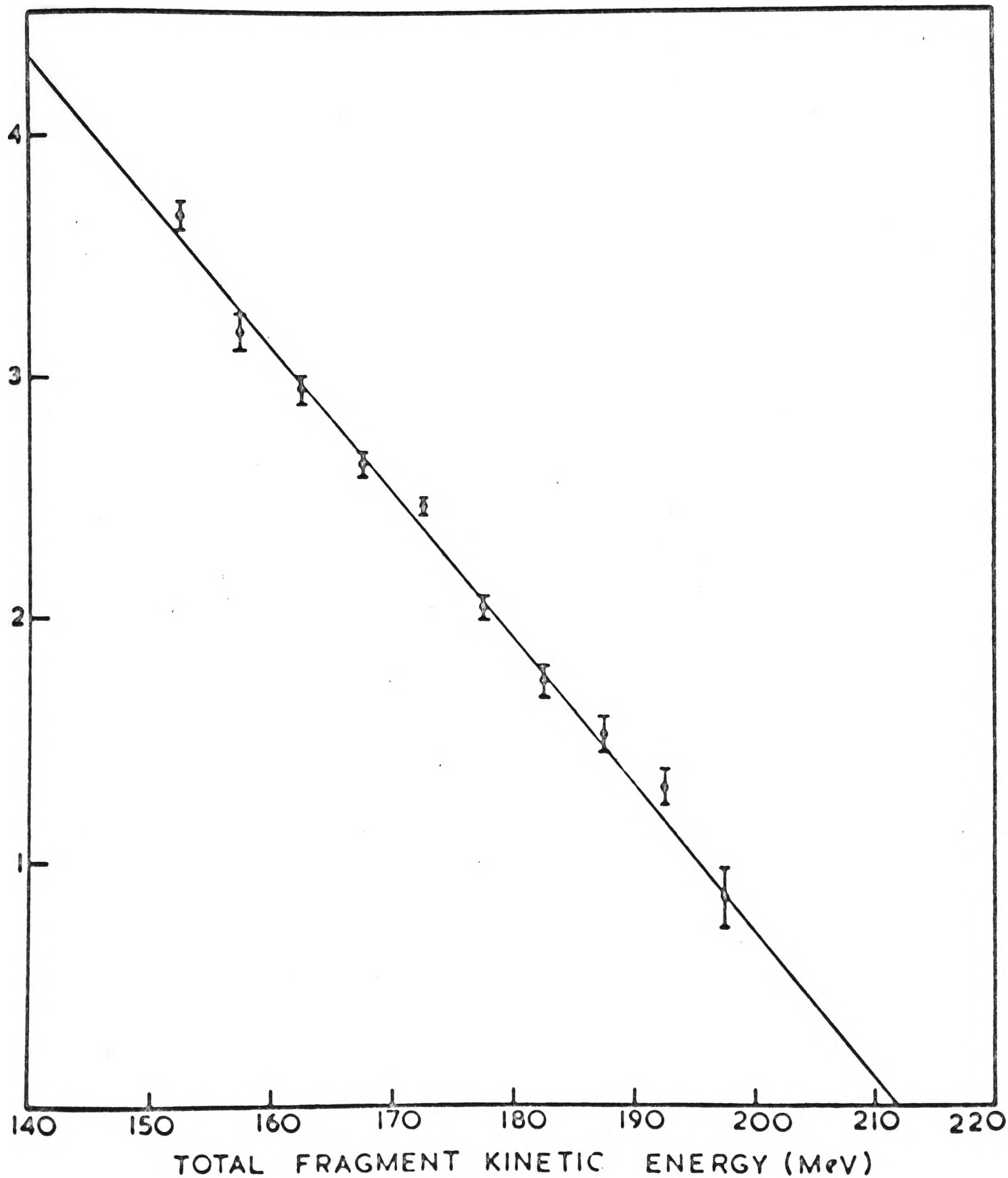

Fig 3.10 TOTAL NEUTRON EMISSION FROM BOTH FRAGMENTS PER FISSION VERSUS TOTAL FRAGMENT KINETIC ENERGY. FROM [14].

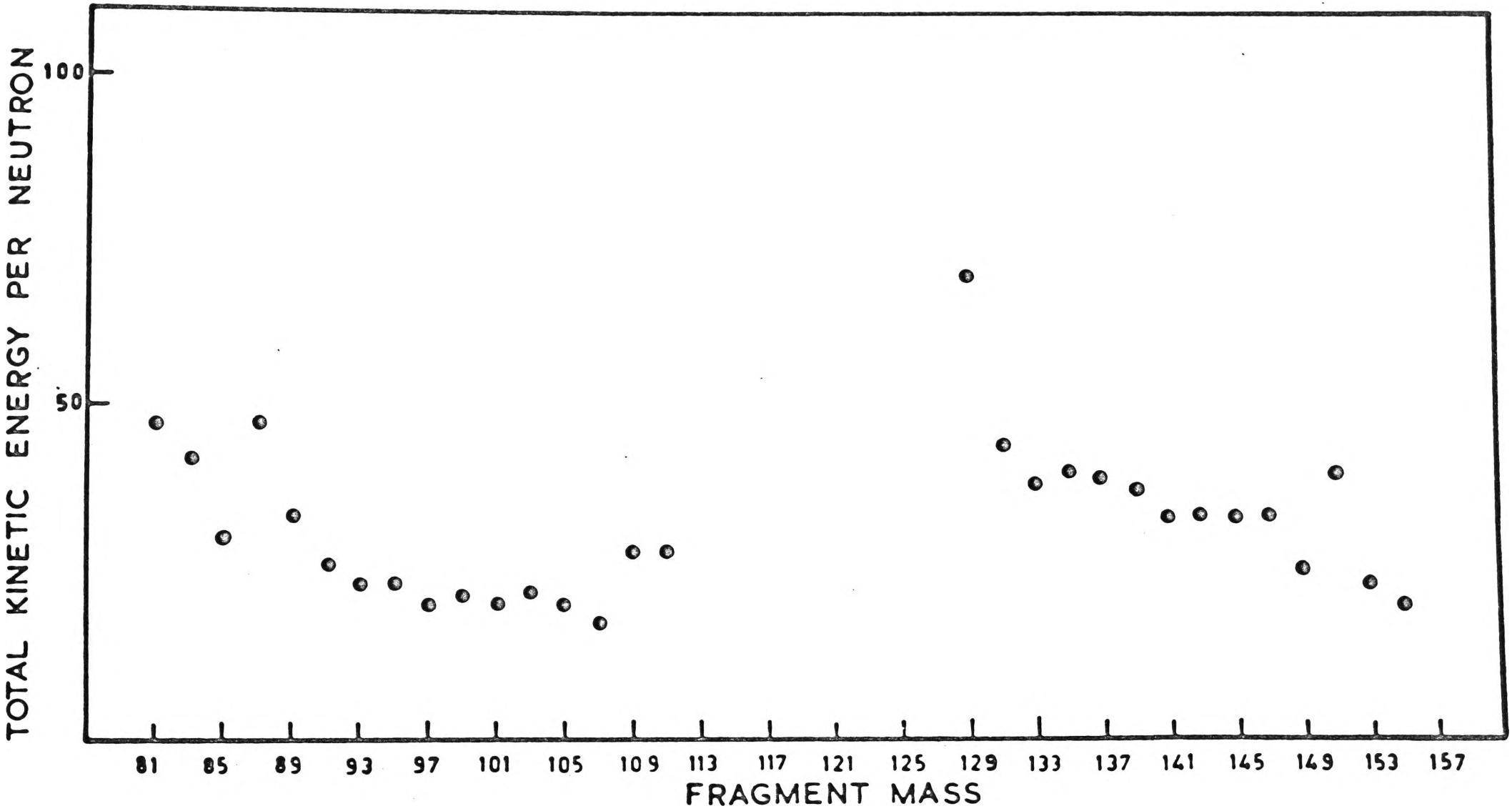

Fig 3.11 THE SLOPE $\frac{dE_T}{d\nu}$ VERSUS FRAGMENT MASS.
FROM [14].

corresponding to the above figure is 9.5 MeV per neutron. Nifenecker et al.[10] found a $\frac{dE^*}{d\nu}$ value of 9 to 10 MeV per neutron for ^{252}Cf, and Maslin et al.[55] found 15.2 MeV per neutron for ^{235}U. These slopes are considerably higher than the figure of 6.6 MeV long regarded as necessary for the emission of a neutron from a fragment (see section 2.3a; also Figure 12 of reference 63). Perhaps some of the additional excitation energy involved is dissipated as gamma ray emission[48]. It is significant that the value of $\frac{d\bar{\nu}}{dE_n}$ (or in other words, of $\frac{d\nu}{dE^*}$) found by Boldeman and Walsh for ^{235}U[12] was 0.107 neutrons per MeV below the pairing gap, giving good agreement with the above.

The linearity of Figure 3.10 is not surprising. From equation (2.18), for E_n and $\bar{E}_\gamma$ constant, the neutron emission (represented by $\bar{E}_n^*$) should decrease as E_K increases. This linearity is also preserved when $\frac{d\nu}{dE_K}$ data is presented for particular mass divisions. However, the slopes of the linear portions are different for different mass divisions. Figure 3.11 shows the individual $\frac{dE_K}{d\nu}$ slopes of reference (14) plotted against fragment mass. The steady decrease of $\frac{dE_K}{d\nu}$ (or 'α') for the light fragment as symmetric fission is approached agrees well with fragment shell theories of fission: the light fragments become progressively easier to deform when approaching symmetry. Similarly the large α value for the heavy fragment just after symmetry agrees with the shell notions of a stiff, hard to deform nucleus at mass values around 132.

3.3 ν Versus Charge

The early radiochemical methods[80] of measuring the charge division in fission involved irradiation of a known sample followed by chemical isolation of the products so formed. However, an average pair of fission fragments undergoes about six beta decays before achieving stability. Also the nuclear potential energy associated with the pair is large, about 22 MeV[81]. Because of this large amount of potential energy the primary fission fragments are for the most part very short lived (average lives of minutes to hours, usually). 'Primary' here means post-neutron emission, but pre-beta emission. Thus the measurement of primary fragment charges for individual fission events was not feasible by radiochemical means. A suitable method presented itself with the discovery of the emission of characteristic fragment X-rays coincident with fission [82,83,84,85]. These X-rays arise through internal conversion of the prompt γ-rays accompanying the de-excitation of the primary fragments. The orbital electron vacancy generated by this conversion, say in the K-electron shell, is filled by an electron dropping down from a higher level shell (L or M say), with the resulting emission of a K X-ray of energy

$$E_{K\ X\text{-}ray} = B_K - B_{L,M} \qquad \ldots(3.9)$$

where B_K is the binding energy of an electron in the K shell. Similarly for B_L, B_M. The K X-ray energies typically lie in the region 15-50 keV.

The K electron shell cannot be further subdivided according to binding energies, whereas the L shell is really composed of a triplet, while the M shell forms a quintet, etc. The subshells are designated L_I, L_{II}, L_{III}; M_I, M_{II}, etc. in order of decreasing binding energies. Thus, for a particular K-shell vacancy, a large number of electron transitions is possible to fill it, each with its own characteristic K X-ray emission energy. An approximate qualitative relation between the K X-ray energy E and the nuclear charge Z of the element emitting it is

$$Z \approx 10\, E^{\frac{1}{2}} \text{ (keV)} \qquad \ldots(3.10)$$

Modified Moseley formula[85]

More accurately, data on electron binding energies of different elements[86] and on the intensities of the various possible transitions[87] make it possible to calculate the average K X-ray energies from a fission fragment of a particular charge. Of course it is assumed here that the electron binding energies and transition intensities for the disrupted electron cloud of a fission fragment are the same as those of the undisturbed atom. Watson[88] has investigated this point and has shown that the increased ionisation of fission fragments does not lead to a substantial modification of the relative energies of the $K\alpha$ and $K\beta$ spectral lines from the singly ionised atom. Table 3.2 lists these average K X-ray energies for individual elements[87].

TABLE 3.2

ENERGIES OF K X-RAYS FROM INDIVIDUAL ELEMENTS[a]

Element	Z	$K\alpha_1$(MeV) ($K\text{-}L_{III}$)	$K\alpha_2$(MeV) ($K\text{-}L_{II}$)	$K\beta_1$(MeV) ($K\text{-}M_{III}$)	$K\beta_2$(MeV) ($K\text{-}N_{III}$)
Kr	36	12.648	12.597	14.112	14.313
Rb	37	13.394	13.335	14.960	15.184
Sr	38	14.164	14.097	15.834	16.083
Y	39	14.957	14.882	16.736	17.011
Zr	40	15.774	15.650	17.666	17.969
Nb	41	16.614	16.520	18.621	18.951
Mo	42	17.478	17.373	19.607	19.964
Tc	43	18.370	18.250	20.612	21.012
Ru	44	19.278	19.149	21.655	22.072
Rh	45	20.214	20.072	22.721	23.165
Pd	46	21.175	21.018	23.816	24.297
Ag	47	22.162	21.988	24.942	25.454
Cd	48	23.172	22.982	26.093	26.641
In	49	24.207	24.000	27.274	27.859
Sn	50	25.270	25.042	28.483	29.106
Sb	51	26.357	26.109	29.723	30.387
Te	52	27.471	27.200	30.993	31.698
I	53	28.670	28.315	32.292	33.016
Xe	54	29.779	29.463	33.644	34.398
Cs	55	30.970	30.623	34.984	35.819
Ba	56	32.191	31.815	36.376	37.255
La	57	33.440	33.033	37.799	38.728
Ce	58	34.717	34.276	35.255	40.231
Pr	59	36.023	35.548	40.746	41.772
Nd	60	37.359	36.845	42.269	43.349

(a) From reference (87)

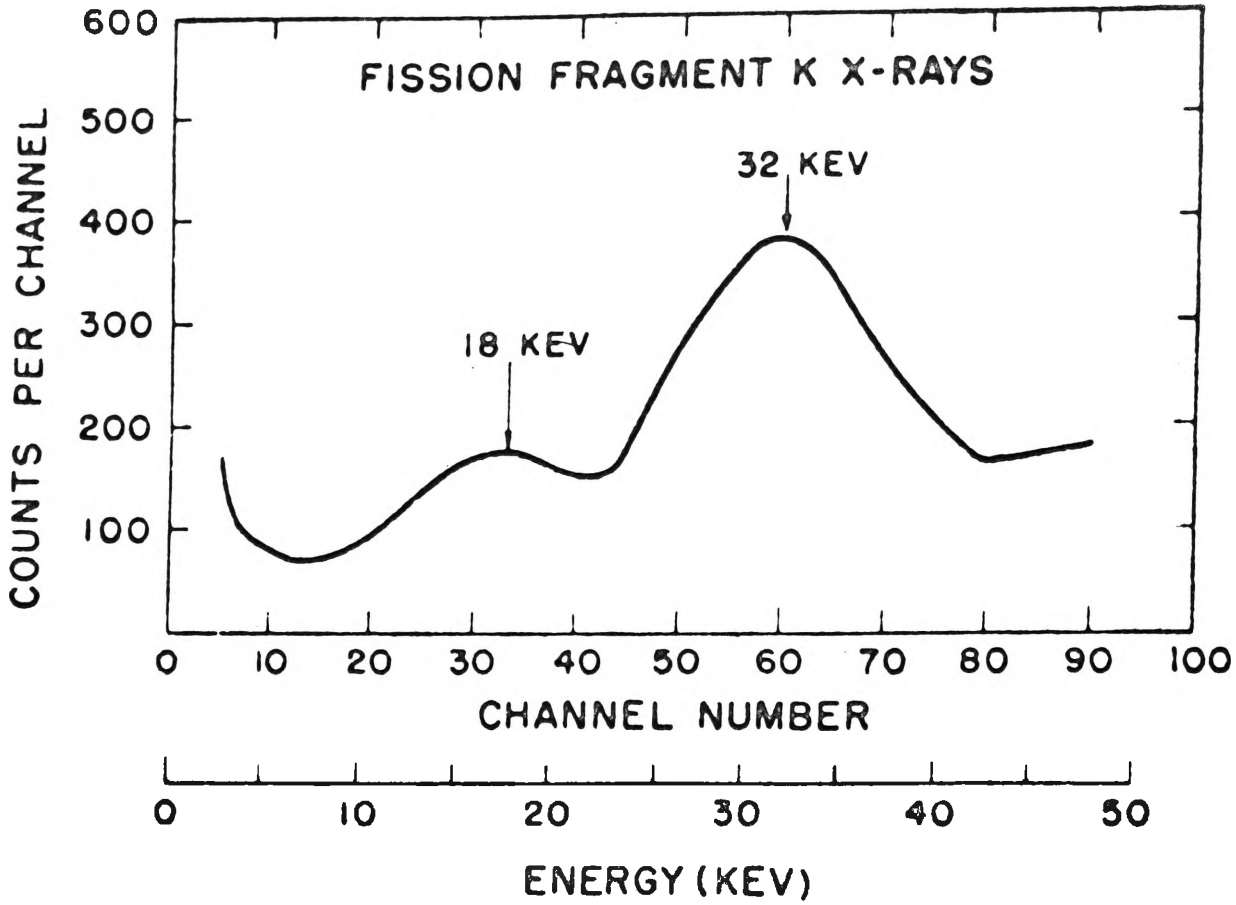

Fig 3.12a Energy spectrum of the K X rays from fission obtained by Carter, Wagner and Wyman with a 0.045-in. NaI crystal. From [84].

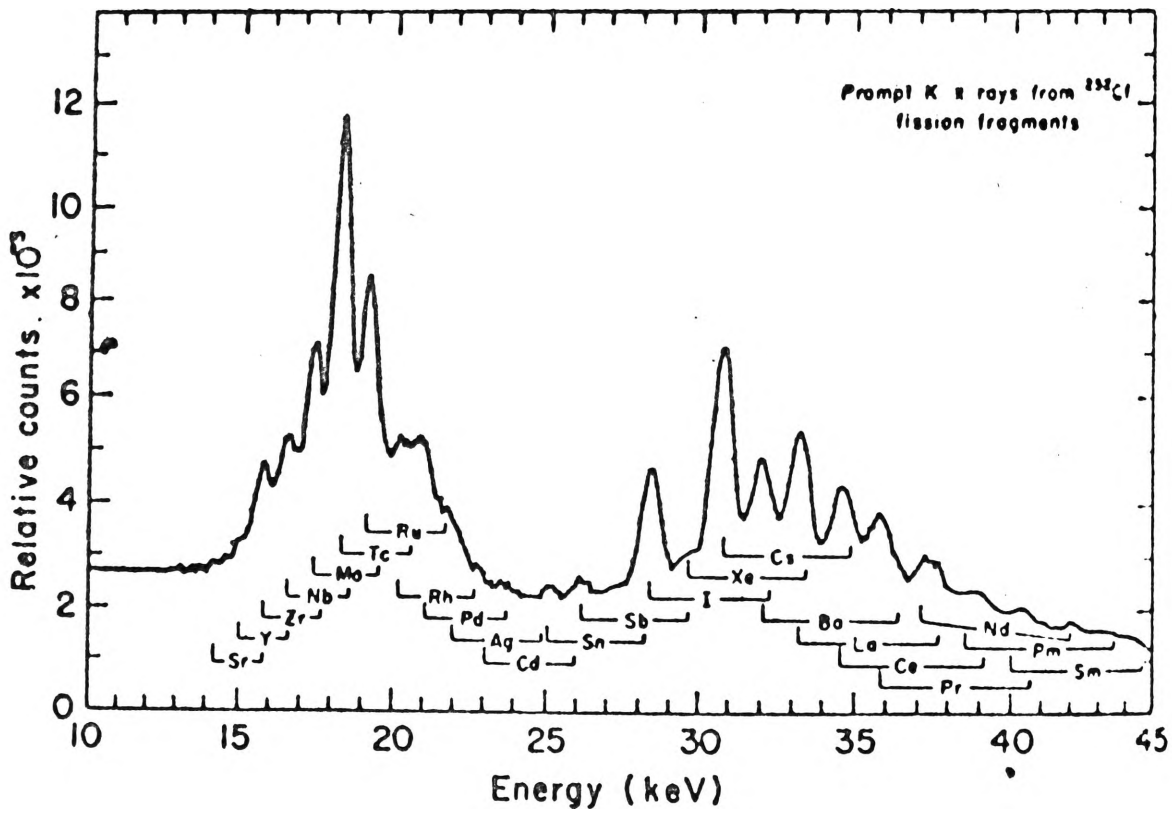

Fig 3.12b The energy spectrum of K x rays emitted by primary ^{252}Ct fission products in coincidence with fission. The locations of the $K\alpha$ and $K\beta$ x-ray groups are indicated for most fission-product elements by brackets. From [89].

The average yield of the K X-rays is 0.55 ± 0.10 per fission for ^{252}Cf[90]. Thirty per cent are emitted within 0.1 ns after fission, another 30 per cent between 0.1 and 1 ns, 25 per cent between 1 and 10 ns, and the remainder >10 ns after fission. The X-rays are accompanied by 50-300 keV conversion electrons, emitted within 2 μs of fission, with a yield of ~1 per fission event[90].

The initial measurements of fission fragment X-rays were hampered by poor resolution. Figure 3.12a shows the spectrum obtained by Carter, Wagner and Wyman for ^{235}U, using a NaI crystal as X-ray detector[84]. Their resolution (FWHM) was probably only about 10 keV. Figure 3.12b shows a much more accurate measurement, this time for ^{252}Cf K X-rays[89]. The resolution here is 820 eV at 26 keV, obtained by the use of a lithium drifted silicon semiconductor detector. The square brackets in Figure 3.12b indicate the location of the Kα and Kβ X-ray groups for most of the fission-product elements. As the X-ray energy resolution is improved, the indentification of different elements with an accuracy close to or better than one charge unit, becomes possible.

A study of the fission neutron emission from a fragment of particular charge Z is important for two main reasons: (i) the high resolution obtainable with Si(Li) X-ray detectors, about one charge unit, is equivalent to a mass resolution of about 2.5 a.m.u. Such mass resolution is comparable to the best time-of-flight measurements. In particular, for ^{252}Cf, the direct neutron counting experiments of Whetstone[62] and Bowman et al.[63] (see Figure 3.3) achieved a mass resolution of only about 6 a.m.u.

(ii) it permits investigation of a possible odd-even Z parity variation in the excitation energy of the fission fragments. This variation arises as follows[9]: the mass formula may be separated into two terms, one of which is a smooth function of Z and A and includes shell effects, while the other is a term which depends only on the parities of the neutron and proton numbers. Thus

$$M(N,Z) = m(N,Z) - \delta_N - \delta_Z \qquad \ldots(3.11)$$

where $\delta_N \approx 1$ MeV for N even

≈ 0 MeV for N odd,

$\delta_Z \approx 1$ MeV for Z even

≈ 0 MeV for Z odd.

M(N,Z) is the mass of a fragment containing N neutrons and Z protons, and m(N,Z) is the smooth function mentioned above. Define $\Delta = \delta_N + \delta_Z$. One can then find the value of Δ for a fragment of given mass number A. If A is odd, then either N or Z is odd, thus

$$\Delta_A^{odd} \approx 1 \text{ MeV} \qquad \ldots(3.12)$$

If A is even, then either N and Z are odd or N and Z are even. Assuming that these two cases are equally probable gives

$$\Delta_A^{even} \approx 1 \text{ MeV} \qquad \ldots(3.13)$$

Thus $$\Delta_A^{even} \approx \Delta_A^{odd} \qquad \ldots(3.14)$$

However, for a given Z, it can similarly be shown that

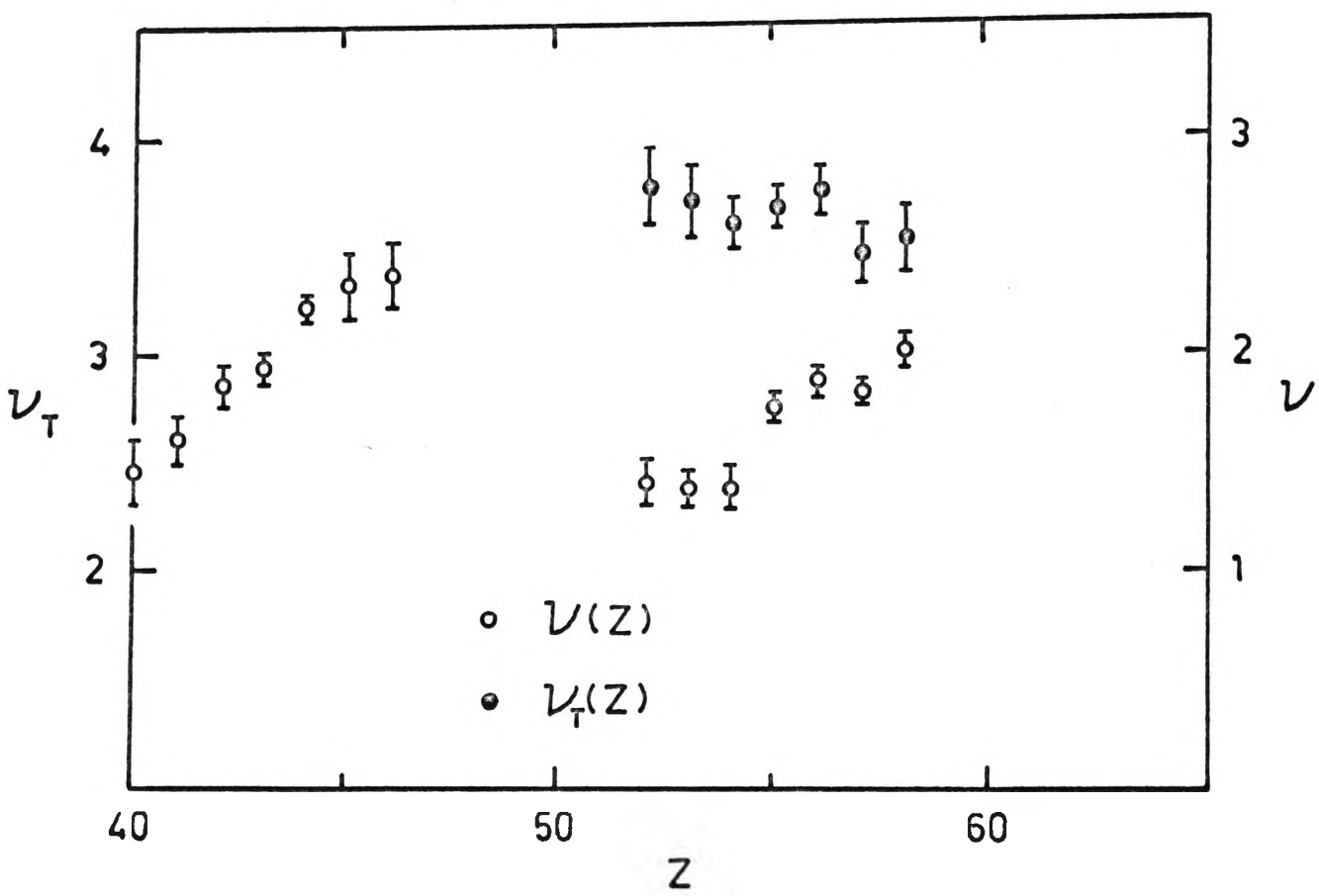

Fig 3.13 AVERAGE NUMBER OF NEUTRONS AS A FUNCTION OF THE FRAGMENT CHARGE. FROM [10].

$$\Delta_Z^{even} \approx 1.5 \text{ MeV}$$

$$\Delta_Z^{odd} \approx 0.5 \text{ MeV}$$

$$\Delta_Z^{even} \approx \Delta_Z^{odd} + 1 \text{ MeV} \qquad \ldots(3.15)$$

In other words fission into two even charge fragments liberates about 2 MeV more energy than fission into two odd charge fragments. It is important to know whether this extra 2 MeV shows up in the kinetic energy of the fragments or in their excitation energy, especially since the fine structure in the mass yield curves has been attributed to such an effect[91]. If the additional energy appears in the fragment excitation energy, then the neutron emission for an even-even split should be enhanced by about 0.2 to 0.3 neutrons (based on $\frac{dE^*}{d\nu}$ values of ~10 MeV/neutron and ~6.6 MeV/neutron respectively, section 3.2).

To date only one experimental study of $\nu(Z)$ has been reported, by Nifenecker et al. for ^{252}Cf[9,10]. The X-ray energy resolution achieved in that work, 1000 eV at 30 keV, was poorer than that achieved in the present experiment, 440 eV at 26 keV. Nifenecker et al. did not find evidence for a Z parity effect in the neutron emission. Their $\nu(Z)$ data are shown in Figure 3.13. The open circles represent the light and heavy fragment data. The familiar sawtooth shape of the $\nu(A)$ curve is reproduced in the $\nu(Z)$ curve. The solid circles denote the total neutron emission from both fragments (ν_T) as a function of the charge of the heavy fragment. Averaging over the even charges Z = 52, 54, 56, 58 and over

the odd charges Z = 53, 55, 57, gives

$$\nu_{T(\text{even } Z)} = 3.66 \pm 0.06$$

$$\nu_{T(\text{odd } Z)} = 3.66 \pm 0.04 \quad ,$$

i.e. no difference in even Z and odd Z neutron emission.

In the same experiment the fragment kinetic energies were measured as a function of Z. Again, no evidence for the Z parity effect was observed.

The X-ray resolution of the French work, 1000 eV at 30 keV, is not really adequate to identify individual fragment charges. The energies of the $K\alpha_1$ lines of the light fragment group are only about 800 eV apart, while those of the heavy group are about 1200 eV apart. The 440 eV X-ray resolution of the present experiment, however, enables a much better identification of individual charges.

CHAPTER 4

EXPERIMENTAL CONSIDERATIONS

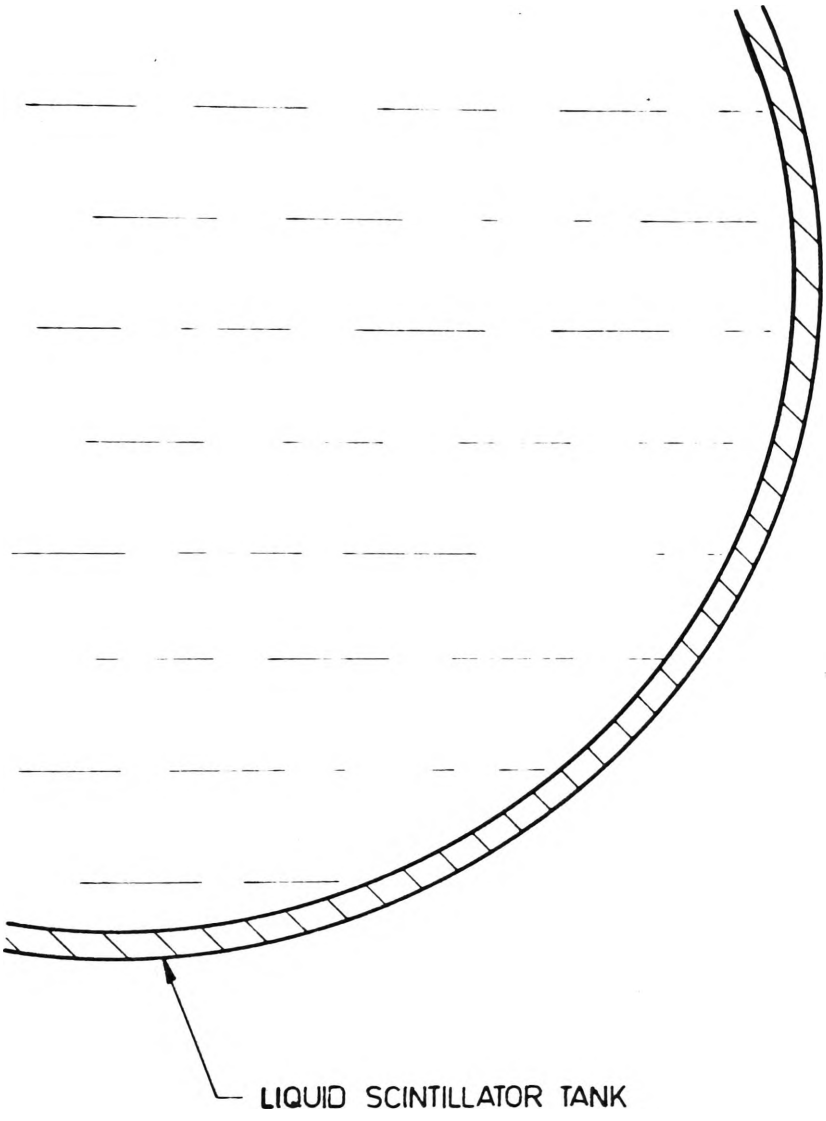

Fig 4.1 EXPERIMENTAL

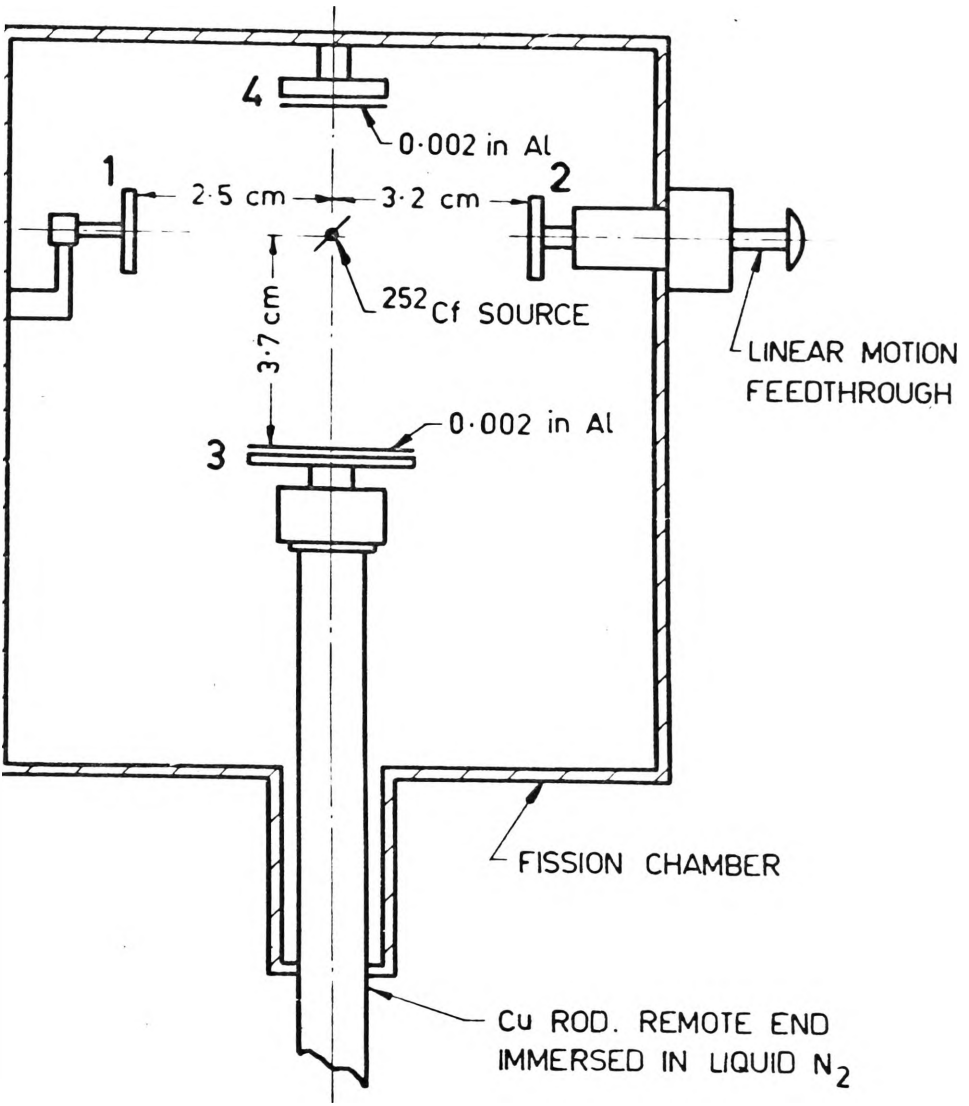

SYSTEM - SCHEMATIC

The experiment is designed to measure the neutron emission from ^{252}Cf spontaneous fission fragments as a function of the mass and charge of the fragments, and also as a function of the total kinetic energy of the two fragments. The energy of the K X-ray detected in coincidence with the fission fragments establishes the fragment charges, and the pulse heights from the fragment detectors establish the total fragment kinetic energy and the fragment masses.

4.1 Apparatus

(a) The Fission Chamber

Figure 4.1 is a schematic diagram of the experimental system. The ^{252}Cf spontaneous fission source (strength 7×10^4 fissions per min.) is situated inside an evacuated fission chamber (pressure $\sim 10^{-8}$ torr). The source is prepared on a 5 μin. thick nickel backing foil by vacuum sublimation, and was supplied by A.E.R.E. Harwell. The source is viewed by four solid state detectors.

Detectors 1 and 2 (see Figure 4.1) are the fission fragment detectors. These are standard gold-coated silicon surface barrier devices, of resistivity ~ 2000 Ω-cm. They are masked to an active area of one cm^2. Detector 1 is situated 2.5 cm from the source and subtends an angle of $\pm 11.3^\circ$ with respect to it. Detector 2 is mounted on a linear motion feedthrough and its distance from the source can be changed from outside the vacuum system. Detector 2 was initially set at 3.2 cm from the source, subtending an angle of $\pm 8.9^\circ$. (This distance was subsequently changed, however. See § 4.3). The source-detector distances are necessarily unequal so as to prevent discrimination against fission events in which

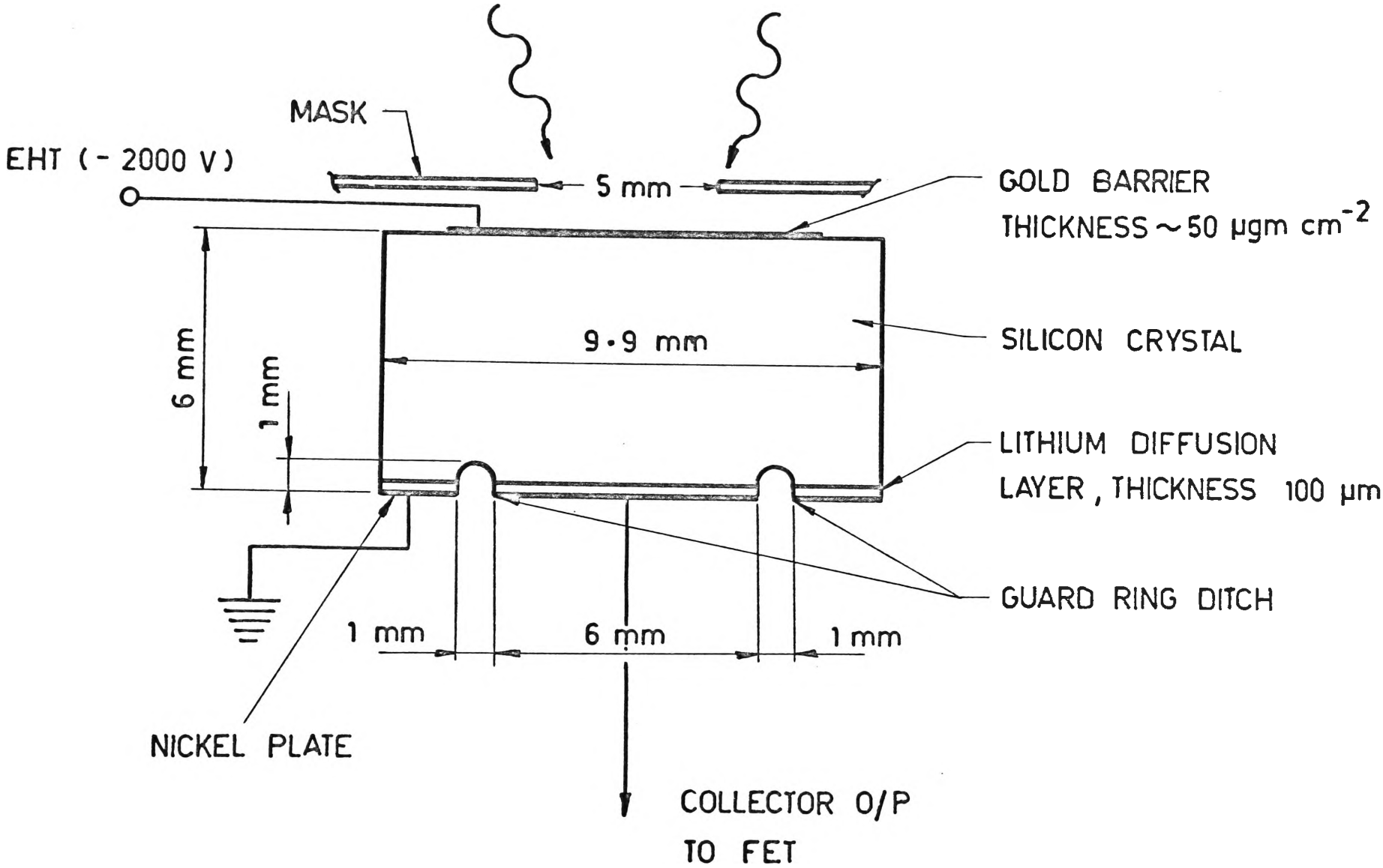

Fig 4·2 THE X-RAY DETECTOR. 90 K Ω - cm n - TYPE SILICON

one fragment emits a large number of neutrons, and is thereby given a larger angular dispersion than normal. In the above geometry, 99% of fragments seen by detector 2 will have their complementary fragment seen by detector 1. Both detectors are operated under reverse bias of about 90 volts (negative).

Detector 3 is the high resolution X-ray detector. This is a 90 KΩ-cm n-type silicon surface barrier device, of guard ring type. Operation is at reverse bias of 2000 volts (negative), for which the leakage current is exceptionally low, $\sim 10^{-14}$ A. Figure 4.2 shows the detector dimensions. The detector is mounted on the end of a copper rod, the remote end of which is kept immersed in liquid nitrogen (-196°K), to provide the necessary cooling for the detector. Because of thermal losses however, the detector end of the rod was some 10°K above liquid nitrogen temperature. As a result of this slight warming, it was found necessary to keep the liquid nitrogen cryostat continually replenished (every four hours) in order to minimize gain drifts in the X-ray line. The detector was shielded from the source by 0.002 in. of aluminium, to protect against alpha particle and fission fragment damage. The X-ray resolution achieved was 440 eV (FWHM) for the 26.36 keV ^{241}Am line.

Detector 4 is identical to detectors 1 and 2. Its purpose is to detect the ternary alpha particle emitted in fission (about one per 300 binary events). The 0.0015 in. aluminium foil shielding it from the source stops ^{252}Cf natural alphas (6.1 MeV) and fission fragments, but allows passage of the higher energy ($>$ 10 MeV) ternary alpha particles. The ternary count rate in Detector 4, coincident with fission, was very

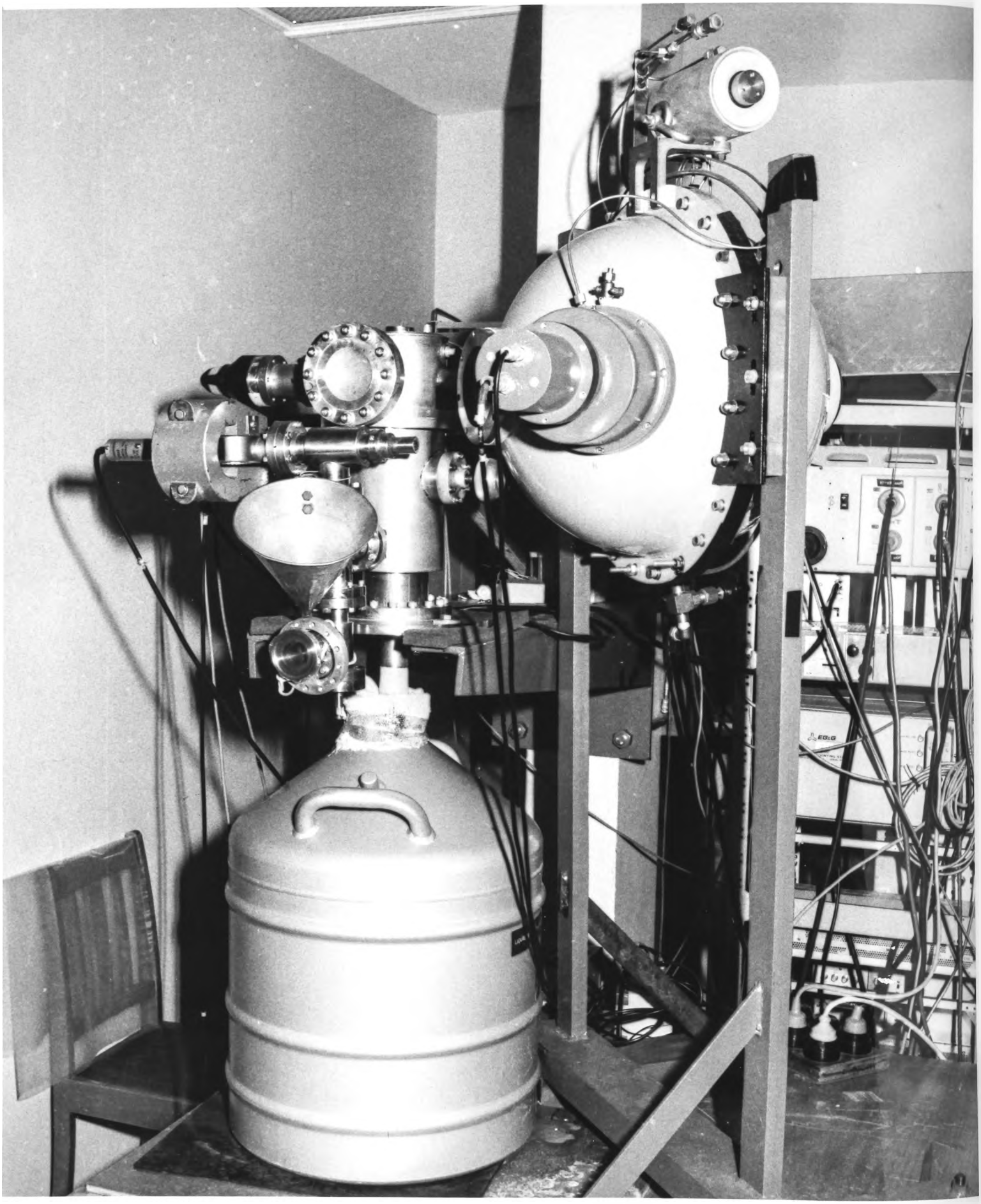

Figure 4.3 The Experimental System

low, about one every 10 mins, and therefore for the purposes of this thesis, only the data taken by Detectors 1, 2 and 3 was utilized.

(b) The Liquid Scintillator Tank

The neutrons emitted in fission are detected in the spherical, liquid scintillator tank (see Figure 4.1). This tank is 40 cm in diameter and contains 32 litres of NE323, a trimethyl benzene scintillator liquid with 0.5% by weight gadolinium loading. Two E.M.I. 9618B photomultiplier tubes mounted on the tank at right angles to the fission axis, and operated in coincidence, detect the scintillations caused by capture gamma rays and knock-on protons in the liquid. The chosen operating voltage of the photomultiplier tubes (1860V) was a compromise between high efficiency and high background count rate. At 1860V, the 4π tank efficiency was ~60%. The tank is located on the fission axis and subtends an angle of $\pm 29.7^{\circ}$ with respect to the source. It is placed directly behind detector 1 and therefore most of the fission neutrons it detects will be those emitted from fragment 1, as a result of the strong neutron peaking in the fragment direction of motion (see section 2.1).

Both the tank and the fission chamber are elevated to a height of 6 ft. above ground, to reduce the contribution of scattered neutrons to the tank background. Figure 4.3 is a view of the system.

(c) Electronics

Figure 4.4 is a block diagram of the electronic system. The X-ray preamplifier is a resistive feedback charge sensitive device. It had been hoped that an opto electronic feedback preamplifier would be supplied by the A.A.E.C. Instrumentation and Control Division, as a fifty per cent

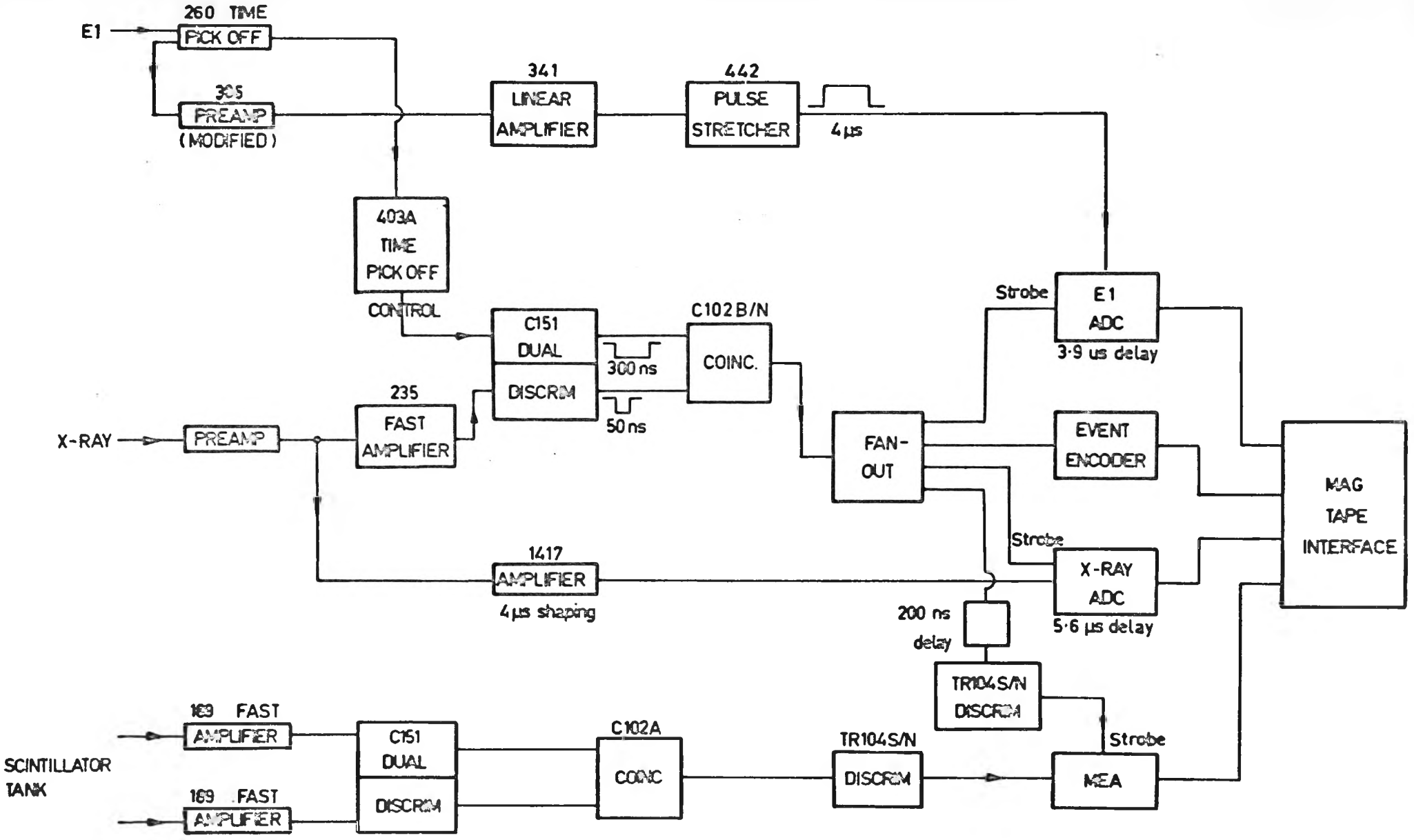

FIG 4.4 Block diagram of electronics for $V(Z)$ measurements. For $V(A, E_{TOT})$ measurements the X-ray line is replaced by an E2 line identical to the E1 line.

improvement in resolution is obtainable with these devices as against the resistive feedback preamplifier. However, only the latter type was eventually available. The pulse height lines for the two fragments and for the X-ray are digitized in three 220 channel AD128 analogue-to-digital converters. The neutron counting line passes into a 'Multiple Event Analyzer' (MEA), which stores the number of times 0, 1, 2 etc. neutrons were observed per counting cycle. A triple coincidence between the two fragment fast lines and the X-ray fast line serves to gate open the three ADC's and the MEA. The gating pulse to the MEA is delayed by $\sim$200 ns however to discriminate against the prompt γ rays accompanying fission. When gated on, the MEA counts neutrons for 40μsec after fission. After a subsequent waiting period of 100μsec the gate opens again for a further period of 40 μs, in order to sample the tank background. Twenty-two counting channels are available, fifteen for foreground data and seven for background data.

The experimental data is recorded event by event on 9 track, 800 bytes per inch, magnetic tape. Thus each particular event gives a record like (label; X; N,B; E_1; E_2) where X is the X-ray pulse height; N, B the foreground and background neutron counts; E_1, E_2 the fragment pulse heights; and 'label' is a number specifying the type of event recorded (double coincidence, triple coincidence, etc.). 'Label' is generated by an 'Event Encoder' which also is strobed by the fast coincidence line. The magnetic tape is analyzed 'off-line' by an IBM 360/50 computer.

4.2 Preliminary Procedures

The preliminary X-ray measurements for the experiment were hampered by microphonic noise arising from the cryostat. At that time the cryostat system consisted of a liquid nitrogen feed-through assembly, in which the cryostat was situated vertically above the X-ray detector and the liquid N_2 flowed down under gravity to provide cooling. It seemed most likely that the microphonic noise arose from bubbling of the liquid N_2 as it flowed downwards. The system was therefore re-designed to operate as an immersion assembly, with the detector mounted on one end of a 3/4 inch diameter copper rod, the remote end of which is immersed in liquid N_2 (see Figure 4.1). This procedure reduced the microphonic noise to a level where high resolution X-ray measurements became possible.

Considerable care was required in the selection and installation of the high-tension feedthrough carrying the X-ray detector bias. This feedthrough passed through the wall of the fission chamber, and it was necessary that it leak only a few picoamps at full detector bias (2000 V). The feedthrough used was a glass-to-metal S.T.C. make, type HS2B. A number of these were cleaned with demineralized water, tested individually for insulation, and the best of these installed in the system. The feedthrough chosen leaked 6 pA at 2000 V.

Thermocouple measurements were made to determine the operating temperature of the detector end of the copper cooling rod. A simple copper-constantan thermocouple was used. The 'cold' junction of this was in thermal contact with the copper rod end via a thermally conducting yet electrically insulating boron nitride washer. The 'hot' junction was

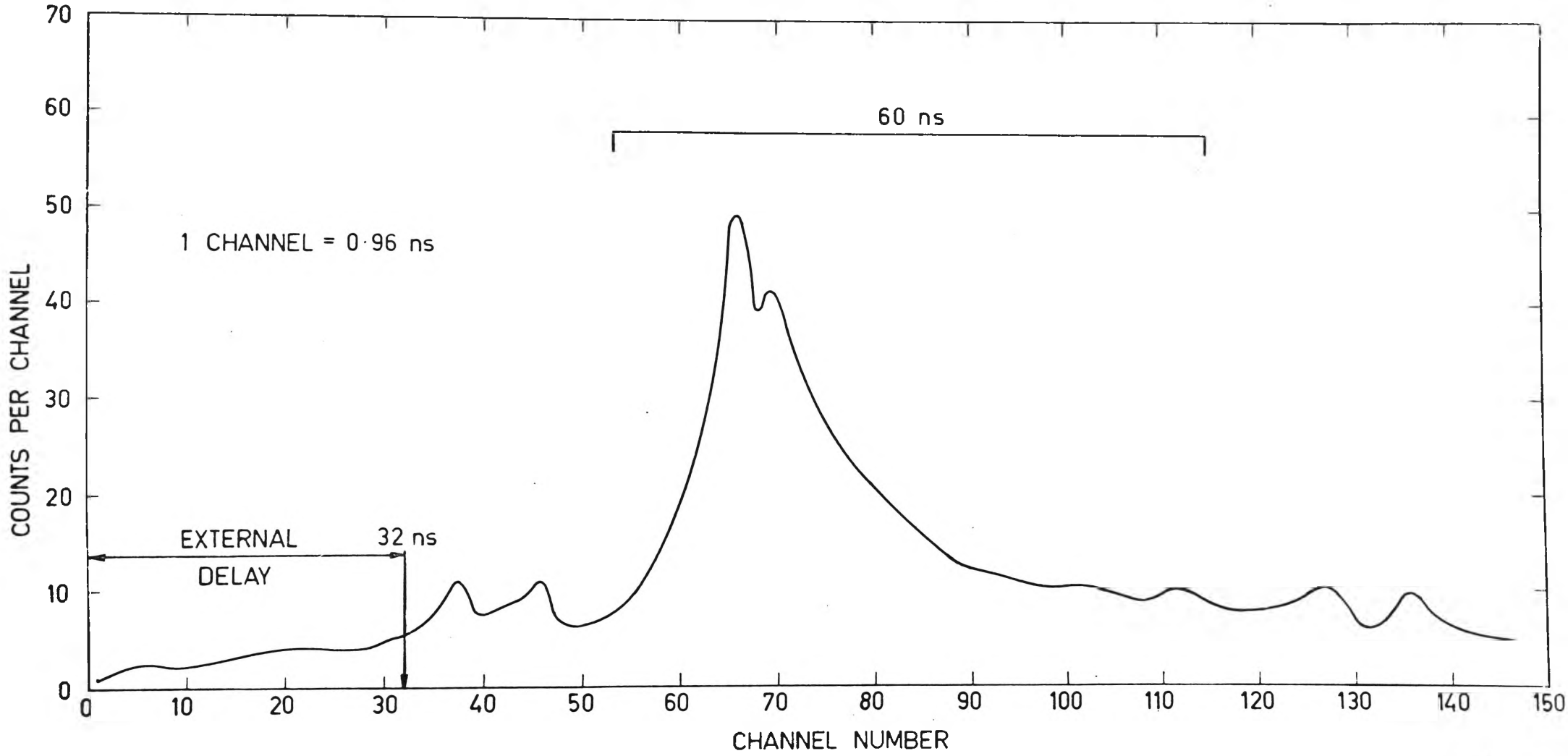

Fig 4·5 TIME DISTRIBUTION OF X-RAY DETECTION FOLLOWING FISSION.

held at $0^{\circ}C$. It was found to be quite important that the thermocouple wires inside the evacuated fission chamber be fairly long, of the order of 40 cm. This minimised penetration of heat from the fission chamber surroundings into the cold junction. The resulting e.m.f. of -5.30 mV indicated an operating point of $-186^{\circ}C$, i.e. 10 K above liquid N_2 temperature.

The two E.M.I. 9618 tubes used were selected for low dark current at the operating bias. The dark currents measured were 0.05 and 0.8 nA for the same gain in the two tubes. The scintillator tank was filled with fresh NE323 liquid, which was then 'bubbled' with dry nitrogen gas. This bubbling removes unwanted oxygen from the liquid, whose presence decreases the tank efficiency.

As mentioned in section 3.3, 30 per cent of K X-rays are emitted within 0.1 ns of fission, 30 per cent between 0.1 and 1 ns, 25 per cent between 1 and 10 ns, and the remainder in two groups of equal intensity with half-lives of 30 and 100 ns[90]. This effect results in a small amount of time 'jitter' between the fragment - X-ray fast coincidence pulse and the peaks of the fragment data line linear pulses. This jitter would cause errors in the ADC recordings of the fragment energies. Figure 4.5 shows the time distribution of detection of an X-ray following a fission event. The fragment fast line fed the 'START' input of an ORTEC 437 time-to-amplitude converter, while the X-ray line fed the 'STOP' input, through an external delay of 32 ns. It is seen that nearly all the later X-rays are detected within about 60 ns of those arriving first. To overcome this time jitter, the fragment linear lines were stretched to ~ 4 μsec width by ORTEC 442 pulse stretchers, with the ADCs being set so

that the peak recording aperture windows opened well into the 'stretched' portion of the linear pulse. Also the fragment fast line was stretched to 300 nsec prior to the fragment-X-ray coincidence requirement. This ensured that the delayed X-ray component was not discriminated against.

4.3 Data Collection

4.3a ν versus Fragment Mass

The $\nu(A)$ data were recorded in a separate run from the $\nu(Z)$ data. As shown in Chapter 5, the $\nu(A)$ results provide a value for the 4π neutron detection efficiency of the scintillator tank. This efficiency value is then used in the analysis of the $\nu(Z)$ data.

With detector 1 at 2.5 cm from the source and detector 2 at 3.2 cm, the coincidence rate in the two detectors was ~200 min^{-1}. The experimental run lasted 2.5 days, which gave ~8 x 10^5 fission events for analysis. Visual inspection of the fragment pulse height spectra for each individual detector before and after the run showed the electronic drifts to be less than 0.3 per cent. The scintillator efficiency was constant to ~2 per cent during the run, as implied from the ~2 per cent variation in scintillator background. The neutron counts observed (corrected for background) were typically 0.15 to 0.3 neutrons per 40 μsec counting gate, with a genuine to background ratio of 1:1.

4.3b ν versus Fragment Charge

The triple coincidence rate between two fragments and an X-ray was extremely low, only 1 every 5 min even with detector 2 situated at the minimum distance of 2.0 cm from the source. Therefore the triple coincidence requirement was dispensed with. The $\nu(Z)$ study was performed with only a double coincidence (between an X-ray and a fragment) needed to

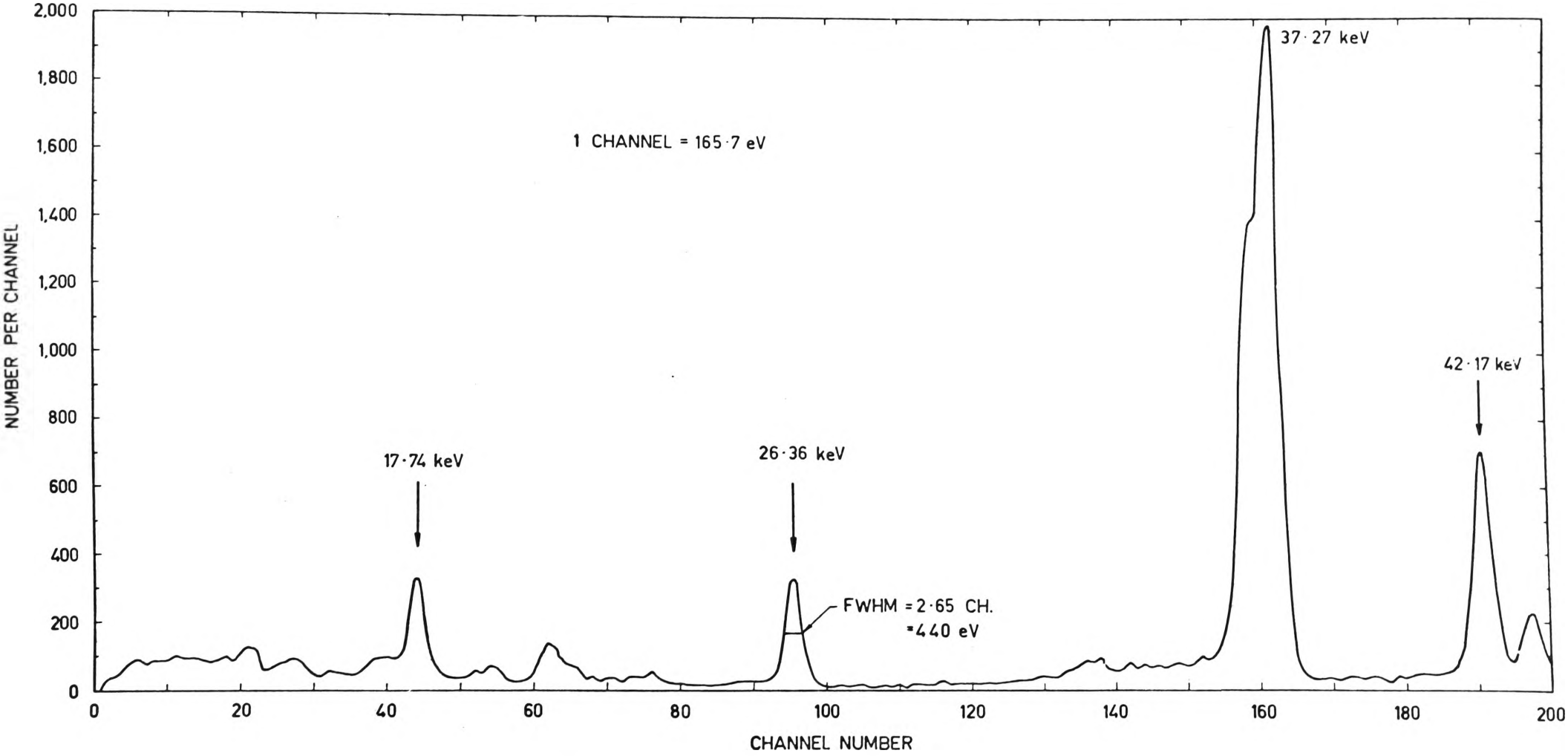

Fig 4.6 TYPICAL ^{241}Am X-RAY LINE CALIBRATION SPECTRUM

strobe the ADCs and MEA. The fragment detector used was detector 2. With this at 2.0 cm from the source, the gross X-ray-fragment coincidence rate was $\sim 5\ min^{-1}$.

A pulser in the X-ray pulse height line served as a check on any gain drifts. Data recording could be stopped at any time and the pulser output monitored in a 512 channel pulse height analyser. Also the pulser output on its own was recorded on the magnetic tape at daily intervals. The X-ray line was found to be stable to ~0.5 per cent over a typical measurement period (7 to 8 days).

Energy calibration of the X-ray pulse height scale was achieved by the use of an ^{241}Am γ ray source. This source could be aimed at the X-ray detector through a thin aluminium window in the fission chamber. The calibration was based on

(i) the 26.36 keV γ ray from $^{241}Am \xrightarrow{\alpha} {}^{237}Np^{*} \xrightarrow[keV]{26.36} {}^{237}Np$. The 59.54 keV γ from americium could not be used as it fell outside the preset acceptance region of the X-ray line ADC (viz 5 to 50 keV);

(ii) the 37.17 keV $K\alpha_1$ and 42.27 keV $K\beta_1$ X-ray lines from neodymium $_{60}Nd$. The americium is encapsulated in neodymium and the Nd $K\alpha_1$ and $K\beta_1$ lines are produced by fluorescence from the 59.54 keV americium line.

The calibration procedure was performed every second day during a data run. Figure 4.6 shows a typical calibration spectrum. The resolution of the 26.36 keV line is 440eV (FWHM).

Every 2 to 3 days, fragment pulse height spectra from detector 2 were recorded. This procedure served to calibrate the fragment line.

The final $\nu(Z)$ data chosen for analysis was based on three separate series of measurements, each series lasting 7 to 8 days. Each particular series consisted of one-day-long $\nu(Z)$ measurements, separated by X line pulser and calibration recordings and by E line calibrations. The individual day-long X-ray spectra in a series were added together off-line on the IBM 360/50 computer to produce a composite X-ray spectrum for that series.

CHAPTER 5

RESULTS AND ANALYSIS

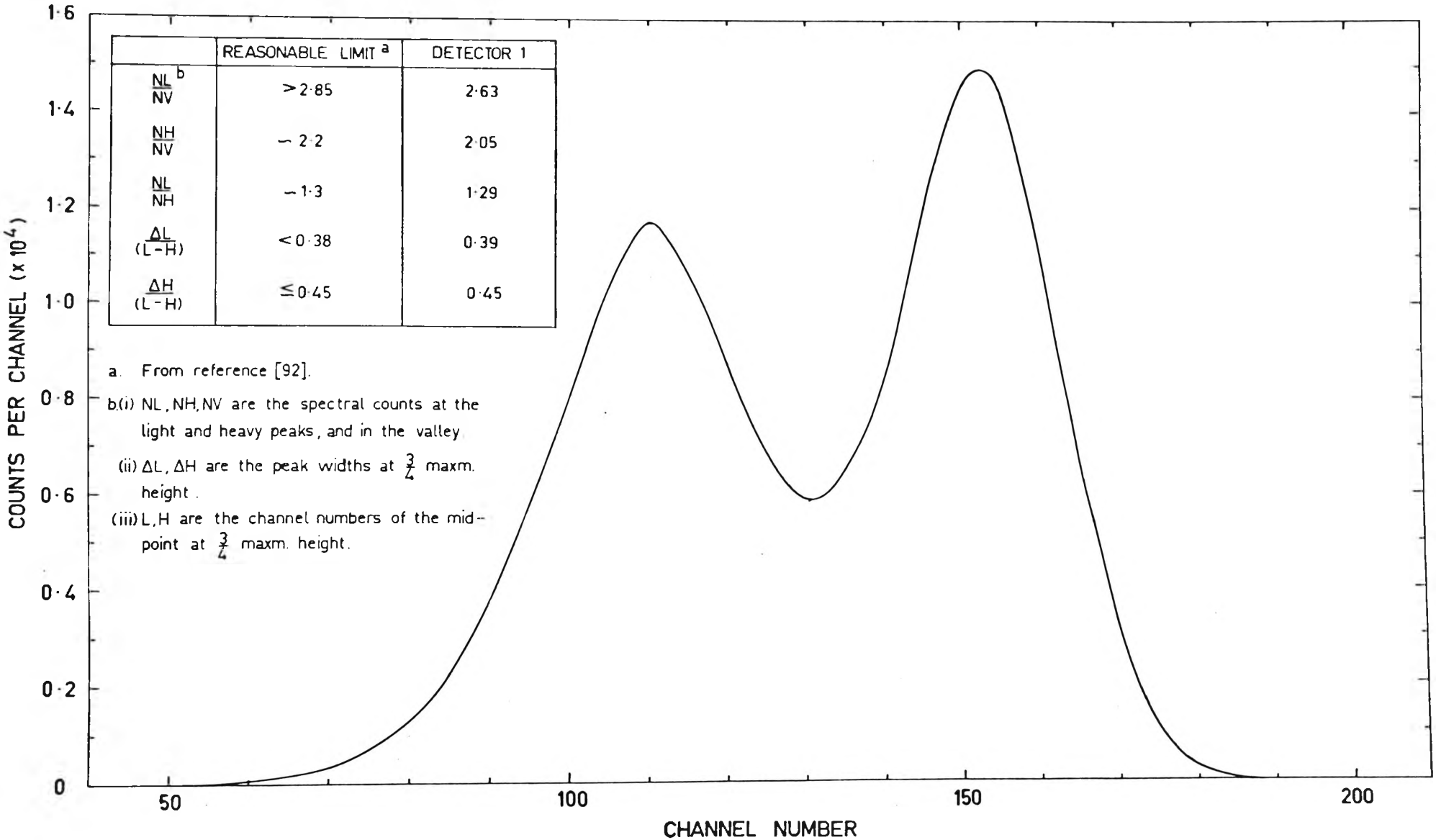

	REASONABLE LIMIT [a]	DETECTOR 1
$\frac{NL}{NV}$ [b]	$>2{\cdot}85$	2·63
$\frac{NH}{NV}$	$\sim 2{\cdot}2$	2·05
$\frac{NL}{NH}$	$\sim 1{\cdot}3$	1·29
$\frac{\Delta L}{(L-H)}$	$<0{\cdot}38$	0·39
$\frac{\Delta H}{(L-H)}$	$\leq 0{\cdot}45$	0·45

a. From reference [92].

b.(i) NL, NH, NV are the spectral counts at the light and heavy peaks, and in the valley

(ii) ΔL, ΔH are the peak widths at $\frac{3}{4}$ maxm. height.

(iii) L, H are the channel numbers of the mid-point at $\frac{3}{4}$ maxm. height.

Fig 5.1 Fragment kinetic energy spectrum for detector 1.

5.1 Mass and Kinetic Energy Study

The raw kinetic energy spectra of the two fragment detectors are shown in Figures 5.1 and 5.2. The spectral characteristics as shown in the figures are similar to the Schmitt values for a 'good' detector[92]. The pre-neutron emission masses and kinetic energies were obtained from the raw kinetic energy data by using the procedures of Schmitt[93] and Terrel[61]. First a linear calibration of the detector pulse height scales was made by using the fragment spectra peak positions and experimental data of Whetstone[94]. For each event, the approximate pre-neutron emission masses M_1 and M_2 were then obtained from the estimated kinetic energies E_1 and E_2 by using the relationships

$$M_1 = \frac{252\ E_2}{E_1 + E_2} \qquad \ldots(5.1)$$

and

$$M_2 = 252 - M_1 \quad . \qquad \ldots(5.2)$$

Post-neutron emission masses were obtained from M_1 and M_2 using the $\nu(M, E_{TOTAL})$ data of Bowman et al.[95] (see Table 5.1). The detector energy scales were recalibrated via the equation

$$E_{POST} = (a + a'\ M_{POST})\ x + b + b'\ M_{POST} \qquad \ldots(5.3)$$

where E_{POST} is the post-neutron emission fragment kinetic energy,

M_{POST} is the post-neutron emission fragment mass,

x is the pulse height in the detector

and a, a', b, b' are constants given in Table 5.2.

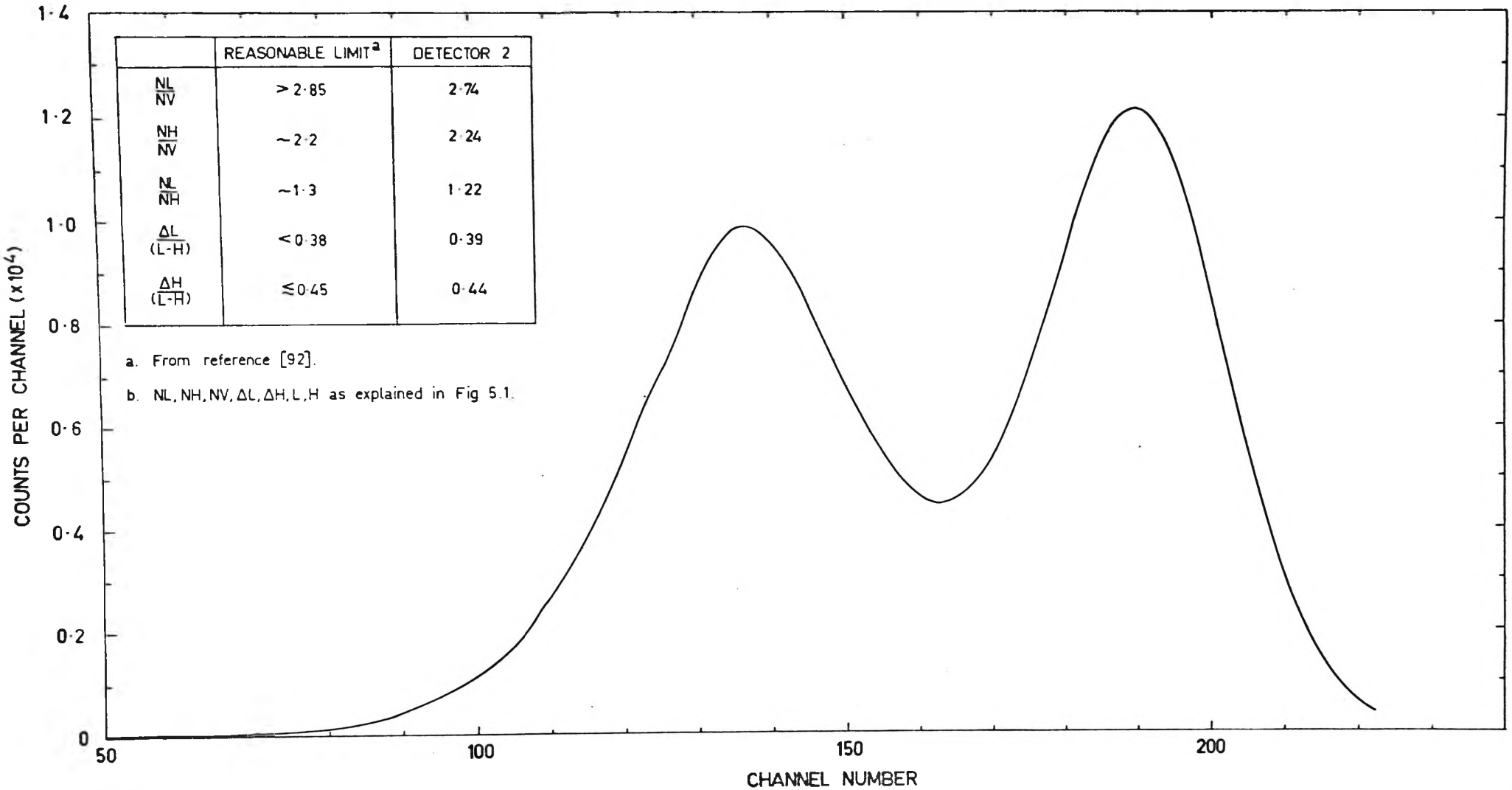

	REASONABLE LIMIT[a]	DETECTOR 2
$\frac{NL}{NV}$	> 2·85	2·74
$\frac{NH}{NV}$	~ 2·2	2·24
$\frac{NL}{NH}$	~ 1·3	1·22
$\frac{\Delta L}{(L-H)}$	< 0·38	0·39
$\frac{\Delta H}{(L-H)}$	≤ 0·45	0·44

a. From reference [92].

b. NL, NH, NV, ΔL, ΔH, L, H as explained in Fig 5.1.

Fig 5·2 Fragment kinetic energy spectrum for detector 2

TABLE 5.1

Matrix showing ^{252}Cf neutron emission as a function of pre-neutron emission fragment mass M and fragment total kinetic energy. Calculated from data of [95].

	K.E. (MeV)										
M	160	165	170	175	180	185	190	195	200	205	210
88	0.0	0.5596	0.6815	0.4386	0.0	0.0	0.0	0.0	0.0	0.0	0.0
90	0.0	0.7550	1.1055	1.1683	0.9153	0.0	0.0	0.0	0.0	0.0	0.0
92	0.0	2.2984	1.3554	1.2849	1.0144	0.0	0.0	0.0	0.0	0.0	0.0
94	0.0	2.5453	1.6867	1.4384	1.1694	0.9980	0.8454	0.0	0.0	0.0	0.0
96	0.0	1.8088	1.9701	1.5678	1.3682	1.0543	0.8315	0.9174	0.0	0.0	0.0
98	0.0	1.9436	1.8399	1.5665	1.2581	1.0422	0.9203	0.8371	0.0	0.0	0.0
100	0.0	2.3048	1.9938	1.6441	1.2629	1.0579	0.8639	0.7275	0.0	0.0	0.0
102	0.0	2.7692	2.3222	1.7650	1.3468	1.0930	0.7151	0.6138	0.6100	0.0	0.0
104	0.0	3.2432	2.6559	1.9968	1.5206	1.2828	0.8667	0.7167	0.5471	0.0	0.0
106	0.0	4.0605	2.9412	2.4517	1.8742	1.4740	1.0570	0.8295	0.6708	0.0	0.0
108	0.0	5.3524	3.5687	2.8867	2.3135	1.7402	1.3066	1.0034	0.8277	0.7905	0.0
110	0.0	6.7181	4.4067	3.1327	2.6829	2.0179	1.5452	1.1949	0.9275	0.8404	0.0
112	0.0	4.6849	4.0484	3.6193	3.2126	2.5211	1.9420	1.5662	1.3578	0.9283	0.0
114	0.0	4.2531	4.7488	4.5271	3.7991	2.8776	2.2574	1.7280	1.3611	1.3060	0.0
116	0.0	0.0	5.9567	5.4750	4.1024	3.2871	2.6011	2.1179	1.7001	1.6074	0.0
118	0.0	0.0	6.6358	6.1020	4.3454	3.8327	3.0817	2.7566	2.2204	1.8931	0.0
120	0.0	5.5468	5.5394	6.5517	5.0636	4.5832	3.8064	3.4696	2.4784	2.3352	0.0
122	0.0	3.0419	5.0124	5.2979	4.8413	4.3443	3.9481	3.8249	3.4960	3.0364	0.0
124	0.0	0.3250	3.8700	4.3682	3.7637	3.1407	2.7300	2.4129	2.1000	0.0	0.0
126	0.0	0.0	2.7200	3.5226	2.7841	2.0465	1.5423	1.1293	0.5500	0.0	0.0
128	0.0	0.5500	2.7000	2.8804	2.2220	1.7705	1.1102	0.7098	0.2000	0.0	0.0
130	0.0	1.2800	3.0400	2.3058	1.7992	1.7673	1.9159	0.5781	0.2400	0.0	0.0
132	0.0	2.0250	3.4000	1.7312	1.3764	1.7642	0.7216	0.4465	0.2900	0.0	0.0
134	0.0	0.0	2.8488	1.5572	1.3558	1.0182	0.7817	0.5061	0.3689	0.0	0.0
136	0.0	2.7148	2.2824	1.8251	1.6680	1.4119	1.0637	0.7642	0.5414	0.4612	0.0
138	0.0	3.7595	3.2690	2.1173	1.8233	1.5434	1.2522	0.9949	0.8109	0.7082	0.0
140	0.0	2.8693	2.4789	2.2752	1.9514	1.5908	1.2646	1.0442	0.9771	0.7571	0.0
142	0.0	3.2774	2.7997	2.4676	2.0451	1.6292	1.3036	1.0448	0.9297	0.8736	0.0
144	0.0	3.9674	3.0567	2.5488	2.1161	1.6337	1.3225	1.0667	0.9115	0.8100	0.0
146	0.0	4.4182	3.2156	2.6040	2.1434	1.6561	1.3277	1.1321	0.9342	0.0	0.0
148	0.0	4.2022	3.3055	2.7581	2.1971	1.7486	1.3368	1.2400	0.9843	0.0	0.0
150	0.0	4.1139	3.6423	2.7034	2.1828	1.8575	1.4350	1.2918	0.9865	0.0	0.0
152	0.0	4.0869	3.3396	2.9250	2.3543	1.8926	1.4983	1.3784	1.0562	0.0	0.0
154	0.0	4.1432	3.1984	3.0067	2.4460	1.9549	1.6047	0.0	0.0	0.0	0.0
156	0.0	4.3444	3.4239	2.7848	2.3493	2.0495	1.7597	0.0	0.0	0.0	0.0
158	0.0	4.8460	3.5312	3.1893	2.7983	2.0907	1.8554	0.0	0.0	0.0	0.0
160	0.0	5.0989	3.8428	3.4014	3.0316	2.1539	0.0	0.0	0.0	0.0	0.0
162	0.0	5.0157	4.3967	3.3523	3.5501	2.2416	0.0	0.0	0.0	0.0	0.0
164	5.3500	6.6500	5.3000	3.0600	2.8400	0.0	0.0	0.0	0.0	0.0	0.0
166	0.0	0.0	2.7300	2.9500	0.0	0.0	0.0	0.0	0.0	0.0	0.0

TABLE 5.2

DETECTOR CALIBRATION CONSTANTS

P_L and P_H are the observed pulse heights corresponding to the mid points between the 3/4 maximum points in the light and heavy mass groups.

$a = \frac{24.0203}{P_L - P_H}$	$a' = \frac{0.03574}{P_L - P_H}$
$b = 89.6083 - aP_L$	$b' = 0.1370 - a'P_L$

The re-calculated post-neutron emission kinetic energies were converted into pre-neutron emission energies via

$$E_{PRE} = E_{POST}\left(1 + \frac{\nu}{M_{POST}}\right) \quad , \qquad \ldots(5.4)$$

again making use of the $\nu(M, E_T)$ data of Table 5.1. The entire process was repeated until the pre-neutron emission masses before and after a particular iteration were the same to within 0.1 amu. The output data for each particular fission event consisted of pre-neutron emission masses and total kinetic energy, plus neutron and background data.

The two major corrections to the data are the scintillator geometry and backscatter corrections. The first of these describes the effect of the particular neutron detection geometry used on the observed neutron detection numbers. Assuming isotropic neutron emission in the C.M.S., the laboratory neutron distribution with respect to fragment direction is[18]

$$\rho_i(V_i, \theta) = \frac{a^2 v_i}{T_i^2} V_i^2 \sin\theta \exp\left(-\frac{a v_i^2}{T_i}\right) \qquad \ldots(5.5)$$

where

V_i is the laboratory velocity of the neutrons

v_i is the neutron centre of mass velocity

$a = 0.5228$

θ is the neutron emission angle with respect to the fragment direction

T_i is the evaporation temperature of fragment i (data of [96]).

V_i is given by

$$V_i^2 = v_i^2 - W_i^2 + 2v_i W_i \cos\theta \qquad \ldots(5.6)$$

where W_i is the laboratory velocity of fragment i (data of [94]).

The scintillator tank subtends $\pm 29.7^\circ$ with respect to the fission source. Thus the probability of forward neutron emission from fragment i into the scintillator geometry is

$$P_{i1} = \int_0^{\infty} \int_0^{29.7^\circ} \rho_i(V_i,\theta)\, dV_i\, d\theta \qquad \ldots(5.7)$$

The backscatter correction relates to backward neutron emission into the scintillator geometry from a fragment travelling away from the tank. For complementary masses M_1 and M_2, if $P_1(M_1,E_T)$ and $P_2(M_2,E_T)$ are the experimentally observed neutron detection numbers, then

$$P_1(M_1,E_T) = \nu_1\, \varepsilon\, P_{11}(M_1,E_T) + \nu_2\, \varepsilon\, P_{22}(M_2,E_T) \qquad \ldots(5.8)$$

and

$$P_2(M_2,E_T) = \nu_2\, \varepsilon\, P_{21}(M_2,E_T) + \nu_1\, \varepsilon\, P_{12}(M_1,E_T) \qquad \ldots(5.9)$$

where ν_1 and ν_2 are the neutron emission numbers per fission from complementary fragments,

ε is the liquid scintillator efficiency

and P_{i1}, P_{i2} are the forward and backward neutron emission probabilities from fragment i (as above).

Equations (5.8) and (5.9) are solved simultaneously to obtain $\varepsilon\nu_i(M_i,E_T)$. Averaging over the kinetic energy distribution then gives $\varepsilon\nu_i(M_i)$.

The geometry and backscatter corrections assumed (a) that the excitation energies of the two fragments are correlated, and (b) that ε is independent of neutron energy. To apply the corrections, the raw data was sorted into a matrix of mean neutron emission numbers per event for mass groups 2 amu wide and for total kinetic energy groups 5 MeV wide. Dead time losses were ignored as they involved a correction of less than one per cent. Firstly, an approximate correction for geometry and backscatter was made assuming that <u>all</u> the neutrons are emitted from the moving fragments. The data obtained were normalised to $\bar{\nu}_p$ (^{252}Cf) = 3.724[97]. This gave an approximate value of the average scintillator detection efficiency and the variation of the total neutron emission ν_T with fragment mass. Assuming that 15 per cent of the neutrons are emitted isotropically in the laboratory system (that is, the scission neutrons[18]), the experimentally observed numbers were adjusted accordingly to remove this component. The remaining component was corrected for detector geometry and backscatter and the variation of $\varepsilon\nu_F$ with fragment mass obtained. Here ν_F refers only to the non-scission component. Assuming that for a particular mass division, the scission neutrons are emitted from the two fragments in the same proportions as those from the moving fragments, the total neutron emission ν from a particular fragment is given by

$$\varepsilon\nu = \frac{\varepsilon\nu_F}{0.85} \qquad \ldots(5.10)$$

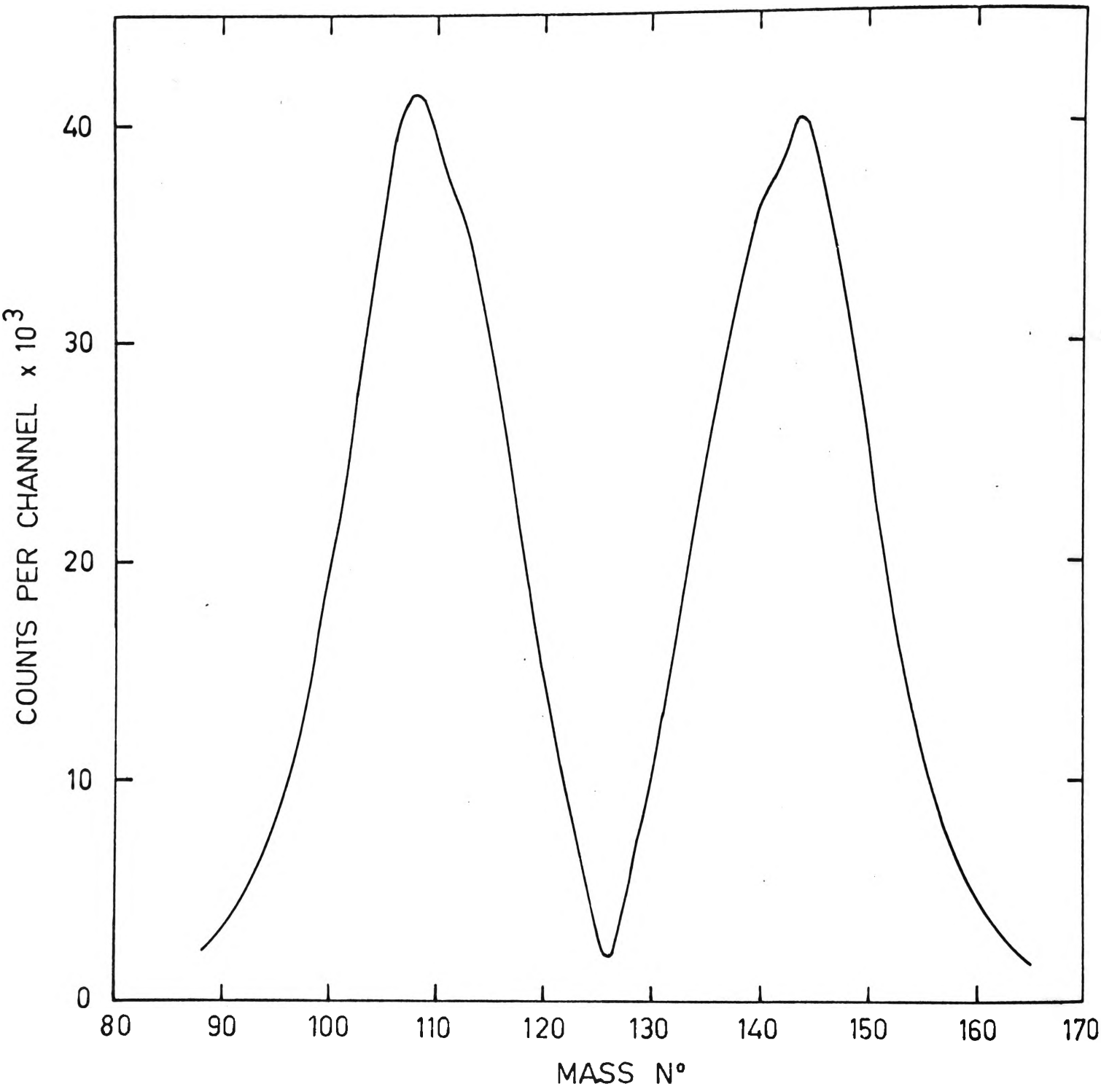

Fig 5·3 Pre-neutron emission mass distribution for ^{252}Cf.

The data were normalised again to $\bar{\nu}_p(^{252}Cf) = 3.724$. It was found unnecessary to repeat the process with the more accurate ν_T and scintillator efficiency data, as subsequent corrections changed the final data by less than one per cent. The scintillator 4π efficiency was found to be 50.2 per cent.

The whole analysis procedure described above was performed off-line on an IBM 360/50 computer using the programs MASSIVE, PCALC and GEOMC. MASSIVE applied the Schmitt detector calibration procedure (equations 5.1 through 5.4) to the raw data and produced the matrix of observed neutron counts per event for mass groups 2 amu wide and total kinetic energy groups 5 MeV wide. PCALC calculated the geometry neutron emission probabilities P_{i1} and P_{i2} (equation 5.7) for each mass and total kinetic energy group. GEOMC applied the geometry and backscatter corrections (equations 5.8 and 5.9). It also corrected for the scission neutron contaminant.

MASSIVE is a lengthy program involving a large amount of computer time - over two hours of central processor time to analyse 800,000 fission events. About two months of software effort was spent in restructuring MASSIVE from an earlier, outmoded form. The analysis of both the $\nu(A)$ and $\nu(Z)$ data was performed after all the experimental runs were finished and took about five months to complete.

The pre-neutron emission mass distribution obtained is shown in Figure 5.3 (uncorrected for mass resolution). 'Shoulders' can be seen at masses 112 and 140, in excellent agreement with the more accurate time of flight mass yield data[65,94]. The (light) fragment peak-to-valley ratio of 20.7:1 is similar to that reported in other surface barrier mass yield work, viz, 19.2 by Stein[65] and 30.0 by Schmitt et al.[98] (mass yield curves uncorrected for mass resolution). These values are all significantly

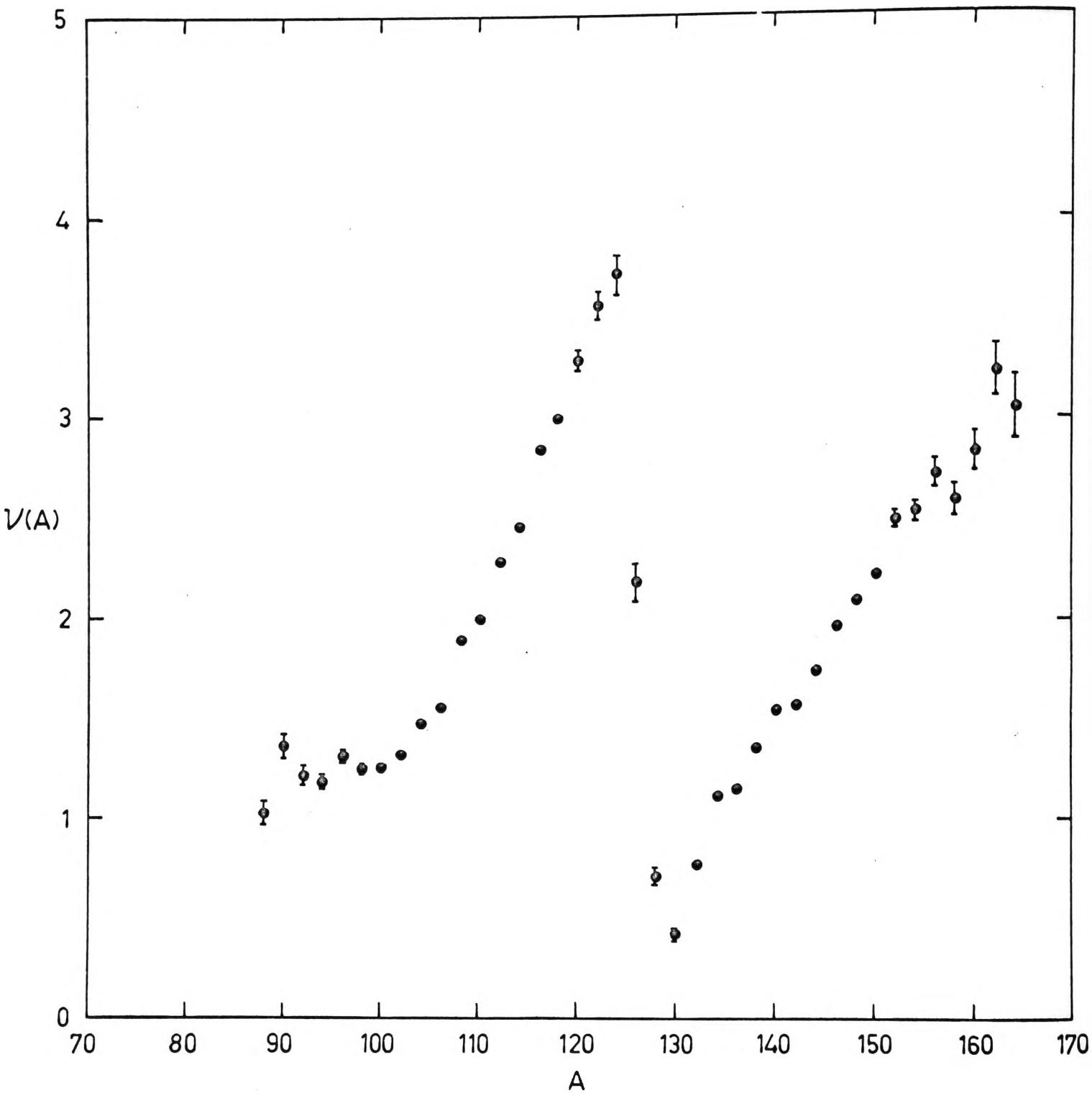

Fig 5.4 Neutron emission versus fragment mass.

lower than the value of around 60:1 found by time of flight methods. The reason for this is the poorer mass resolution near symmetry associated with double-energy measurements; probably ± 4 to 5 amu compared with $\pm$ 3 amu for double-velocity measurements. If a mass resolution correction is made to the double-energy data[98] the peak-to-valley ratio is seen to approach that of the double-velocity studies.

The $\nu(A)$ results of this work are listed in Table 5.3 and shown in Figure 5.4. The errors given are the statistical errors. No correction for mass resolution has been applied. Figure 5.5 shows the present results compared with the early time of flight data of Whetstone[62], the later, more accurate, time-of-flight data of Bowman, Milton et al.[63] and the indirect data of Terrel[61]. The general agreement between the Bowman and Terrel data and the present data is good. In particular, the Bowman high neutron emission values at masses ~120 to 124 are reproduced in the present work. This may be contrasted with the situation for neutron induced fission of ^{235}U wherein the recent double-energy measurements[14,55] did not find the high neutron emission values at the light fragment sawtooth peak which were reported in the ^{235}U time of flight work of Milton and Fraser[66].

The data of Figure 5.4 show humps at masses 90 and 96 for the light fragment and at mass 156 for the heavy fragment. The Bowman et al. data (Figure 5.5) also has a maximum at mass 96, though no such effect at mass 90. Milton and Fraser, in their ^{235}U study[66], reported significant maxima at masses 90, 96 and 101. It is important to note that these masses correspond exactly to the location of the fine structure peaks observed in the ^{252}Cf and ^{235}U mass yield curves[67].

TABLE 5.3

MEASURED AVERAGE NEUTRON EMISSION VERSUS FRAGMENT MASS[c]

Mass No.A	$\nu(A)$[a]	Mass No.A	$\nu(A)$	$\nu_{TOTAL}(A)$[b]
88	1.02 ± 0.06	164	3.05 ± 0.16	4.07 ± 0.17
90	1.36 ± 0.06	162	3.23 ± 0.13	4.59 ± 0.14
92	1.21 ± 0.05	160	2.83 ± 0.10	4.04 ± 0.11
94	1.18 ± 0.04	158	2.59 ± 0.08	3.77 ± 0.09
96	1.31 ± 0.03	156	2.72 ± 0.07	4.03 ± 0.08
98	1.24 ± 0.03	154	2.53 ± 0.05	3.77 ± 0.06
100	1.25 ± 0.02	152	2.49 ± 0.04	3.74 ± 0.04
102	1.32 ± 0.02	150	2.22 ± 0.04	3.54 ± 0.04
104	1.47 ± 0.02	148	2.09 ± 0.03	3.56 ± 0.04
106	1.55 ± 0.02	146	1.96 ± 0.03	3.51 ± 0.04
108	1.88 ± 0.02	144	1.73 ± 0.02	3.61 ± 0.03
110	1.99 ± 0.02	142	1.56 ± 0.02	3.55 ± 0.03
112	2.28 ± 0.03	140	1.54 ± 0.02	3.82 ± 0.04
114	2.46 ± 0.03	138	1.35 ± 0.02	3.81 ± 0.04
116	2.84 ± 0.04	136	1.14 ± 0.03	3.98 ± 0.05
118	2.99 ± 0.04	134	1.12 ± 0.03	4.11 ± 0.05
120	3.28 ± 0.05	132	0.76 ± 0.03	4.04 ± 0.06
122	3.55 ± 0.07	130	0.42 ± 0.03	3.97 ± 0.08
124	3.70 ± 0.10	128	0.71 ± 0.04	4.41 ± 0.11
126	2.17 ± 0.09	126	2.17 ± 0.09	4.34 ± 0.13

(a) The errors shown are statistical errors only, owing to the difficulty of calculating any errors that might be associated with the backscatter and geometry corrections. These latter are expected to be slight in any case.

(b) Total neutron emission from both fragments versus heavy fragment mass.

(c) Data normalised to $\bar{\nu}_p$ (^{252}Cf sp.) = 3.724.

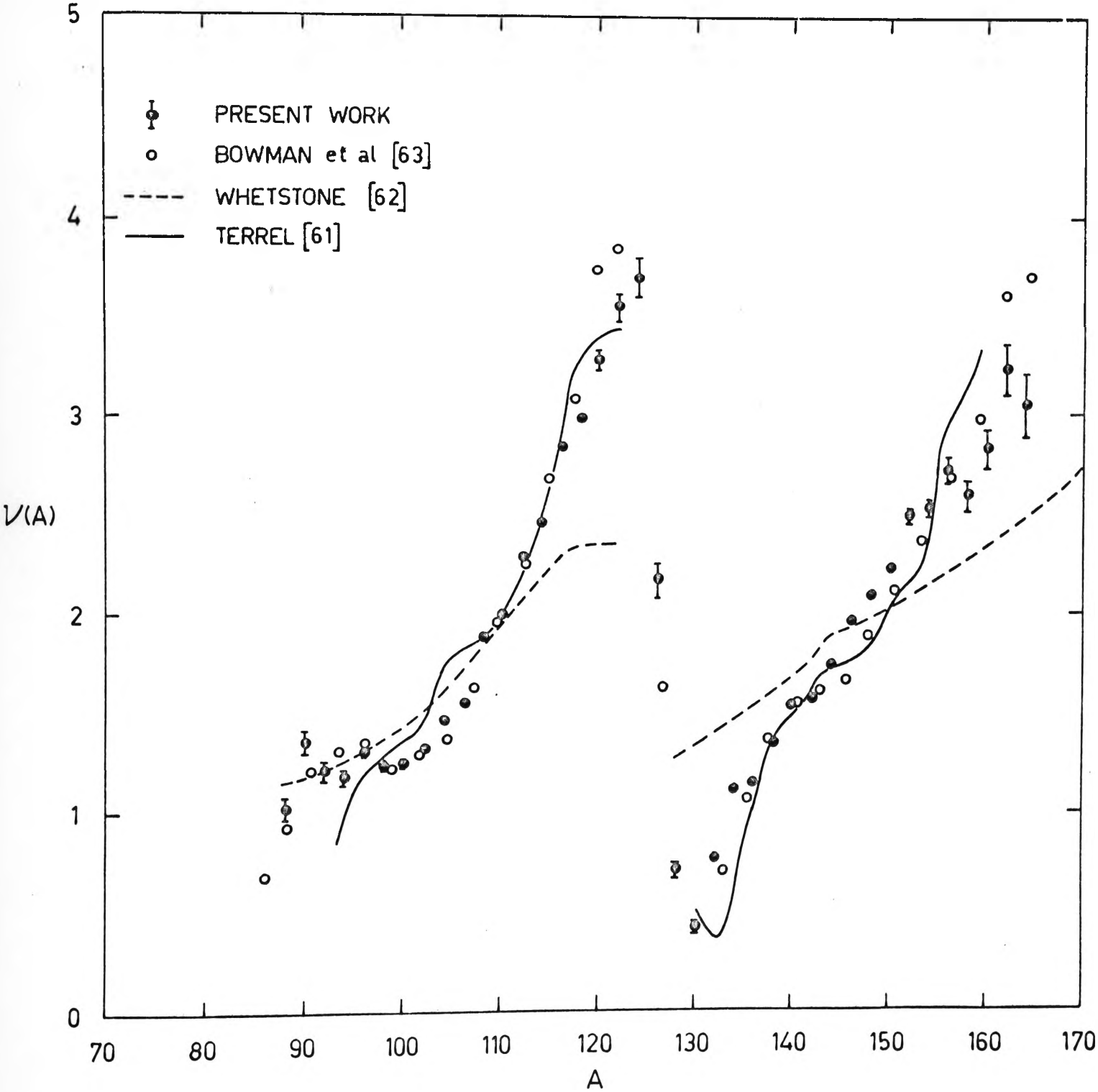

Fig 5.5 Neutron emission versus fragment mass – present work + others.

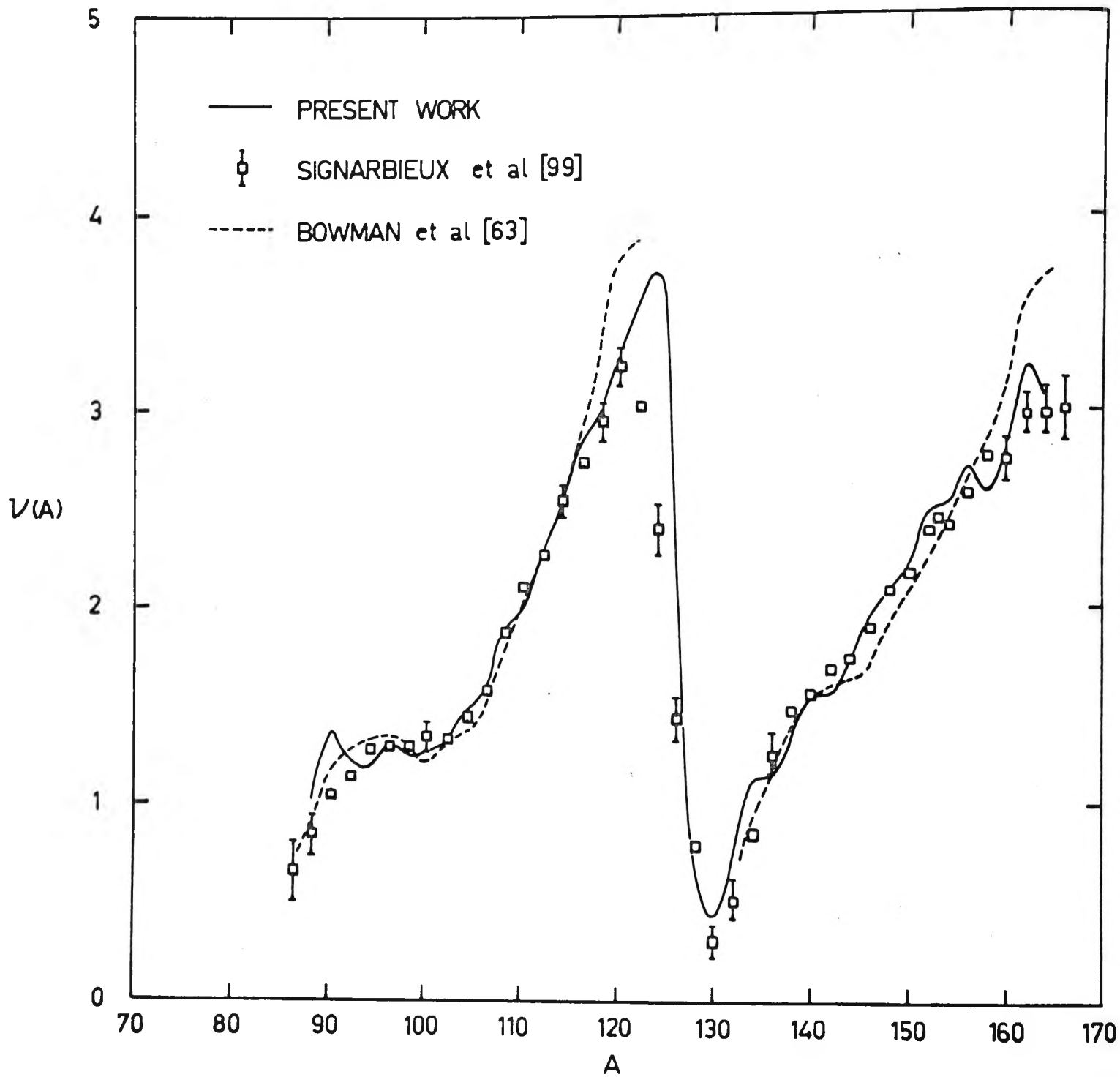

Fig. 5.6 Neutron emission versus fragment mass — present work + others.

As mentioned in section 3.1, the data of Bowman et al., and to a lesser degree the indirect data of Terrel, imply a flattening of the $\nu(A)$ curve for the heavy fragment in the mass region 140 to 146, i.e. a 'plateau' in the region of the most probable mass yield. The present data show no real evidence of this flattening.

The ratio of the neutron emission from the light fragment to that from the heavy fragment was found to be $\nu_L/\nu_H = 1.195 \pm 0.005$, where the error is the statistical error. Whetstone[62] reported 1.02 ± 0.02, while Bowman et al.[63] reported 1.17 ± 0.03. Thus the present value confirms the Bowman result. $\nu_L/\nu_H \sim 1.2$ agrees with the values of 1.15 to 1.25 found in the majority of ^{235}U studies[14,55,64].

Figure 5.6 compares the present results with the recent data of Signarbieux et al. at Saclay[99]. These authors carried out a double-energy ^{252}Cf study very similar in design to the present experiment. Also shown for comparison in Figure 5.6 is the data of Bowman et al.[63]. Both the Signarbieux and Bowman data sets have been corrected for mass resolution. Over most of the range the agreement between the Signarbieux data and the present work is excellent. The Signarbieux data, however, misses the high neutron emission values at masses 120 to 124, their data decreasing rapidly after mass 120. Also Signarbieux et al. do not report any humps at masses 90 and 96. Their data does contain a suggestion of a hump at mass 158 however, which is close to the hump at mass 156 in the present data. In like fashion to this work, the Signarbieux data has no 'plateau' in the mass region 140 to 146. The Bowman data show a smoother $\nu(A)$ variation than is observed in the other two data sets.

The total neutron emission from both fragments as a function of the mass of the heavy fragment $\nu_T(A)$ is given in Figure 5.7 for the present

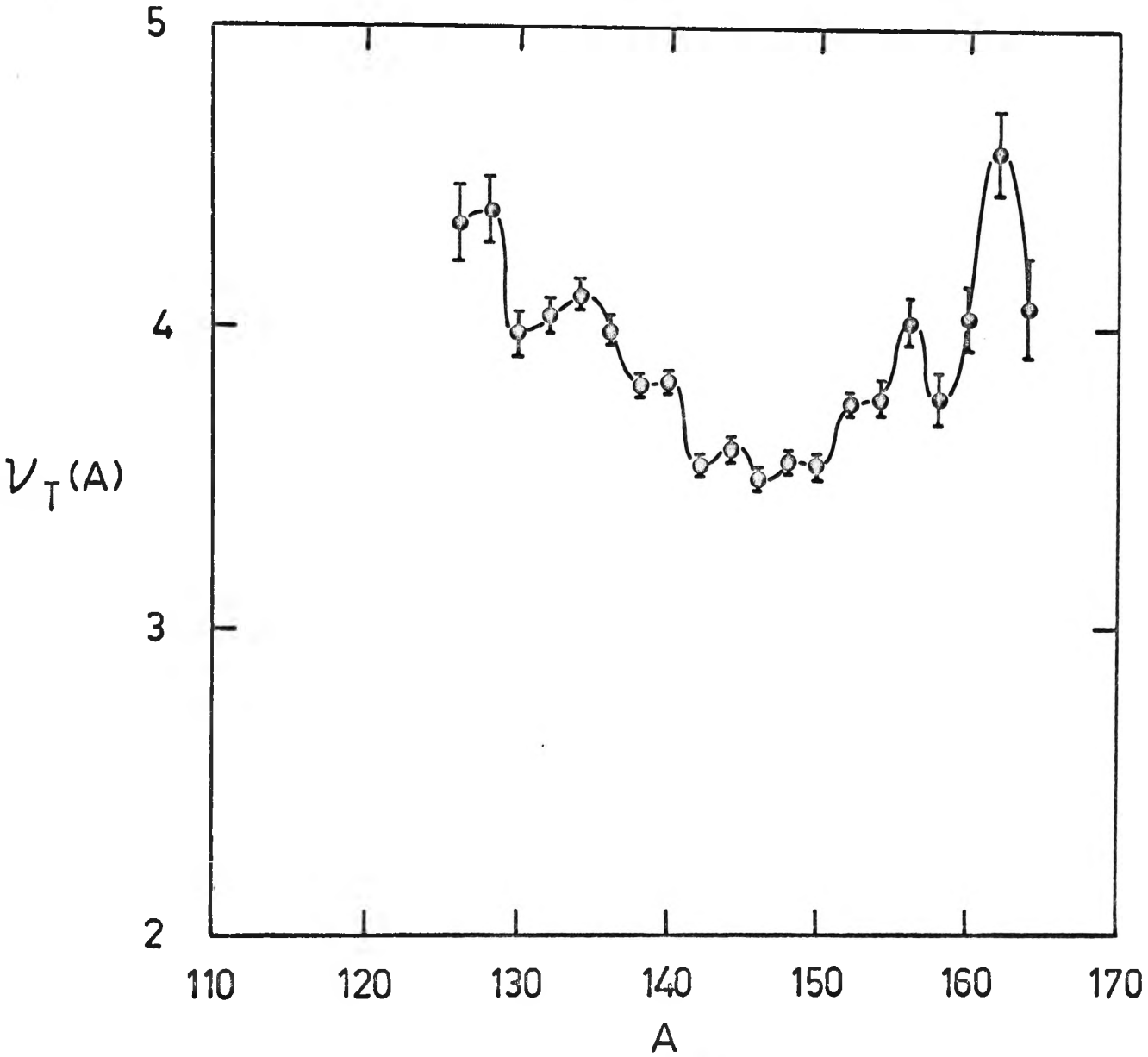

Fig 5.7 Total neutron emission versus mass of heavy fragment.

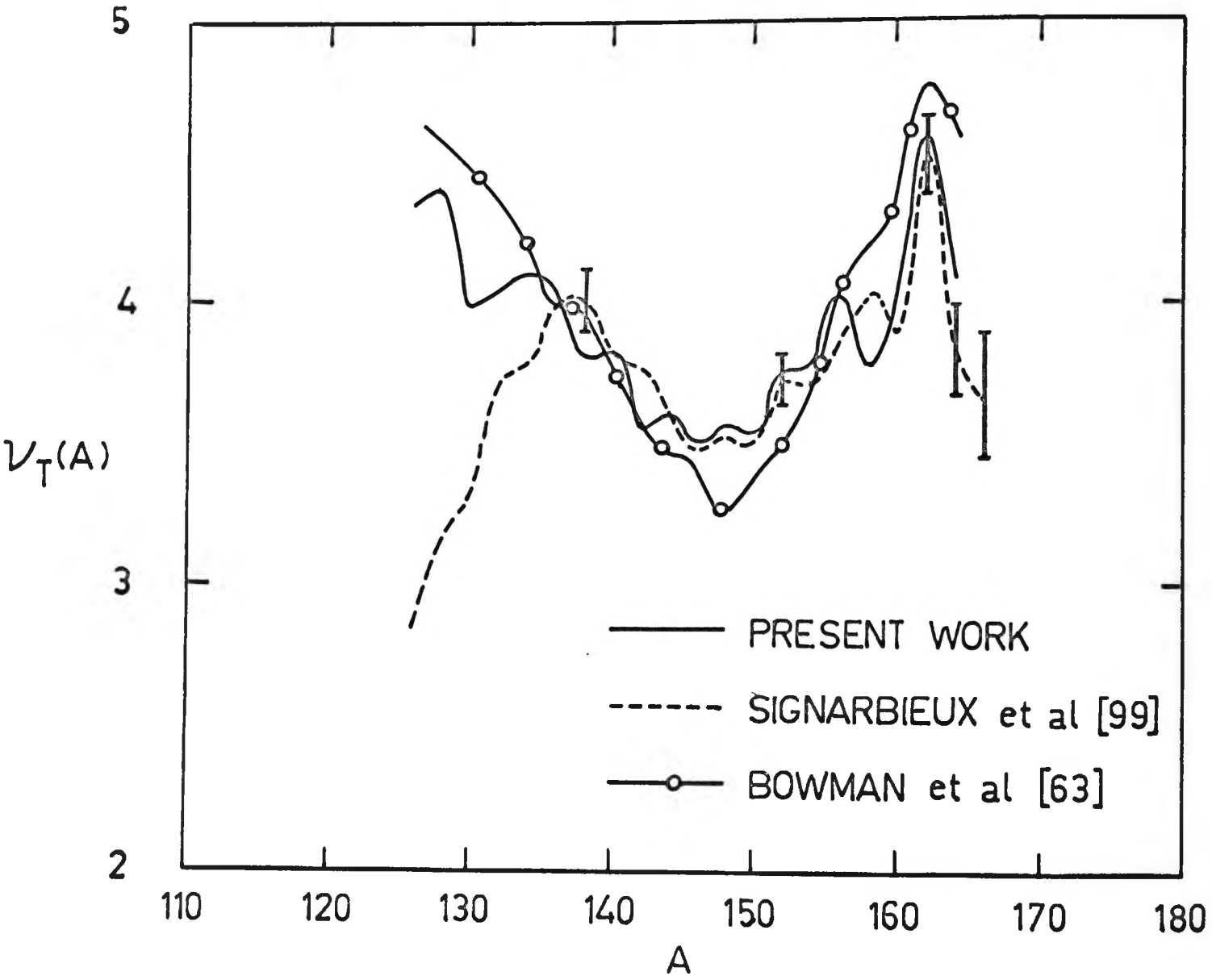

Fig 5·8 Total neutron emission versus heavy fragment mass – present work + others.

work. This curve is obtained by adding together the complementary $\nu(A)$ values from the light and heavy fragment groups (Table 5.3). Figure 5.8 shows the $\nu_T(A)$ curves for the three data sets of Figure 5.6. A few of the error bars of the Signarbieux work are shown. For masses $\gtrsim 135$, the Signarbieux ν_T data are in good agreement with the present work, as is to be expected in view of their similarity in Figure 5.6. Below mass 135 the Signarbieux curve falls away markedly. This anomalous behaviour is a direct result of the low neutron emission values reported by these authors for the light group for masses >120.

Of major interest in Figure 5.7 are the humps associated with the present data. These humps occur at masses 134, 140, 144, 148, 152, 156 and 162. Five of these seven locations, viz, 134, 140, 152, 156 and 162 correspond exactly to the locations of the fine structure peaks observed in the ^{252}Cf and ^{235}U mass yield curves[67]. The mass yield curves display a fine structure peak at mass 146 also. This peak is not reproduced in the present ν_T data. The Signarbieux et al. ν_T curve (Figure 5.8) also displays humps at masses 148, 152 and 162, in close agreement with the present work. Further, their data show a peak at mass 158, which is near the peak at mass 156 of this work. In fact, for masses >146, the agreement in the ν_T shape between this work and that of Signarbieux et al. is outstanding.

The early time-of-flight data of Whetstone[62] also contain evidence of $\nu(A)$ peaks at masses ~156 and ~162. (The Whetstone curve given in Figure 5.5 merely shows the general trend of his data. The $\nu(A)$ peaks in Whetstone's data can be seen in Figures 2 and 3 of reference (61)). Again, the Bowman ν_T behaviour in Figure 5.8 is much smoother

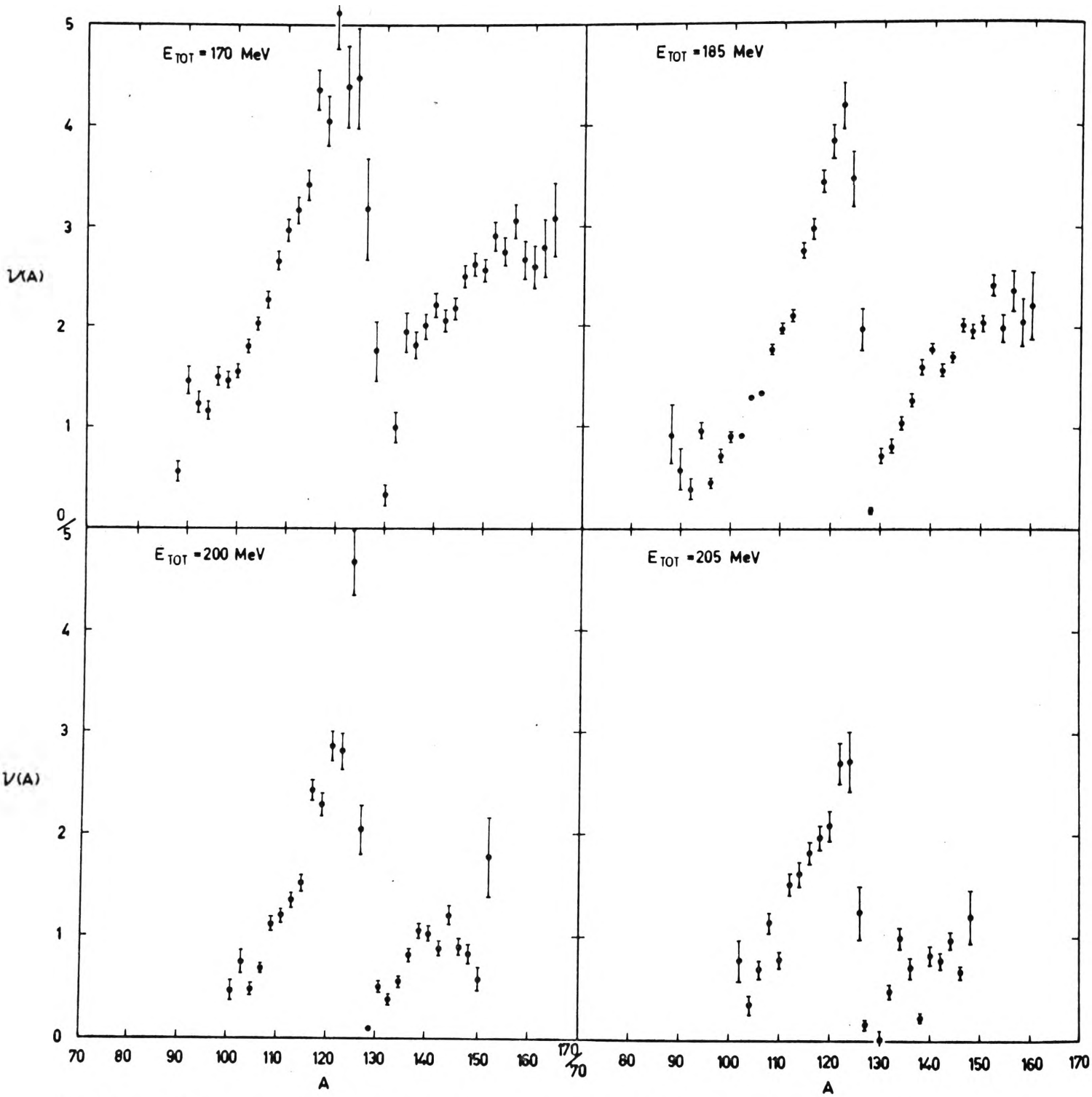

Fig 5.9 Neutron emission versus fragment mass for four regions of fragment total kinetic energy.

than the other two curves, while still giving good agreement overall.

The $\nu(A)$ behaviour for particular total kinetic energy regions is given in Figure 5.9. It may be seen that the basic sawtooth shape is preserved over the full range of kinetic, and hence excitation, energies. A flattening of the heavy fragment $\nu(A)$ curve above mass ~140 becomes apparent as the total kinetic energy increases. This flattening has also been observed by Bowman et al.[63] for ^{252}Cf and by others for ^{235}U[14,55]. It is thought that this flattening is caused by increased de-excitation competition from low energy gamma transitions[55].

The total neutron emission from both fragments is plotted as a function of the total kinetic energy E_T in Figure 5.10 and listed in Table 5.4. A least squares fit to the data points gives $dE_T/d\nu_T$ = -13.7 MeV per neutron. This may be compared with the Bowman[63] value of about -6.6 MeV per neutron and values of -16.7 and -18.5 MeV per neutron from ^{235}U results[14,55].

The average total kinetic energy of ^{252}Cf fission fragments was found in this work to be 183 $\pm$ 1.5 MeV, a value intermediate between the 182.1 MeV result of Fraser et al.[67] and the 185.7 MeV result of Whetstone[94], both of which were time-of-flight experiments.

The variation of total fragment kinetic energy with heavy fragment mass is given in Figure 5.11. The 4 MeV 'dip' at symmetry is markedly smaller than the corresponding dip of about 30 MeV found for ^{235}U, ^{233}U and ^{239}Pu[100]. Milton and Fraser[101] found a dip for ^{252}Cf of about 5 MeV by the time-of-flight method, as did Gibson, Thomas and Miller[102] using semiconductor counters. However, the time-of-flight measurement of Whetstone[94] found a kinetic energy dip of 25 MeV for ^{252}Cf. Above mass

TABLE 5.4

MEASURED TOTAL NEUTRON EMISSION VERSUS TOTAL FRAGMENT KINETIC ENERGY[b]

E_{TOTAL} (MeV)	ν_{TOTAL} [a]
160	5.65 ± 0.02
165	5.253 ± 0.016
170	4.769 ± 0.012
175	4.340 ± 0.010
180	4.074 ± 0.009
185	3.608 ± 0.008
190	3.261 ± 0.008
195	2.877 ± 0.008
200	2.494 ± 0.010
205	2.287 ± 0.014
210	1.98 ± 0.02

(a) Errors shown are statistical errors

(b) Data normalised to $\bar{\nu}_p$ (^{252}Cf sp.) = 3.724

130 the three data sets[101,102,94] are similar, and are in good agreement with the curve of Figure 5.11.

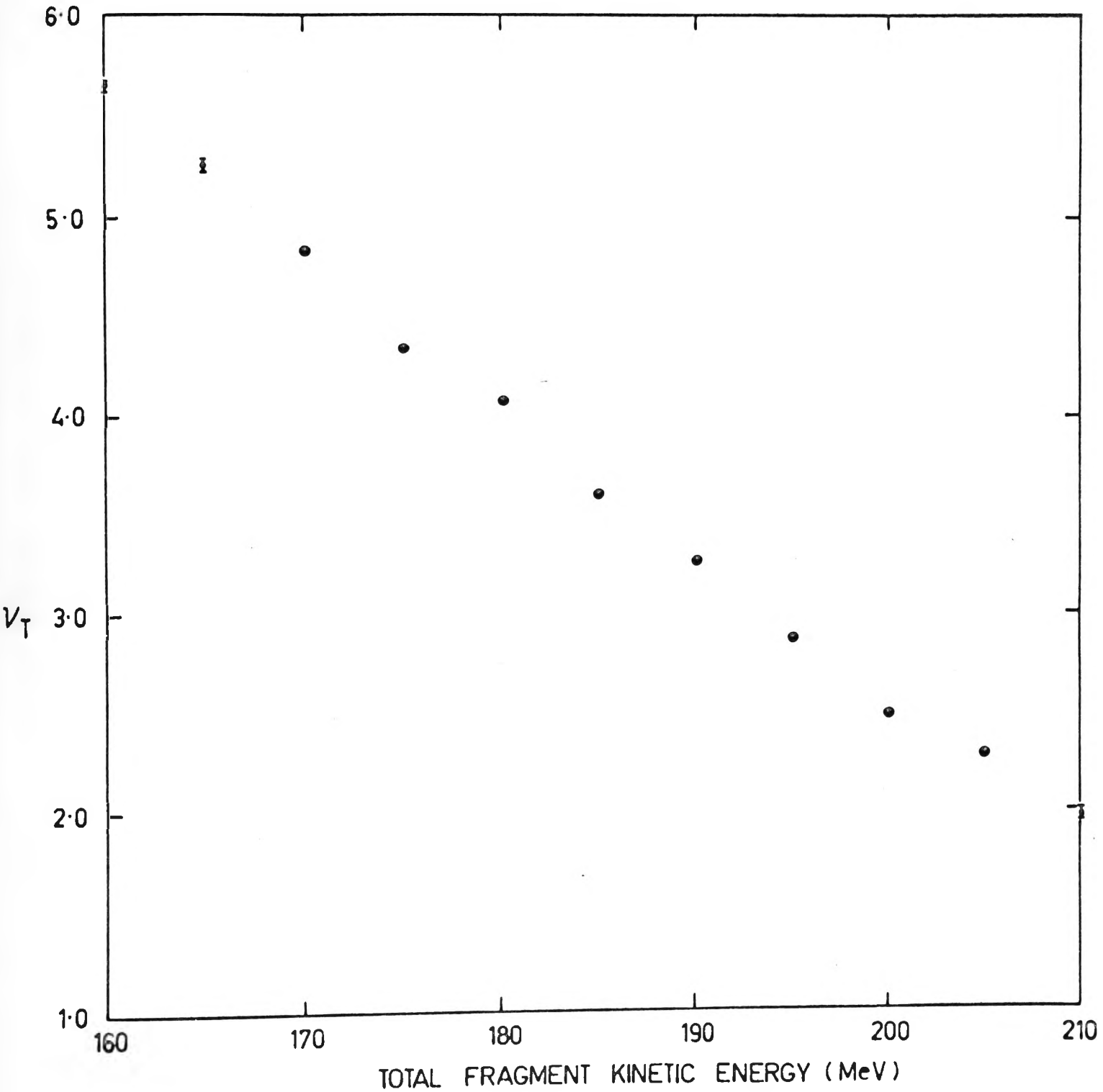

Fig 5.10 Total neutron emission versus total fragment kinetic energy. Where errors are not shown they are smaller than the points.

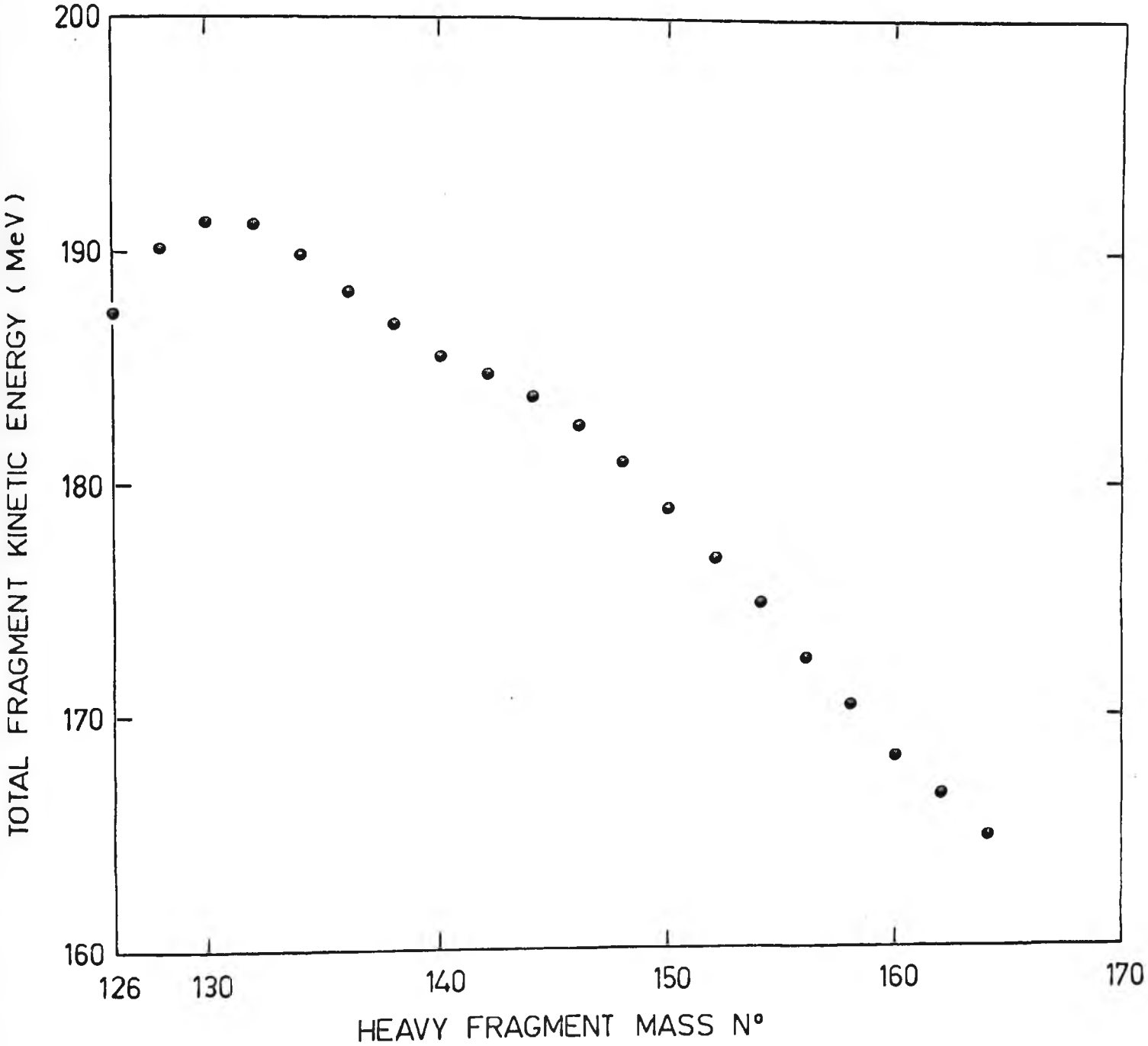

Fig 5.11 Total fragment kinetic energy versus heavy fragment mass

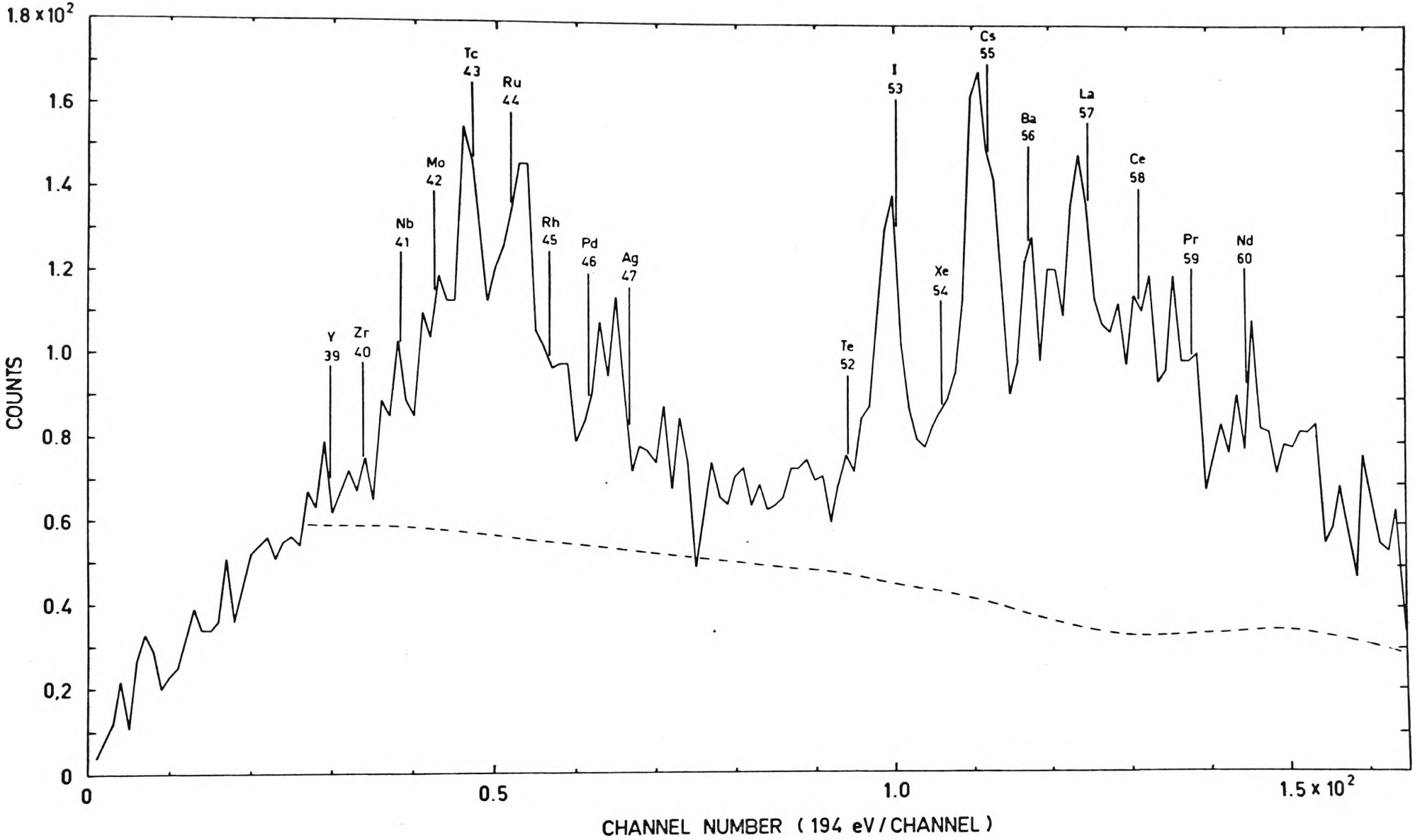

Fig 5.12 Observed raw energy spectrum of K X-rays from ^{252}Cf fission fragments. The expected positions of the $K\alpha_1$ peaks for a number of fragments are shown. The dashed curve shows the normalised Compton background.

5.2 Charge Study

As mentioned in section 4.3, the v(Z) data analysis was based on three separate series of measurements. The raw X-ray energy spectrum for one such series is shown in Figure 5.12. The expected position of the $K\alpha_1$ peaks for a number of elements are also shown (from the data of [87]). It is clear that identification of individual elements is possible in the data by using appropriate X-ray energy 'windows'.

Before choosing the particular windows however, it was necessary to subtract from the raw X-ray spectrum the background due to Compton scattering of prompt fission gamma rays. In each fission event about 7 or 8 prompt fission photons are emitted, each with average energy about 1 MeV. If one of these photons suffers Compton scattering in the body of the detector and the Compton electron so produced has energy 5 to 50 keV, then this (Compton scatter-fragment) coincident event will be indistinguishable from a genuine (X-ray-fragment) coincidence. To measure the Compton contribution, a copper shield of sufficient thickness to stop the genuine K X-rays ($\lesssim$50 keV) was inserted in front of the X-ray detector. The high energy prompt fission gammas could still reach the detector however. The Compton background spectrum so obtained is shown as the dashed curve in Figure 5.12. The Compton curve has been normalised up to the data curve by multiplying by a factor n, where n is the ratio of data measurement duration to background measurement duration. The normalised background curve was subtracted from the raw data off-line to produce a nett X-ray spectrum for each of the three series. One such nett spectrum is shown in Figure 5.13. The expected

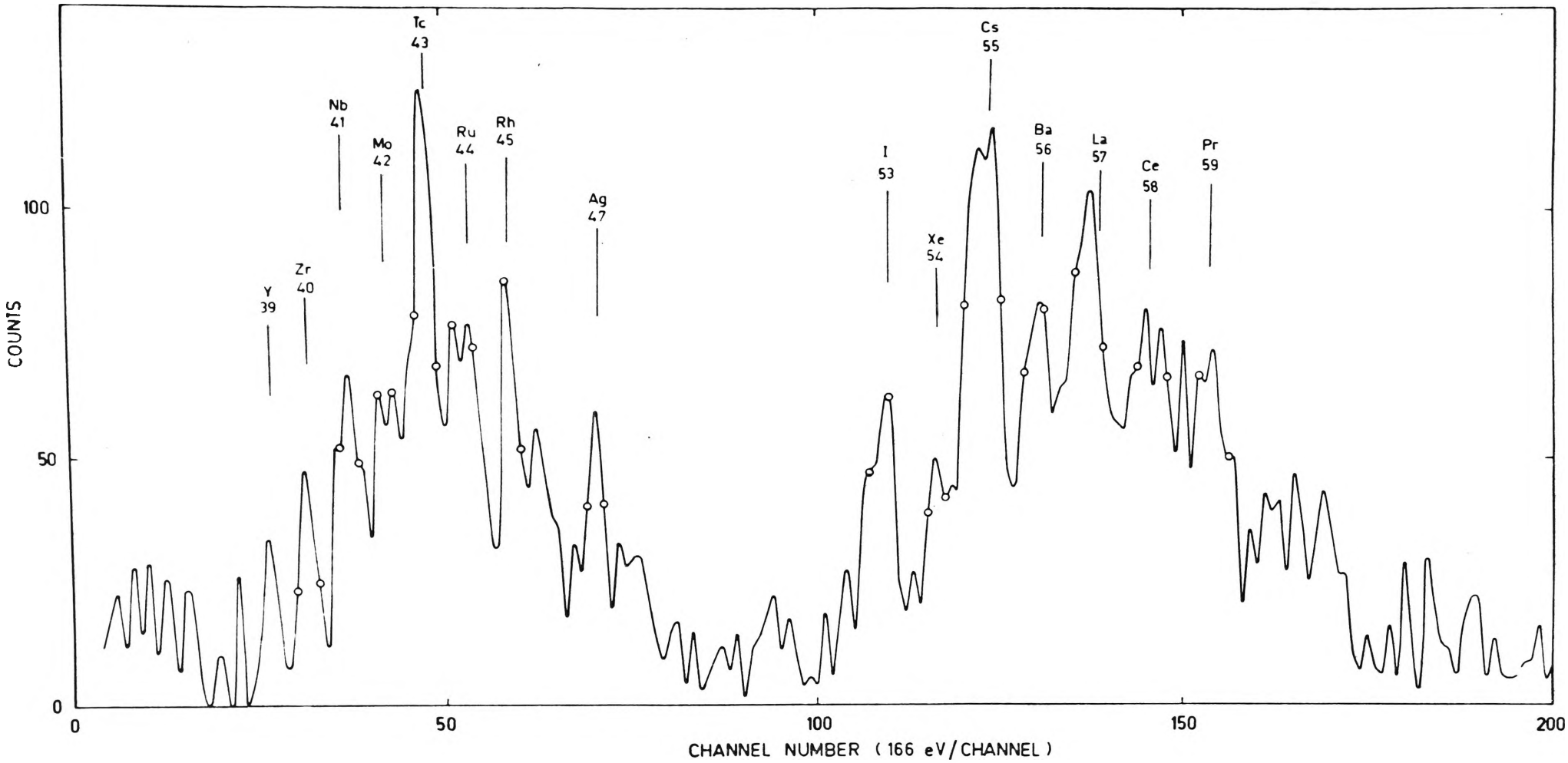

Fig 5.13 Energy spectrum of K X-rays from ^{252}Cf fission fragments – after Compton background subtraction
(i) The circles show the limits of the energy windows chosen for each peak. The windows contain $K\alpha_1$ and $K\alpha_2$ contributions from a given Z fragment. $K\beta$ contribution to any particular window from a fragment of lower Z is $\lesssim 10\%$ of total.
(ii) Data on Z=39 fragments derived solely from data on Z=59 fragments moving away from tank (see text).

positions of the $K\alpha_1$ peaks for various elements are shown, again confirming that the contributions from individual elements to the spectrum have been identified.

To determine the neutron emission from a particular element, an energy window (in terms of channel numbers) was set by eye across the X-ray peak for that element. By restricting the analysis of neutron data to those events whose X-ray energies (pulse heights) lay within this window and whose fragment kinetic energy values lay in the appropriate region (that is labelling a light or heavy fragment) the neutron emission from that element was found. The kinetic energy restriction (via the E line data) was required because for an X-ray detection event in a given window it was not known which fragment emitted the X-ray and was therefore being labelled, the one moving towards the scintillator tank (and thus the one supplying the neutron for that event), or the one moving away from the tank. However, the E line pulse height information resolved this difficulty. For example, an event with X-ray pulse height between channels 120 and 125 would mean detection of a cesium, Z = 55, fission fragment. Thus the neutrons counted in this event were emitted either by the cesium fragment (cesium moving towards tank and complementary technetium, Z = 43, fragment hitting surface barrier detector 2, Figure 4.1), or by the technetium fragment (cesium moving away from tank and hitting surface barrier detector). Thus for this particular event $155 \leq$ (E pulse height in channels) ≤ 220 identified cesium as the neutron emitter, while $50 \leq$ (E pulse height) ≤ 154 identified technetium as the neutron emitter. The E line division point for classification into light or heavy fragment groups was chosen as the channel corresponding to the mid-point of the dip at symmetry, taken from the

observed fragment pulse height spectrum for detector 2.† Application of the X and E line windows to the data was accomplished off-line by the computer program NBDIFF. This program also printed out a neutron detection frequency table for both foreground and background, for each single set of X and E windows. Finally, the program printed the mean number of neutrons per event for foreground and background and their difference.

This mean number of neutrons observed per event, $\bar{n}_k^{obs}$ say, for window k, then had to be corrected for the neutrons associated with the Compton scatter events mentioned above. The corrected mean number of neutrons per window, $\bar{n}_k$, is given by

$$\bar{n}_k = \frac{\bar{n}_k^{obs} - a_k \bar{B}_c}{1 - a_k} \qquad \ldots(5.11)$$

where a_k = ratio of number of Compton events to total number of events, for window k; a_k usually ~ 0.35.

$\bar{B}_c$ = mean number of neutrons per event associated with Compton scatter events; $\bar{B}_c = 0.128 \pm 0.013$.

$\bar{B}_c$ was determined in the Compton background measurement above, and was assumed to be the same for each window. To determine a_k a rather lengthy procedure was needed. This is as follows. Information on each element Z_k comes from N_k^d direct observations and N_k^i indirect observations, such that $N_k^d + N_k^i = N_k$, the total number of observations of element Z_k. In the N_k^d direct observations, the number of Compton events C_k^d is

$$C_k^d = N_k^d \times \left(\frac{C_k}{N_k^d + N_{98-k}^i} \right) \qquad \ldots(5.12)$$

† This procedure is discussed more fully at the end of this section.

where C_k is the number of Compton events for window k, determined in the Compton background measurement,

N^i_{98-k} is the number of indirect observations of the element complementary to k that fell in window k.

Thus

$$\left(\frac{C_k}{N^d_k + N^i_{98-k}} \right)$$

represents the fraction of total events in window k that were Compton. It is assumed that this Compton fraction is constant for any subgroup of events within window k, e.g. the subgroup N^d_k. Similarly, for N^i_k we have

$$C^i_k = N^i_k \times \left(\frac{C_{98-k}}{N^i_k + N^d_{98-k}} \right) \quad . \qquad \ldots(5.13)$$

a_k is then given by

$$a_k = \frac{C^d_k + C^i_k}{N_k} \quad . \qquad \ldots(5.14)$$

Substitution into equation (5.11) then gives $\bar{n}_k$.

No correction was applied to $\bar{n}_k$ to take account of random coincidences between the X-ray line and the fission line, as this rate was estimated to be less than one per 200 genuine coincidences.

About 50 per cent of the X-rays are emitted relatively late after fission at time intervals of $\sim$0.5 ns and beyond. These will be Doppler shifted by up to a few hundred eV since the detected X-ray is not emitted at right angles to the fragment velocity direction. This effect tends to complicate the setting of the X-ray windows by smearing the peaks into one another. This problem was overcome by selecting for analysis only those

events which fell near the centre of an X-ray peak, being well away from the 'wings' of the peak where ambiguities are more likely to occur. The energy windows chosen are shown in Figure 5.13 for a number of elements.

The next correction applied to the $\nu(Z)$ data was the geometry and backscatter correction. This procedure was analogous to that described in section 5.1 for the $\nu(A)$ data. For each pair of complementary charges the most probable pre-neutron emission masses were taken from the data of Watson et al.[103].

The final step was to correct for the scintillator detection efficiency. It was originally intended to use the value of ε derived from the $\nu(A)$ data. However, because of technical difficulties, the $\nu(Z)$ measurements were performed with slightly smaller gains in the photomultiplier tube amplifiers than was used for the $\nu(Z)$ runs. Hence the value of ε used in section 5.1 did not apply to the $\nu(Z)$ data. Therefore the total neutron emission found in the present work (weighted over the charge distribution observed) was normalised to the accurate, weighted total neutron emission found by Nifenecker et al.[11] for the same Z region, Z = 39-45, to determine the tank efficiency. This means, of course, that the present $\nu(Z)$ values are relative values, rather than absolute. Still, it is the <u>shape</u> of the $\nu(Z)$ curve which is of primary importance and the shape is not affected by this method of normalisation. This procedure implied a 4π neutron detection efficiency of 37 per cent.

It should be mentioned that it is not permissible to simply normalise the total neutron emission observed in the $\nu(Z)$ data up to $\bar{\nu}_p$ (^{252}Cf)= 3.724 for two reasons:

(i) 'selectivity' of X-ray emission wherein different fragments have different probabilities of emitting an X-ray. This biases the fragment yield distribution observed in charge

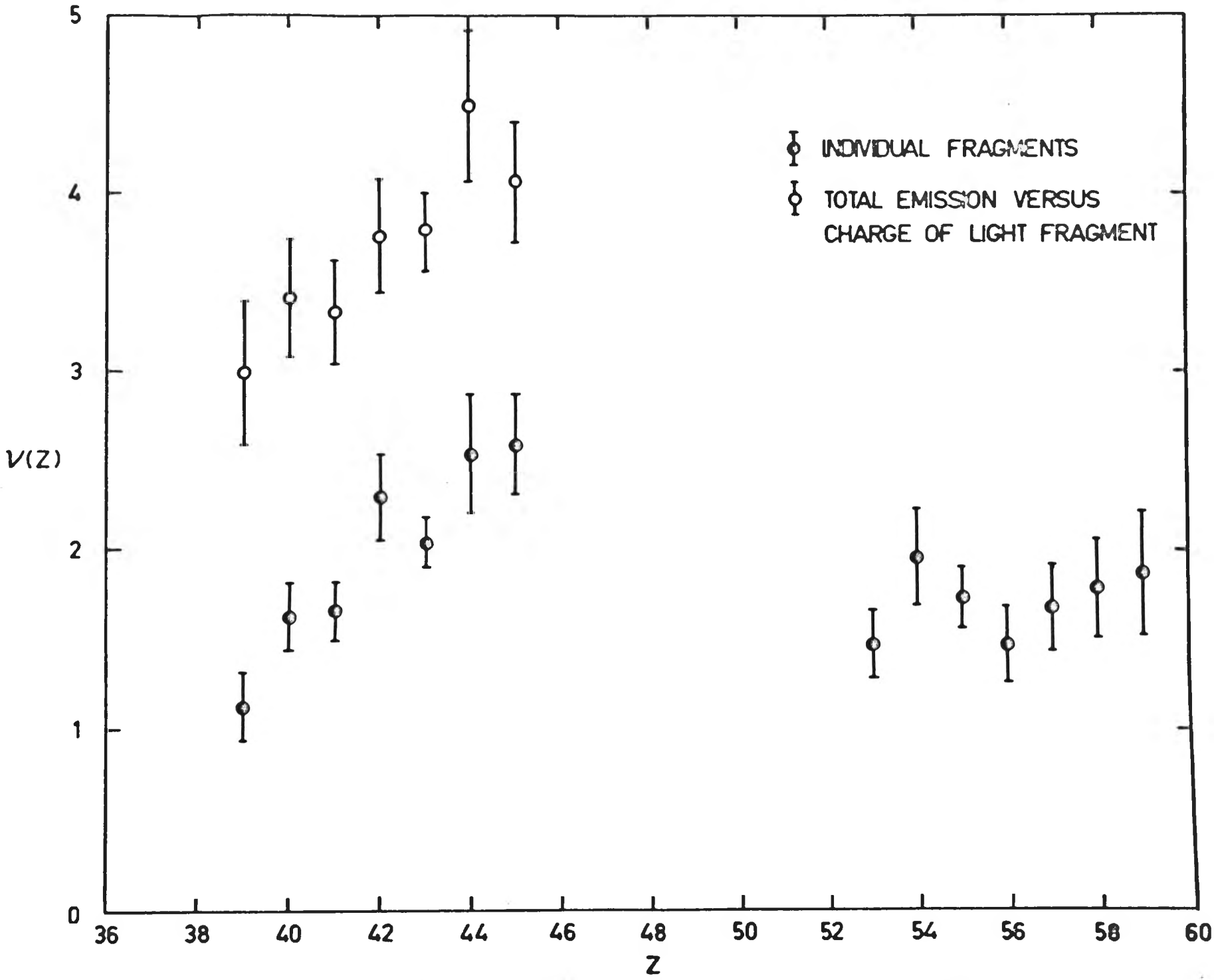

Fig 5.14 Neutron emission versus fragment charge.

studies away from the familiar mass-yield distribution.

(ii) Even if selectivity were not present, only seven charge pairs have been measured in the present experiment. This is too few to be representative of the full spectrum of fission fragment masses.

The final $\nu(Z)$ results are listed in Table 5.5. Also given are the values of $\nu_{total}(Z)$, the total neutron emission from a fragment pair versus the charge of the light fragment. Table 5.6 lists the experimental errors. Figure 5.14 shows the $\nu(Z)$ and $\nu_{total}(Z)$ curves. The expected 'sawtooth' behaviour for $\nu(Z)$ is clearly seen. However, the $\nu(Z)$ slope for the heavy fragment group is substantially lower than that measured by Nifenecker et al.[9]. The present data is compared with the data of (9) in Figure 5.15. A new feature is that data for the pair Z = 39, 59 has been obtained in this experiment. Assuming that the pronounced peak at Z = 54 seen in this work is not a genuine effect, then the present data implies $d\nu/dZ$ (Z = 53-59) $\sim$0.07 neutrons per Z, whereas the data of (9) implies $d\nu/dZ$ (Z = 53-58) $\sim$0.14 neutrons per Z. For the light fragment group however, the agreement between the two sets of data is good. The points at Z = 42, 44, 45 of this work are slightly higher than those of (9), but this is not really significant as the present errors are relatively large and the two data sets are based on slightly different normalisation procedures. The effect of the lower slope for the heavy group is to produce a significantly larger slope in the present $\nu_{total}(Z)$ data than that observed in (9). From this work $d\nu_{total}/dZ$ (Z = 40-45) $\sim$0.13 neutrons per Z. From (9) $d\nu_{total}/dZ$ (Z = 40-45) $\sim$0.035 neutrons per Z. Even though the final errors associated with the present results are about three times larger than those of Nifenecker et al., the factor of about three difference in

TABLE 5.5

MEASURED AVERAGE NEUTRON EMISSION VERSUS FRAGMENT CHARGE [a]

Z	$\nu(Z)$	Z	$\nu(Z)$	$\nu_{TOTAL}(Z)$
39	1.12 ± 0.19	59	1.87 ± 0.35	2.99 ± 0.40
40	1.62 ± 0.19	58	1.79 ± 0.27	3.41 ± 0.33
41	1.65 ± 0.16	57	1.68 ± 0.24	3.33 ± 0.29
42	2.29 ± 0.24	56	1.47 ± 0.21	3.76 ± 0.32
43	2.04 ± 0.14	55	1.74 ± 0.17	3.78 ± 0.22
44	2.53 ± 0.33	54	1.96 ± 0.27	4.49 ± 0.43
45	2.59 ± 0.28	53	1.47 ± 0.19	4.06 ± 0.34

(a) Data normalised to total neutron emission of (11)

TABLE 5.6

SOURCE OF ERRORS IN $\nu(Z)$ RESULTS

Z	% Error in $\nu(Z)$ [a] (Statistical)	% Error in $\nu(Z)$ [b] (Statistical plus Compton)
39	11.3	17.4
40	7.7	12.0
41	6.2	9.6
42	6.6	10.5
43	5.1	7.0
44	8.1	13.0
45	6.8	11.0
53	8.1	13.0
54	8.8	14.0
55	6.3	9.8
56	8.3	14.5
57	7.8	14.2
58	9.3	15.0
59	12.5	18.7

(a) Error calculated solely from total number of neutrons observed.

(b) Final error after Compton neutron background correction applied (equation 5.11). Error in $\bar{B}_c$ is 10%; error in a_k is 4%.

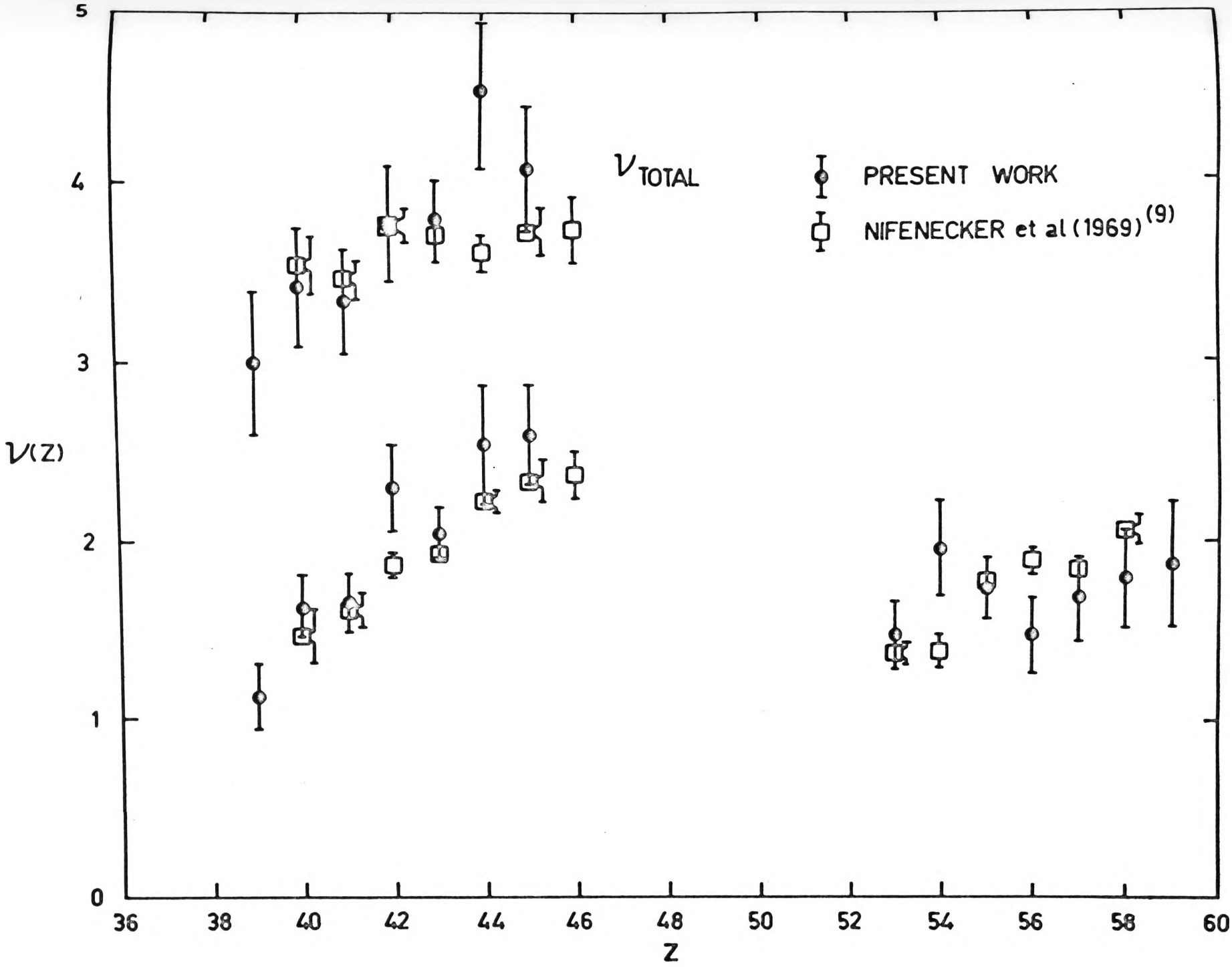

Fig 5.15 Neutron emission versus fragment charge.

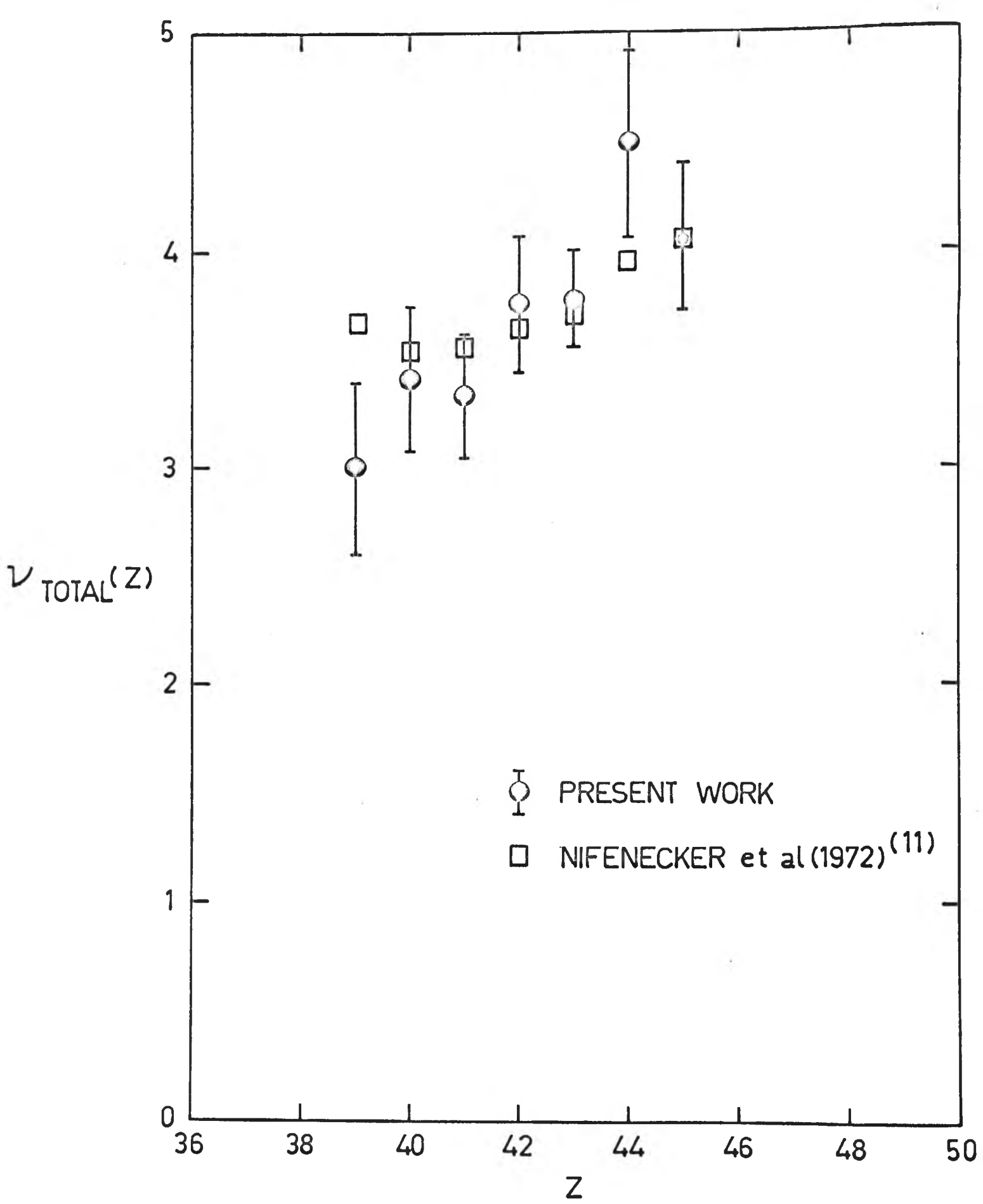

Fig 5.16 Total neutron emission versus charge of light fragment.

$d\nu_{total}/dZ$ between the two data sets certainly appears to be genuine.

In December 1972, when the measurements for the present work were close to completion, Nifenecker et al., in a private communication to the candidate[11], reported the results of a study of total neutron emission versus Z for ^{252}Cf spontaneous fission. In this experiment the californium source was placed at the centre of a large liquid scintillator tank. With this 4π neutron detection geometry, neutrons from individual fragments could not be measured - only the total neutron emission from a given fragment pair could be recorded. However, such an experimental design provides much higher fission counting rates than can be obtained in studies of individual fragments, enabling greater accuracy of results. The accuracy achieved for $\nu_{total}(Z)$ in (11) was markedly better than that of (9). Figure 5.16 shows the very accurate results of (11) compared with the data of the present experiment for the same range of Z. The data of (11) implies $d\nu_{total}/dZ$ (Z = 40-45) ~ 0.10 n/Z, in good agreement with the value of ~0.13 n/Z found in the present work.

From Figure 5.16 the high value for ν_{total} (Z = 44, 54) in the present work appears non-genuine. It is caused mainly by the spuriously high $\nu(Z)$ value for fragment Z = 54. Also, the ν_{total} (Z = 39, 59) value of this work is considerably lower than that of (11). However the ν_{total} (Z = 39, 59) point of this work is the least accurate of all the data points, its percentage error being 14 per cent compared with 8 to 9 per cent for most of the rest (see Table 5.6).

The present results do not suggest the existence of the odd-even Z effect in the neutron emission, which was described in section 3.3. A weighted average over the even charges Z = 40, 42, 44, gives

$$\nu_{total}\ (Z = 40,\ 42,\ 44) = 3.61 \pm 0.19$$

A weighted average over the odd charges Z = 41, 43, 45 gives

$$\nu_{total}\ (Z = 41,\ 43,\ 45) = 3.52 \pm 0.15$$

The odd-even difference measured is thus 0.09 ± 0.24 neutrons. This is to be compared with the expected difference of 0.2-0.3 neutrons. The errors associated with this work are relatively large however, and therefore these results do not definitely deny the existence of the odd-even effect in $\nu(Z)$. It is only with the evidence from the recent accurate French work[11] on total neutron emission that one can confidently say the effect does not exist. Nifenecker et al.[11] found ν_{total} (even charges) = 3.712 ± 0.005 and ν_{total} (odd charges) = 3.685 ± 0.005, a difference of 0.027 ± 0.007 neutrons. The final chapter of this thesis examines the consequences of this effect not being found.

Nifenecker et al.[9] reported the existence of two plateau regions in their heavy group $\nu(Z)$ data, one plateau for charges 52-53-54 and another for charges 55-56-57 (see Figure 3.13). They claimed a correlation between this 'fine structure' and the fine structure observed in the mass yield curve. This suggestion is discussed more fully in the following chapter. The present data contain no evidence of plateaux in the same region.

Unfortunately, there was not enough time available to obtain results for single fragment kinetic energy versus Z, i.e. $E_K(Z)$. This situation arose mainly because of unforeseen computer software delays in modifying the program MASSIVE to perform the ^{252}Cf $\nu(A)$ analysis.

In the $\nu(Z)$ analysis above, the E line pulse height information was used to classify fragments into the light or heavy mass group. The dividing line was chosen as the symmetry mid-point of the pulse height spectrum of detector 2. This was originally intended to be only an approximate method. If the $E_K(Z)$ analysis had been done, the classification into light or heavy mass groups would have been known exactly (because the fragment mass for each event would have been known). It is unlikely however that this approximate classification method has introduced any significant error to the present $\nu(Z)$ results. The time-of-flight measurements of Whetstone[94] showed that ~5 per cent of the heavy fragments have kinetic energies greater than the energy at the symmetry mid-point, while only ~1.5 per cent of the light fragments have energies less than this value. However, the majority of these fragments have masses in the symmetric region A = 120-135, a region not covered by the present $\nu(Z)$ data.

The error bars on the present data are larger than those of (9) (Figure 5.15). The reason is the larger statistical errors. The present counting rate was necessarily reduced by a factor of two over that planned because at the time the apparatus was set up only small, 1 cm^2 active area surface barrier detectors were available, rather than the larger 2 cm^2 area detectors that it was originally intended to use. Also, a significant amount of data recording time was lost through malfunction of the magnetic tape deck control unit. This unit displayed a tendency to lock into a mode wherein the last 'bit' of each eight bit word was not generated, thus providing unusable data. It should be mentioned again though that the present data have been obtained with markedly better charge resolution than was used in (9).

CHAPTER 6

DISCUSSION

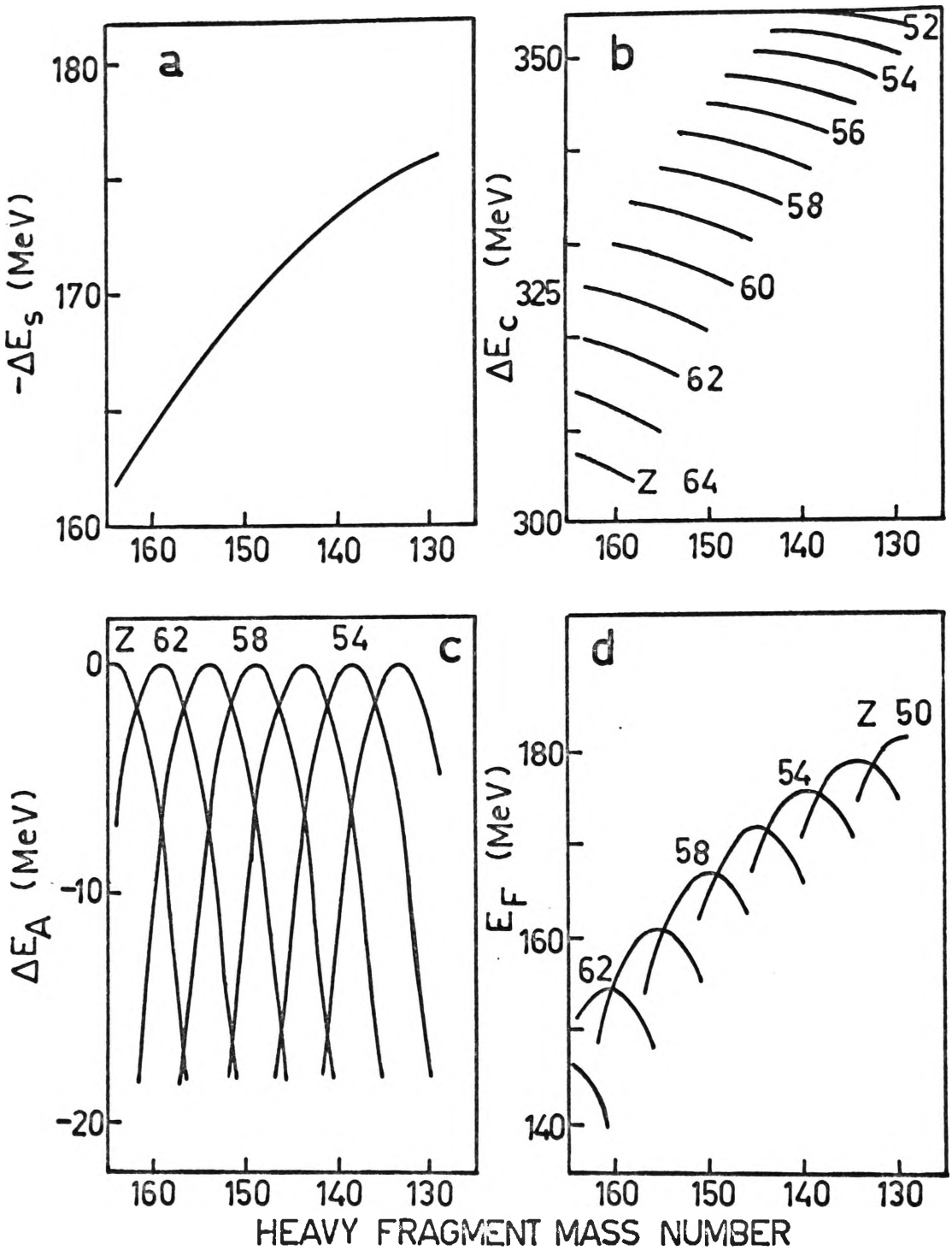

Fig 6.1 Surface (a), Coulomb (b), asymmetry (c), and total (d) energy changes for the fission of U^{236}, as calculated from a semi-empirical mass formula. From [8].

The ν versus Z work is the major endeavour of this thesis and will therefore be discussed first.

6.1 Charge Study

6.1a Odd-even Z Effect

The results of the present work and also of Nifenecker et al.[11] imply that the expected 0.2 to 0.3 neutrons excess emission of evenly charged fragments over oddly charged fragments does not exist. It is necessary therefore at this point, to examine the theoretical basis for expecting such an effect. The following is a more exhaustive examination of the argument which was presented in restricted form in section 3.3.

Equation (6.1) shows a form[8] of the semi-empirical mass equation which is a somewhat simpler version of the more common mass equations (58, 104, 105).

$$E_f = A_c \left[\frac{Z^2}{A^{\frac{1}{3}}} - \frac{Z_1^2}{A_1^{\frac{1}{3}}} - \frac{Z_2^2}{A_2^{\frac{1}{3}}} \right] + A_s \left(A^{\frac{2}{3}} - A_1^{\frac{2}{3}} - A_2^{\frac{2}{3}} \right) +$$

$$+ A_a \left[\frac{(A-2Z)^2}{A} - \frac{(A_1-2Z_1)^2}{A_1} - \frac{(A_2-2Z_2)^2}{A_2} \right] + \Delta \qquad \ldots(6.1)$$

Here E_f is the total energy released in the fission of a compound nucleus (A, Z) into two fragments (A_1, Z_1) and (A_2, Z_2). A_s, A_c and A_a are the surface, Coulomb and asymmetry coefficients respectively and Δ is a term to represent shell and pairing effects. Figures 6.1a, b and c (taken from the work of Thomas and Vandenbosch[8]) show the behaviour of each of the first three terms of equation (6.1) for the compound nucleus ^{236}U. Their sum is shown in Figure 6.1d. The parabolae shown in Figure 6.1d connect points corresponding to a given division of charge, for even Z-even N

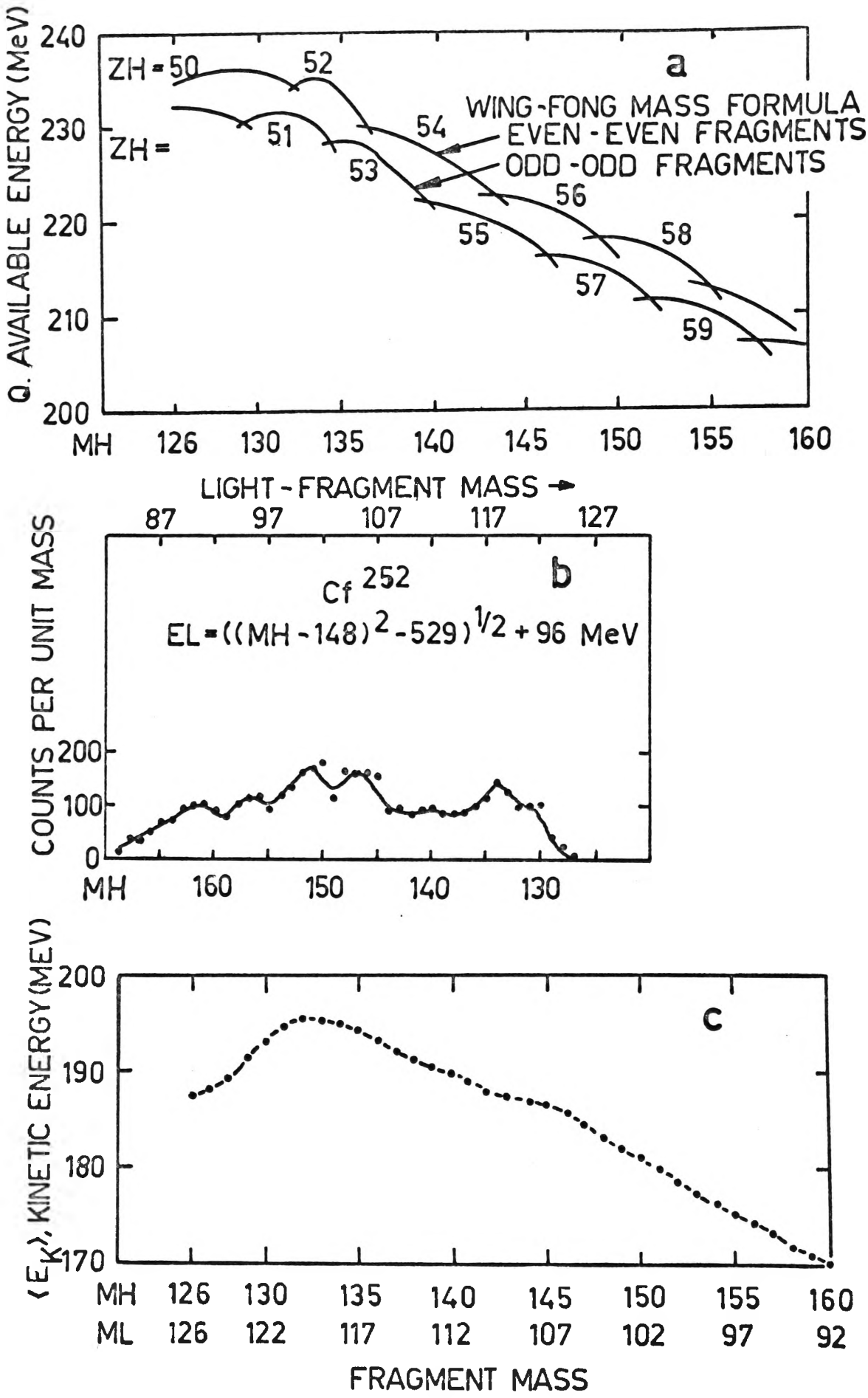

Fig 6.2 (a),(b),(c) See text.

fragments. The peaks of the oscillations are very nearly 5 mass units apart. This is because the mass number of the most stable nuclide for a given Z changes about 2.5 units for a unit change in Z. Adding in the effect of the Δ term in equation (6.1) causes the energy release surface for odd-mass fragments to be depressed below that for even-even fragments. This feature is illustrated by Figure 6.2a, which shows the energy release surfaces for ^{252}Cf as calculated by Schmitt et al.[98] using the mass equation of Wing-Fong. The upper parabolae are for even Z-even N fragments, while the lower parabolae are for odd Z-odd N fragments. The Q values for fission into odd A nuclei form a set of parabolae at energies between the two sets shown. As before, each parabola connects points of constant charge division.

The validity of the calculations of the energy release curves can be seen by comparing Figures 6.2b and c with Figure 6.2a. Figure 6.2b shows the ^{252}Cf mass yield for a particular region of light fragment energy[91]. (This region is one which follows the average position of a contour in the ^{252}Cf mass-energy surface). The fine structure peaks in the mass yield curve coincide with the peaks of the even-even energy release curves. These occur at heavy fragment mass numbers 134, 140, 146, 152, 156 and 162. Figure 6.2c shows the ^{252}Cf total fragment kinetic energy versus mass curve[98]. Fine structure effects can be seen at masses 140, 146 and 156. Now the total energy release for even-even fragments is greater than for odd A and odd-odd fragments. Thus the even-even configurations are energetically preferred in the fissioning system. Therefore the structure in the mass surface should be preferentially determined by the mass surface for even-even fragments, as distinct from

the odd A or odd-odd fragments. And this is precisely what is observed!

This agreement in location between mass yield fine structure and even-even fragment energy release curves also occurs for thermal neutron fission of ^{235}U, ^{233}U and ^{239}Pu[8,100,106]. Indeed, for each of the four fissioning systems considered, the fine structure is associated with identically the same heavy fragment mass numbers. This fact is suggestive of the universal nature of the fine structure phenomenon and lends further support to the semi-empirical mass equation calculations[8] described above.

The basis for postulating an odd-even Z effect in fragment neutron emission (note that 'odd-even' here describes Z only) can be easily seen by referring to Figure 6.2a. An even Z fragment can have N either even or odd. If N is even, the total energy release Q (for <u>two</u> such even Z fragments) will be given by one of the upper curves. If N is odd, Q will lie on a nearby intermediate energy curve.

Assuming that each possibility is equally probable, then the average Q for two even Z fragments will be approximately midway between the upper and intermediate energy curves. By the same argument the average Q for two odd Z fragments lies approximately midway between the lower odd-odd curves and the intermediate energy curves. Using the energy scale shown in Figure 6.2a, one finds the average Q for the even Z pair to be about 2 MeV larger than that for the odd pair. Assuming that this extra total energy passes wholly into fragment excitation E^*, then the E^* for an even Z pair should be enhanced by about 2 MeV over that for the odd Z pair. It is well known that the majority of fragment excitation energy appears finally as neutron emission. Assuming $dE^*/d\nu \sim 6.6$-10 MeV/neutron (see

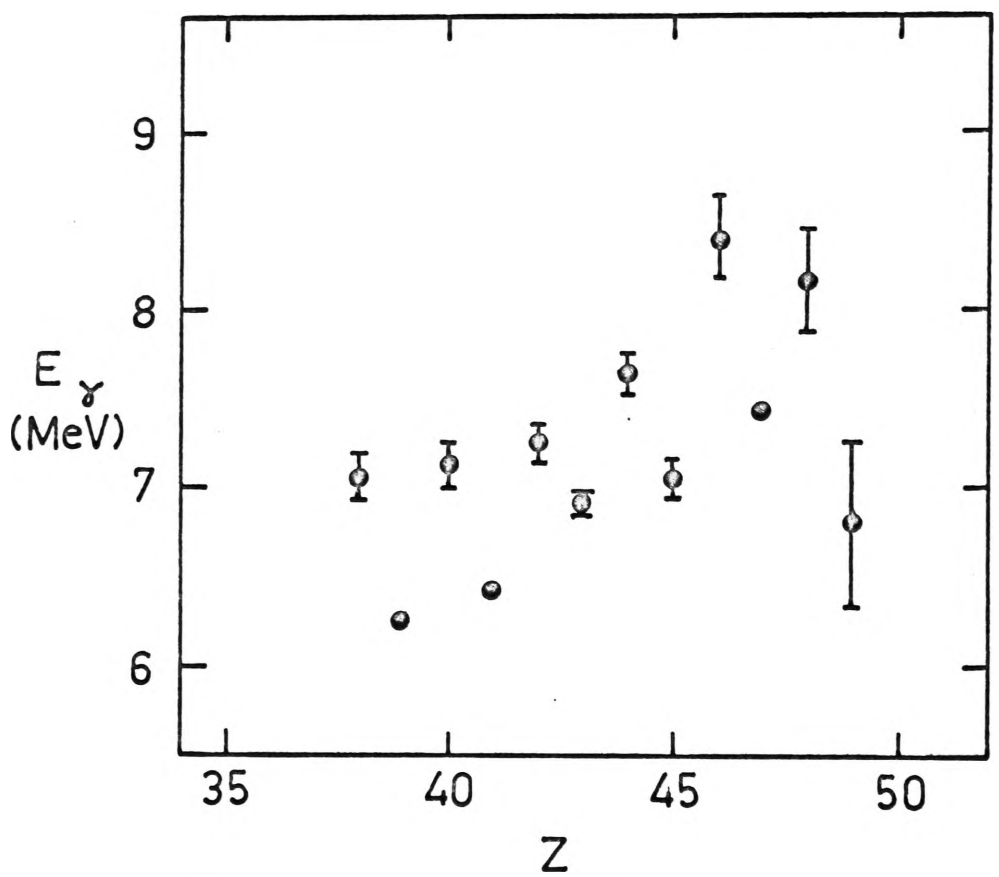

Fig 6.3 Average total gamma ray energy versus charge of light fragment. From [11].

section 3.2) gives a neutron enhancement for the even pair of 0.2 to 0.3 neutrons over the odd pair.

However, experimentally no such effect on the neutron emission is observed. Clearly though, the effect is genuine for the total energy release. Therefore either

(i) the excess energy release passes not into fragment excitation energy but into fragment kinetic energy, or

(ii) the excess does pass into fragment excitation, but this extra excitation passes not into neutron emission but into prompt gamma ray emission, or even perhaps into the average energy carried away by the neutrons.

Nifenecker et al.[10] investigated possibility (i) and found no odd-even Z effect in the fragment kinetic energies. Possibility (ii), however, is more promising. In their recent study on total neutron emission[11], Nifenecker et al. also measured the total prompt gamma ray energy E_γ in ^{252}Cf fission as a function of the charge of the fragments. They found a distinct odd-even effect. The average E_γ for the even Z fragment pairs exceeded the average E_γ for the odd pairs by 0.66 ± 0.05 MeV. Figure 6.3 shows their data for the light fragments. Even though this result is an important step forward, the value of 0.66 MeV is still too small to account for the 2 MeV excess energy available from the total energy release.

It may well be that the 'missing' 1.3 MeV of energy contributes to the energy carried off by the neutrons. That is, the neutrons emitted from a pair of evenly charged fragments have about 1.3 MeV more energy associated with them than those emitted from two oddly charged fragments.

The energy carried away per neutron is equal to the sum of the binding energy and the centre of mass kinetic energy of the neutron. It is known from mass tables that the neutron binding energies show odd-even fluctuations with respect to the number of neutrons but not to the number of protons in the nuclei[11]. Therefore it is likely that the remainder of the excess Z pairing energy appears as neutron kinetic energy. Unfortunately, no direct measurements of the charge dependence of the fission neutron kinetic energy have been reported. Such a measurement needs to be done to resolve the problem.

6.1b $\nu(Z)$ Behaviour for Heavy Fragment

There are two other important findings associated with the $\nu(Z)$ measurements of this thesis. The first is the significantly lower slope for the heavy fragment $\nu(Z)$ curve. The present work found a slope of about 0.07 neutrons per Z. This value is half that found by Nifenecker et al.[9], viz 0.14 neutrons per Z. For the light fragment group however, both data sets are similar. The present work found a slope of 0.19 neutrons per Z, while Nifenecker et al.[9] found 0.17 neutrons per Z. The lower heavy fragment $\nu(Z)$ slope reported in this thesis is the more likely to be correct. This is so for two reasons. Firstly, from the $\nu(A)$ data (Figure 5.6) $d\nu(A)/dA$ (A = 135-150, heavy group) is about one half $d\nu(A)/dA$ (A = 100-115, light group). The mass regions considered here correspond to the charge regions of Figure 5.14, viz Z = 39-45 and Z = 53-59, respectively. Therefore, because of the correspondence between A and Z, one would expect a similar ratio of slopes for the $\nu(Z)$ data. Secondly, as mentioned in section 5.2, the lower $\nu(Z)$ slope

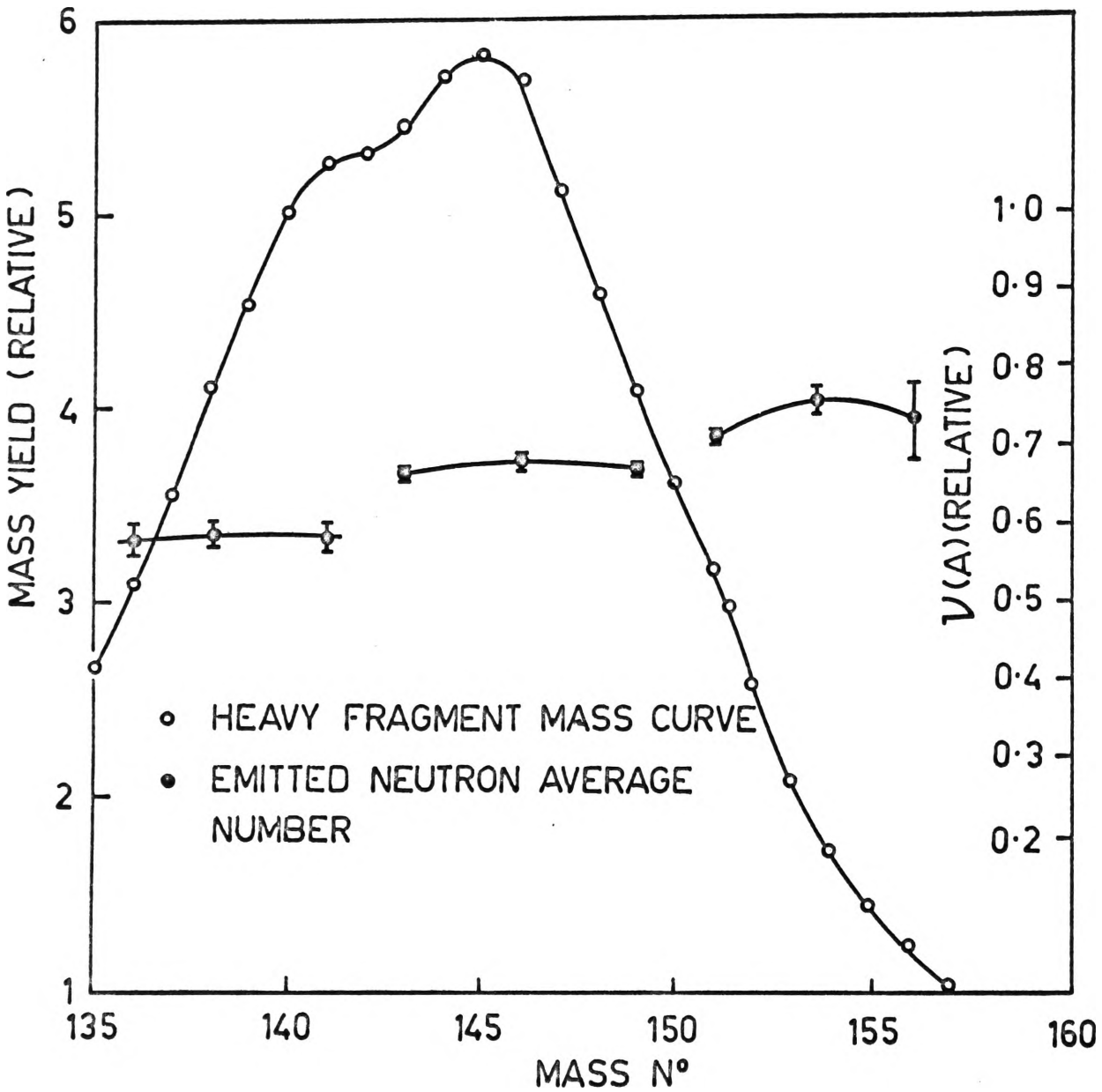

Fig 6.4 Calculated $\nu(A)$ behavior compared with mass yield curve [101]. The $\nu(A)$ values are derived from $\nu(Z)$ data. From [9].

for the heavy group produces a $d\nu_{total}/dZ$ slope in good agreement with the recent accurate $d\nu_{total}/dZ$ slope reported by Nifenecker et al.[11]

The second finding to be noted is the clear absence of plateaux at Z = 52-53-54 and Z = 55-56-57 as reported in (9). Nifenecker et al. converted their heavy fragment $\nu(Z)$ data to $\nu(A)$ data via

$$\bar{m} = Z \times \frac{252}{98} - 2 \quad , \qquad \ldots(6.2)$$

where $\bar{m}$ is the most probable fragment mass for a given charge Z, and obtained the curve shown in Figure 6.4. Also shown is the ^{252}Cf heavy fragment mass yield curve of Fraser et al.[91] Nifenecker et al. suggested a correlation between the $\nu(A)$ plateaux (at A = 136-141 and A = 143-149) and the 'humps' in the mass yield curve in the same region. They claimed that if this correlation is genuine, then the mass yield fine structure might not be a Z parity effect as has been generally thought[8,67]. The authors suggested an alternative explanation in terms of the cluster model of fission[107]. According to this model, certain cluster structures formed in the compound nucleus <u>before</u> fission remain essentially unaffected throughout the fission process. Further, the fragment excitation energies are directly related to the different cluster structures. According to Nifenecker et al. then, if each mass yield hump corresponds to a given cluster, it is not surprising that the excitation energy appears to be constant in the mass (charge) region corresponding to a given hump.

However, it is probable that this plateau effect is not genuine. The $\nu(A)$ data show no evidence of plateaux at mass regions 136-141 and 143-149 (Figure 5.6). Also the $\nu(Z)$ data of the present work show no

indication of such an effect.

6.2 Mass and Kinetic Energy Study

The most important outcome of the ν versus mass and kinetic energy work was the finding of fine structure peaks in the total neutron emission, Figure 5.7, and in the $\nu(A)$ curve of Figure 5.4 which correlate exactly with the positions of the fine structure peaks in the mass yield curves. This is a major result. The only previous workers to have reported similar fine structure effects were Milton and Fraser, for the light fragment $\nu(A)$ curve of ^{235}U[66]. The $\nu_T(A)$ data of Signarbieux et al. (Figure 5.8) suggest fine structure also, however these authors have made no comment on this fact[99]. The question then arises as to why Bowman et al[63] missed seeing this structure. Their $\nu_T(A)$ curve shows only a smooth variation with mass (Figure 5.8). The statistical errors of the Bowman data points are about the same as those of the present data (Table 5.3). The Bowman mass resolution however was 6.2 amu (FWHM). Recently, the mass resolution of silicon surface barrier fission detectors calibrated by the Schmitt procedure[93] has been investigated in detail and has been found to be ~4 amu (FWHM)[108]. The method used was to study the yield of mass-sorted K X-rays in coincidence with fission. The spread of the measured yields provides an upper limit to the experimental fragment mass resolution. The surface barrier detectors and associated electronics of (108) were similar to that used here. Therefore the mass resolution of the present work is probably ~4 amu (FWHM) also. The fine structure in the mass yield curves occurs with spacings of 4 and 6 amu. Most likely the Bowman et al. resolution of 6.2 amu was just sufficiently large to smear out the fine structure peaks in the neutron yield curves.

The present results have not yet been corrected for mass resolution. It is expected though that this correction will be small, amounting to dispersion shifts of $\lesssim$1 amu[61,108]. This expectation is borne out by the good agreement above mass 136 between the present $\nu_T(A)$ data and the data of Signarbieux et al.[99], which have been resolution corrected (Figure 5.8).

It is interesting that whereas the 'expected' odd-even Z effect in the neutron emission is not observed experimentally the neutron emission versus mass data do contain fine structure. As discussed in the preceding section this fine structure arises from the parabolic behaviour (versus fragment mass) of the total energy release curves for the energetically preferred even Z-even N configurations (Figure 6.2a). Thus one can conclude that the gross total energy release fluctuations are reflected in the neutron emission, but not to the detailed extent needed to produce an odd-even effect in $\nu(Z)$.

CONCLUDING REMARKS

Recently new surface barrier fragment detectors have been acquired. These have an active area four times that of the detectors used in the present work. It is intended to insert these detectors into the experimental system to provide higher count rates and to thereby reduce the present $\nu(Z)$ statistical errors. The X-ray pulse height analysis will be performed using 1024 channels rather than the present 220 channels.

With increased data rates it will be feasible to use <u>two</u> fragment detectors in coincidence to study the charge dependence of the ^{252}Cf <u>total</u> fragment kinetic energy. No work has been reported on this. A high (X-ray) resolution measurement is needed here to improve on the lower resolution single fragment kinetic energy data[9], so that the problem of the 'missing' 1.3 MeV of excess energy might be nearer solution.

REFERENCES

1. Hahn, O. and Strassman, F. - Naturwiss 27 (1939) 11.
2. Frisch, O. R. - Nature 143 (1939) 276.
3. Joliot, F. - Comptes Rendus 341, 208 (1939) 647.
4. Von Halban, Jr. H., Joliot, F. and Kowarski, L. - Nature 143 (1939) 470.
5. Anderson, H. L., Fermi, E. and Hanstein, H. B. - Phys. Rev. 55 (1939) 797.
6. Proc. First U.N. Conf. on Peaceful Uses Atomic Energy, Geneva (1955).
7. Proc. Second U.N. Conf. on Peaceful Uses Atomic Energy, Geneva (1958).
8. Thomas, T. D. and Vandenbosch, R. - Phys. Rev. 133 (1964) B976.
9. Nifenecker, H., Ribrag, M., Frehaut, J. and Gauriau, J. - Nucl. Phys. A131 (1969) 261.
10. Nifenecker, H. Frehaut, J. and Soleilhac, M. - 2nd IAEA Symp. on Phys. and Chem. of Fission, Vienna 1969, p. 491.
11. Nifenecker, H. et al. - Private communication (1972).
12. Boldeman, J. W. and Walsh, R. L. - J. Nucl. En. 24 (1970) 191.
13. Walsh, R. L. and Boldeman, J. W. - J. Nucl. En. 25 (1971) 321.
14. Boldeman, J. W., Musgrove, A. R. de L. and Walsh, R. L. - Aust. J. Phys. 24 (1971) 821.
15. Walsh, R. L. and Boldeman, J. W. - $\bar{\nu}_p$ for ^{239}Pu from 0-2 MeV - to be submitted to J. Nucl. En.
16. Boldeman, J. W. and Walsh, R. L. - Fragment Kinetic Energy Study for ^{233}U - Soviet National Conference on Neutron Physics, Kiev, May 28-June 1, 1973.

REFERENCES (cont'd)

17. Fraser, J. S. - Phys. Rev. 88 (1952) 536.

18. Bowman, H. R., Thompson, S. G., Milton, J. C. D. and Swiatecki, W. J. - Phys. Rev. 126 (1962) 2120.

19. Quoted by R. B. Leachman in Paper P/592, Proc. Int. Conf. Peaceful Uses At. Energy, UN, New York (1956).

20. Terrel, J. - Phys. Rev. 113 (1959) 527.

21. Feather, N. - USAEC, Document BR335A, 1942 (unpublished).

22. Weisskopf, V. F. - Phys. Rev. 52 (1937) 295.

23. Tables of Normal Probability Functions - Natl. Bureau of Standards, Applied Maths., Series No. 23 (US Govt. Printing Office, Washington D.C., 1953).

24. Smith, A. B., Fields, P. R. and Roberts, J. H. - Phys. Rev. 108 (1957) 411.

25. Grundl, J. A. - Nucl. Sci. Eng. 31 (1968) 191.

26. McElroy, W. N. - Nucl. Sci. Eng. 36 (1969) 109.

27. Gemmell, W. - private communication (1971).

28. Hopkins, J. C. and Diven, B. C. - Nucl. Phys. 48 (1963) 433.

29. Mather, D. S., Fieldhouse, P. and Moat, A. - Phys. Rev. 133 (1964) B1403.

30. Okolovich, V. N., Smirenkin, G. N. and Bondarenko, I. I. - Sov. J. At. Energy (English trans.) 12 (1963) 491.

31. Protopopov, A. N. and Shiriaev, B. M. - Sov. Phys. JETP 7 (1958) 231.

32. Blyumkina, Yu. A., Bondarenko, I. I., Kuznetsov, V. F., Nesterov, V. G., Okolovitch, V. N., Smirenkin, G. N. and Usachev, Z. N. - Nucl. Phys. 52 (1964) 648.

33. Meadows, J. W. and Whalen, J. F. - J. Nucl. En. 21 (1967) 157.

REFERENCES (cont'd)

34. Bohr, A. - Proc. 2nd U.N. Conf. Peaceful Uses Atom. Energy, Geneva, 2 (1956) 151.

35. Northrop, Y. A., Stokes, R. H. and Boyer, K. - Phys. Rev. 115 (1959) 1277.

36. Moldauer, P. A. - ANL-6323 (1961).

37. Auerbach, E. H. and Perey, F. G. J. - BNL-765 (1962).

38. Boldeman, J. W. and Dalton, A. W. - AAEC/E172, March 1967.

39. Ajitanand, N. N. and Boldeman, J. W. - Nucl. Phys. A144 (1970) 1.

40. Dyachenko, P. P., Kuzminov, B. D., Mikhaiolov, V. B., Semenko, V. I., Senchenko, V. I. and Utyenzhnikov, A. N. - Sov. J. Nucl. Phys. 6 (1968) 848.

41. Bol'shov, V. I., Kuznetsov, V. F., Smirenkin, G. N. Ermagambetov, S. B. and Okolovitch, V. N. - Sov. J. Nucl. Phys. 6 (1968) 844.

42. Kuzminov, B. D., Sergachev, A. I., Dyachenko, P. P., Vorobeva, V. G., Senchenko, V. I. and Taracho, M. S. - Nucl. Data for Reactors, IAEA, Vienna, 2 (1967) 85.

43. Strutinsky, V. M. - Nucl. Phys. 122 (1968) 1.

44. Strutinsky, V. M. and Pavlinchuk, V. A. - Proc. IAEA Symp. Physics and Chem. of Fission, Salzburg, 1 (1965) 127.

45. Huizenga, J. R., Unik, J. P. and Wilkins, B. D. - Proc. IAEA Symp. Physics and Chem. of Fission, Salzburg, 1 (1965) 11.

46. Strutinsky, V. M. and Pauli, H. C. - Proc. 2nd IAEA Symp. Phys. and Chem. of Fission, Vienna 1969, p. 155.

47. Britt, H. C., Stokes, R. H., Gibbs, W. R. and Griffin J. J. - Phys. Rev. Letters 11 (1963) 343.

48. Thomas, T. D. and Grover, J. R. - Phys. Rev. 159 (1967) 980.

49. Norenberg, W. - Proc. 2nd IAEA Symp. Phys. and Chem of Fission, Vienna 1969, p. 51.

REFERENCES (cont'd)

50. Diven, B. C., Martin, H. C., Taschek, R. F. and Terrel, J. - Phys. Rev. 101 (1956) 1012.

51. Hicks, D. A., Ise, J. Jr. and Pyle, R. V. - Phys. Rev. 101 (1956) 1016.

52. Milton, J. C. D. and Fraser, J. S. - Phys. Rev. 111 (1958) 877.

53. Terrell, J. - Phys. Rev. 108 (1957) 783.

54. Milton, J. C. D. and Fraser, J. S. - Canad. J. Phys. 40 (1962) 1626.

55. Maslin, E. E., Rodgers, A. L. and Core, W. G. F. - Phys. Rev. 164 (1967) 1520; also AWRE O-43/67 (1967).

56. Leachman, R. B. - Phys. Rev. 101 (1956) 1005.

57. Gordon, G. E. and Aras, N. K. - Proc. IAEA Symp. Phys. and Chem of Fission, Salzburg 1965, Vol. II, p. 73.

58. Seeger, P. A. - Nucl. Phys. 25 (1961) 1.

59. Glendenin, L. E., Unik, J. P., Griffin, H. C. and Reisdorf, W. - Proc. 2nd IAEA Symp. Phys. and Chem. of Fission, Vienna 1969, p. 781.

60. Fraser, J. S. and Milton, J. C. D. - Phys. Rev. 93 (1954) 818.

61. Terrel, J. - Phys. Rev. 127 (1962) 880.

62. Whetstone, S. L. Jr. - Phys. Rev. 114 (1959) 581.

63. Bowman, H. R., Milton, J. C. D., Thompson, S. G. and Swiatecki, W. J. - Phys. Rev. 129 (1963) 2133.

64. Apalin, V. F., Gritsyuk, Yu. N., Kutikov, I. E., Lebedev, V. I. and Mikaelian, L. A. - Nucl. Phys. 71 (1965) 553.

65. Stein, W. E. - Proc. Symp. on Physics and Chem. of Fission, Salzburg 1965, Vol. I, p. 491.

66. Milton, J. C. D. and Fraser, J. S. - Proc. Symp. on Physics and Chem. of Fission, Salzburg 1965, Vol. II, p. 39.

REFERENCES (cont'd)

67. Fraser, J. S., Milton, J. C. D., Bowman, H. R. and Thompson, S. G. - Can. J. Phys. 41 (1963) 2080.

68. Myers, W. D. and Swiatecki, W. J. - Univ. Cal. Report UCRL-11980 (1965).

69. Milton, J. C. D. and Fraser, J. S. - Phys. Rev. 111 (1958) 877.

70. Stein, W. E. - Phys. Rev. 108 (1957) 94.

Whetstone, S. L. Jr.. - private communication to Terrel.

71. Katcoff, S. - Nucleonics 16, 4 (1958) 78.

Nucleonics 18, 11 (1960) 201.

72. Walker, W. H. - AECL report CRRP-913 (unpublished) Ontario 1960.

73. Nervik, W. E. - Phys. Rev. 119 (1960) 1685.

74. Milton, J. C. D. and Fraser, J. S. - Phys. Rev. Lett. 7 (1961) 67.

75. Britt, H. C., Wegner, H. E. and Gursky, J. - Phys. Rev. Lett. 8 (1962) 98.

76. Vandenbosch, R. - Nucl. Phys. 46 (1963) 129.

77. Fong, P. - Phys. Rev. Lett. 11 (1963) 375.

78. Stelson, P. H. and McGowan, F. K. - Phys. Rev. 110 (1958) 489.

79. Myers, W. D. and Swiatecki, W. J. - Nucl. Phys. 81 (1966) 1.

80. 'Radiochemical Studies: The Fission Products'. (Coryell, C. D., and Sugarman, E., Eds.) Natl. Nuclear Energy Series IV-9, McGraw-Hill, New York (1951).

81. Way, K. and Wigner, E. P. - 'Radiochemical Studies: The Fission Products', ibid., Book 1, paper 43.

82. Voitovetskii, V. K.,Levin, B. A. and Marchenko, E. V. - Sov. Physics JETP 5 (1957) 184.

83. Skliarevskii, V. V., Fomenko, D. E. and Stepanov, E. P. - Sov. Physics JETP 5 (1957) 220.

84. Leachman, R. B. - Proc. 2nd U.N. Int. Conf. Peaceful Uses At. Energy, Geneva, 15 (1958) 331.

REFERENCES (cont'd)

85. Skliarevskii, V. V., Stepanov, E. P. and Medvedv, B. A. - Sov. Phys. JETP 36 (1959) 225.

86. Cauchois, Y. - J. Phys. Radium 13 (1952) 113; 16 (1955) 253.

87. Wapstra, A. H., Nijgh, G. J. and van Lieshout, R. - Nuclear Spectroscopy Tables, North-Holland Publishing Co., Amsterdam, 1959 .

88. Watson, R. L. - Thesis, Ph.D., Univ. of California; also UCRL-16798 (1966), unpublished.

89. Watson, R. L., Bowman, H. R. and Thompson, S. G. - Phys. Rev. 162, 4 (1967) 1169.

90. Glendenin, L. E., Unik, J. P. and Griffin, H. C. - Proc. IAEA Symp. Phys. and Chem. of Fission, Salzburg 1965, Vol. 1, p. 369.

91. Fraser, J. S., Milton, J. C. D., Bowman, H. R. and Thompson, S. G. - Can. J. Phys. 41 (1963) 2080.

92. Schmitt, H. W. and Pleasonton, F. - N.I.M. 40 (1966) 204.

93. Schmitt, H. W., Gibson, W. M., Neiler, J. H., Walter, F. J. and Thomas, T. D. - IAEA Symp. on Phys. and Chem. of Fission, Salzburg 1965, Vol. 1, p. 531.

94. Whetstone, S. L. Jr. - Phys. Rev. 131, 3 (1963) 1232.

95. Bowman, H. R., Milton, J. C. D., Thompson, S. G. and Swiatecki, W. - Report UCRL-10139 Rev. This report contains the full experimental data of references (18) and (63).

96. Kluge, Gy. and Lajtai, A. - Phys. Lett. 27 (1968) 65.

97. 2nd IAEA Panel Meeting on Neutron Standard Reference Data, Vienna, Nov. 1972.

REFERENCES (cont'd)

98. Schmitt, H. W., Neiler, J. H. and Walter, F. J. - Phys. Rev. 141 (1966) 1146.

99. Signarbieux, C., Poitou, J., Ribrag, M. and Matuszek, J. - Phys. Lett. 39B (1972) 503.

100. Milton, J. C. D. and Fraser, J. S. - Can. J. Phys. 40 (1962) 1626.

101. Milton, J. C. D. and Fraser, J. S. - Phys. Rev. 111 (1958) 877.

102. Gibson, W. M., Thomas, T. D. and Miller, G. L. - Phys. Rev. Lett. 7 (1961) 65.

103. Watson, R. L., Jared, R. C. and Thompson, S. G. - Phys. Rev. C 1 (1970) 1866.

104. Cameron, A. G. W. - Can. J. Phys. 35 (1957) 1021.

105. Wing, J. and Fong, P. - Phys. Rev. 136 (1964) B923.

106. Vandenbosch, R. and Thomas, T. D. - Brookhaven National Lab. Report BNL-5876.

107. Faissner, H. and Wildermuth, K. - Phys. Lett. 2 (1962) 212.

108. Reisdorf, W., Unik, J. P., Griffin, H. C. and Glendenin, L. E. - Nucl. Phys. A177 (1971) 337.